Novel mechanisms of NAD^+ dependent inhibition of Alzheimer's disease and AI-based technologies in related mechanistic studies and drug discovery

(Alice) Ruixue Ai

Thesis for the degree of Doctor Philosphiae (Dr. Philos)

Main supervisor: Associate Prof. Evandro F. Fang

Co-supervisors: Prof. Linda Hildegard Bergersen

Prof. Farrukh Abbas Chaudhry

Department of Clinical Molecular Biology, Akershus University Hospital

Faculty of Medicine, University of Oslo

Norway

2023

Series of dissertations submitted to the
Faculty of Medicine, University of Oslo

ISBN 978-82-348-0246-1

Cover: UiO.
Print production: Graphic center, University of Oslo.

Acknowledgements

This thesis is a summary of my three years of work, which I completed from 2020 to 2023 at the Department of Clinical Molecular Biology (EpiGen) at Akershus University Hospital and the Faculty of Medicine, the University of Oslo, Norway. My work has been generously supported by the China Scholarship Council (CSC) and by funding from the Evandro F. Fang Laboratory.

I would like to show my sincere gratitude to my supervisor, Associate Prof. Evandro F. Fang. I am honored to be the first 'doctor' trained from the Fang Lab. We have experienced so much together. I am very grateful that you are allowing me to study here. I sincerely appreciate all the advice you gave me on my research projects. The ample flexibility and independence in research in the Fang Lab has enabled me to develop into an independent researcher. I appreciate you considering my scientific viewpoints, and taking into account my circumstances, as well as the help making backup plans. I genuinely admire how persistent and upbeat we are in the face of challenges. Thanks to Karl Stavem for your support and revising the Acknowledgment section.

I'd like to express my gratitude to my co-mentors, Prof. Farrukh Abbas Chaudhry, Department of Molecular Medicine, Institute of Basic Medical Sciences, and Prof. Linda Hildegard Bergersen, Department of Oral Biology, for their scientific guidance and support on my projects. I have been inspired and supported by Prof. Jon Storm-Mathisen from the Department of Molecular Medicine: both inside the lab and outside of it, you have given me much support. You consistently provided me with great assistance in a timely manner, which gave me hope for the future. I want to express my gratitude to all my co-authors for their significant contributions and support to my work.

Additionally, I'd want to thank all of the members of the Fang Lab, both past and present, as well as my co-workers at EpiGen. I had the great fortune of having Dr. Chenglong Xie (now faculty in Wenzhou Medical University, China) as my first daily mentor. It can be extremely challenging for a dentist to enter a brand-new field of study. It was you who helped me make rapid progress and familiarize myself with this scientific field at the laboratory level. My second, and current daily mentor, is postdoc Dr. Maria Jose Lagartos Donate: I greatly value your advice and assistance on my projects. I would like to thank DPhil student Caroline Shi-qi Zhang, who has made a big contribution to my projects and is also a close friend in my life. I truly appreciate Thale Patrick-Brown for language editing of my papers and thesis. Thank you to all my lovely male colleagues, they are DPhil student Tomás Schmauck-Medina, DPhil student Alexander (Sasha) Anisimov, master student Jared Rice, former postdoc Dr. Yahyah Aman, former exchange Dr. Bai-lei Li, as well as postdoc Dr. Sifang Liao and Dr. Junping Pan. I thank my darling female colleagues postdoc Dr. Shuqin Cao, postdoc Dr. Sofie H. Lautrup, postdoc Dr. Niome Villaseca González, DPhil student Ping-Jie Wang, as well as former colleagues Dr. Domenica Caponio and Rina Ruiyu Han. Also, I would like to thank Janet Jian-ying Zhang and He-ling Wang for the joint scientific journey from the Netherlands to Norway. Also, I thank our Epi-Gen Lab manager Dr. Anna Frengen for your management and daily help.

I want to show my gratitude to everyone in my personal life: they have supported me through all of my challenging circumstances over the past three years. Thank you for being there with me, my friends. I can't imagine what life would be like without you.

Finally, I have no words to adequately convey how appreciative I am to my family (my parents, my little brother, and my boyfriend). You have always been a source of encouragement for me, especially during my doctoral studies. I thank you for your understanding and support over the past four years, wherein I am grateful. Without you by my side, I cannot challenge myself to have the Dr. Philos. degree (Doctor Philosophiae).

Oslo, 23 December 2022
(Alice) Ruixue Ai

Contents

Abbreviations

A3SS	Alternative 3′ splice site
A5SS	Alternative 5′ splice site
AASEs	Aberrant alternative splicing events
AD	Alzheimer's disease
AI	Artificial intelligence
AMBRA1	Autophagy and beclin 1 regulator 1
APP	Amyloid precursor protein
ARIH1	Ariadne RBR E3 ubiquitin protein ligase 1
ATF4	Activating transcription factor 4
ATF5	Activating transcription factor 5
ATFS-1	Activating Transcription Factor associated with Stress
Aβ	Amyloid-beta
Bag-1	BAG cochaperone 1
BCL2L13	BCL2 like 13
BNIP3L	BCL2 interacting protein 3 like
bZIP	Basic Leucine Zipper Domain
Card.	Cardiolipin
CHOP	DNA damage inducible transcript 3
CLPP	Caseinolytic mitochondrial matrix peptidase proteolytic subunit
eiF2α	α subunit of eukaryotic initiation factor 2
ES	Exon skip
EVA1-C	Eva-1 homolog C
FKBP8	FKBP prolyl isomerase 8
FUNDC1	FUN14 domain containing 1
GPUs	Graphics processing units
GWAS	Genome-wide association studies
HSP70	Heat shock protein 70
IMM	Inner mitochondrial membrane
IR	Intron retention
ISR	Integrated stress response
LONP1	Ion peptidase 1
MAPT	Microtubule associated protein Tau
MES	Multiple exon skip
MFN1	Mitofusin 1
MFN2	Mitofusin 2
mRNA	Messenger ribonucleic acid
MTS	Mitochondrial targeting sequence
NAD	Nicotinamide adenine dinucleotide
NAD^+	Nicotinamide adenine dinucleotide (oxidized form)
NBR1	NBR1 autophagy cargo receptor
NDP52	Calcium binding and coiled-coil domain 2
NFTs	Neurofibrillary tangles
NGS	Next-generation sequencing
NIX	BCL2 interacting protein 3 like
NLS	Nuclear localization signal

NMN	Nicotinamide mononucleotide
NR	Nicotinamide riboside
OMM	Outer mitochondrial membrane
OPTN	Optineurin
OXPHOS	Oxidative phosphorylation
p62	Sequestosome 1
PHB2	Prohibitin 2
PINK1	PTEN induced kinase 1
PPI	Protein–protein interaction
RNA	Ribonucleic acid
SIAH1	Siah E3 ubiquitin protein ligase 1
TAXIBP1	Tax1-binding protein 1
TBK1	TANK binding kinase 1
ULK-1	Unc-51 like autophagy activating kinase 1
uORFs	Upstream open reading frame
UPR^{mt}	Mitochondrial unfolded protein response
VDAC	Mitochondrial outer membrane protein porin of 36 kDa like

List of publications

*First author
#Corresponding author

The thesis is based on the following original articles:

1. **Project 1**
   Ruixue Ai*, Shi-Qi Zhang*, Junping Pan*, Chenglong Xie*, Maria Jose Donate Lagartos, Xiongbin Kang, Pingjie Wang, Domenica Caponio, Tanima SenGupta, Lipeng Mao, Francisco José Naranjo-Galindo, Ruiyu Han, Zhipeng Lin, Sofie Hindkjær Lautrup, Yimeng Zhang, Linda Hildegard Bergersen, Jon Storm-Mathisen, Hilde Loge Nilsen, Oscar Junhong Luo, Guobing Chen#, Evandro Fei Fang#. NAD^+ Replenishment improves life span and health span in Alzheimer's disease via coordinating mitophagy and mitochondrial unfolded protein response. (Paper submitted)

2. **Project 2**
   Ruixue Ai*, Lipeng Mao*, Xurui Jin*, Shiqi Zhang, Junping Pan, Maria Jose Donate Lagartos, Shuqin Cao, Guang Yang, Chenglong Xie, Xiongbin Kang, Pingjie Wang, Linda Hildegard Bergersen, Jon Storm-Mathisen, Niome Villaseca González, Zhangming Niu, Guobing Chen, Oscar Junhong Luo#, Evandro Fei Fang#. NAD^+ normalizes the landscape and biological relevance of alternative splicing events in tauopathies. (Paper submitted)

3. **Project 3**
   Chenglong Xie*, Xu-Xu Zhuang*, Zhangming Niu*, **Ruixue Ai***, Sofie Lautrup, Shuangjia Zheng, Yinghui Jiang, Ruiyu Han, Tanima Sen Gupta, Shuqin Cao, Maria Jose Lagartos-Donate, Cui-Zan Cai, Li-Ming Xie, Domenica Caponio, Wen-Wen Wang, Tomas Schmauck-Medina, Jianying Zhang, He-Ling Wang, Guofeng Lou, Xianglu Xiao, Wenhua Zheng, Konstantinos Palikaras, Guang Yang, Kim A Caldwell, Guy A Caldwell, Han-Ming Shen, Hilde Nilsen, Jia-Hong Lu#, Evandro F Fang# (2022). Amelioration of Alzheimer's disease pathology by mitophagy inducers identified via machine learning and a cross-species workflow. Nat Biomed Eng, 6(1), 76-93.

Additional research articles that are not included in the thesis:

4. Qian, Shuangjie; He, Hai-Jun; Xiong, Xi; Ye, Qianqian; **Ruixue Ai**; Zhao, Xuemiao; Feng, Feifei; Zhou, Shuoting; Xia, Kai; Xie, Cheng-Long. Amyloid-β and tau accumulation are independently associated with future cognitive decline. (Paper submitted)

5. Haijun He; Xi Xiong; Liu Shi; Qianqian Ye; **Ruixue Ai**; Shuangjie Qian; Shuoting Zhou; Feifei Feng; Xuemiao Zhao; Evandro F. Fang; Chenglong Xie. Alzheimer's disease diagnostic accuracy by fluid and neuroimaging ATN framework and cognitive decline prediction. eClinicalMedicine. (Paper submitted)

6. **Ruixue Ai***, Xu-Xu Zhuang*, Alexander Anisimov, Jia-Hong Lu#, and Evandro F#. Fang. "A synergized machine learning plus cross-species wet-lab validation approach identifies neuronal mitophagy inducers inhibiting Alzheimer disease." Autophagy 18, no. 4 (2022): 939-941.

7. Naranjo-Galindo, Francisco José, **Ruixue Ai**, Evandro Fei Fang, Hilde Loge Nilsen, and Tanima SenGupta. "*C. elegans* as an Animal Model to Study the Intersection of DNA Repair, Aging and Neurodegeneration." Frontiers in Aging (2022): 68.

8. **Ruixue Ai**, Xurui Jin, Bowen Tang, Guang Yang, Zhangming Niu, and Evandro F. Fang. "Ageing and Alzheimer's Disease: Application of Artificial Intelligence in Mechanistic Studies, Diagnosis, and Drug Development." In Artificial Intelligence in Medicine, pp. 1-16. Cham: Springer International Publishing, 2021.

9. Esther Meron, Maria Thaysen, Suzanne Angeli, Adam Antebi, Nir Barzilai, Joseph A Baur, Simon Bekker-Jensen, Maria Birkisdottir, Evelyne Bischof, Jens Bruening, Anne Brunet, Abigail Buchwalter, Filipe Cabreiro, Shiqing Cai, Brian H Chen, Maria Ermolaeva, Collin Y Ewald, Luigi Ferrucci, Maria Carolina Florian, Kristen Fortney, Adam Freund, Anastasia Georgievskaya, Vadim N Gladyshev, David Glass, Tyler Golato, Vera Gorbunova, Jan Hoejimakers, Riekelt H Houtkooper, Sibylle Jager, Frank Jaksch, Georges Janssens, Martin Borch Jensen, Matt Kaeberlein, Gerard Karsenty, Peter De Keizer, Brian Kennedy, James L Kirkland, Michael Kjaer, Guido Kroemer, Kai-Fu Lee, Jean-Marc Lemaitre, David Liaskos, Valter D Longo, Yu-Xuan Lu, Michael R MacArthur, Andrea B Maier, Christina Manakanatas, Sarah J Mitchell, Alexey Moskalev, Laura Niedernhofer, Ivan Ozerov, Linda Partridge, Emmanuelle Passegué, Michael A Petr, James Peyer, Dina Radenkovic, Thomas A Rando, Suresh Rattan, Christian G Riedel, Lenhard Rudolph, **Ruixue Ai**, Manuel Serrano, Björn Schumacher, David A Sinclair, Ryan Smith, Yousin Suh, Pam Taub, Alexandre Trapp, Anne-Ulrike Trendelenburg, Dario Riccardo Valenzano, Kris Verburgh, Eric Verdin, Jan Vijg, Rudi GJ Westendorp, Alessandra Zonari, Daniela Bakula, Alex Zhavoronkov, Morten Scheibye-Knudsen (2022). Meeting Report: Aging Research and Drug Discovery. Aging (Albany NY), 14(2), 530.

Summary

Dementia is one of the most common diseases in the elderly, devastating the quality of life of the patients as well as brining formidable socio-economic challenges. Over 50 million people are affected with dementia worldwide, among them an estimated 70-120 K in Norway. Alzheimer's disease (AD) is the most common (70%) form of dementia, with disease defining pathological features including extracellular Aβ plaques and intracellular Tau tangles. There is still no cure for AD, mostly due to our limited understanding of the aetiology of this disease.

Accumulation of damaged mitochondria and disruption of aberrant alternative splicing events (AASEs) contribute to the progression of AD. Nicotinamide adenine dinucleotide (oxidized form, NAD^+) is a pivotal metabolite in life, health, and neuroprotection. NAD^+ supplementation mitigates memory loss in AD animal models, partially via mitochondrial maintenance through mitophagy. However, whether and how NAD^+ affects other mitochondrial maintenance pathways, such as mitochondrial unfolded protein response (UPR^{mt}), are elusive. Furthermore, whether and how NAD^+ influences AASEs in AD remains unclear.

Artificial intelligence (AI) refers to the modeling of intelligent behavior by machines with little involvement from humans. The use of AI in the medical industry is expanding with common applications including data collection, analysis, mechanistic prediction, clinical disease diagnosis, and medication discovery. In this doctoral program, my colleagues and I conducted thorough research from two angles by combining cutting-edge AI and traditional wet laboratory methods in the AD field: (1) Novel mechanisms of NAD^+-dependent inhibition of AD; and (2) the development and application of novel AI-based approaches in mechanistic studies and anti-AD drug discovery.

My first project showed that the two mitochondrial quality control pathways, UPR^{mt} and mitophagy, are damaged in AD, partially due to depleted NAD^+-activating transcription factor 5 (ATF5)-UPR^{mt}/mitophagy axis. NAD^+ is reduced in AD while its augmentation mitigates AD pathologies. Mechanistically, NAD^+ mediates nuclear translocation of the core UPR^{mt} protein ATF5 via phosphorylating eiF2α, α subunit of eukaryotic initiation factor 2; higher nuclear ATF5 upregulates the expression of genes involved in UPR^{mt}, leading to resilience of glutamatergic and cholinergic neurons, improved memory, reduced Tau pathologies, and improved mitochondrial homeostasis. Intriguingly, the UPR^{mt} protein ATF5 also regulates mitophagy (majorly PINK1/Parkin-dependent mitophagy), highlighting a novel role of ATF5 in regulating mitochondrial homeostasis via coordination of both UPR^{mt} and mitophagy. Our findings point to new druggable strategy against AD by fine-tuning the NAD^+-ATF5-UPR^{mt}/mitophagy axis in preserving mitochondrial quality and minimizing Tau pathology.

My second project investigated the effect of NAD^+ on AASEs in AD mouse models and AD human cell models. Eva-1 homolog C (EVA1-C) is a protein that is expressed by axons in the developing spinal cord, forebrain, and other areas of the nervous system. It plays a role in the formation of neural circuits through its interaction with Slit and Robo proteins, which regulate axon guidance and pathfinding. EVA1C appears to have both Robo-dependent and Robo-independent functions in these processes, suggesting that it plays a multifaceted role in the development of the nervous system. NAD^+ normalizes AASEs in Tauopathy as exemplified by the regulation of Eva-1 homolog C (EVA1-C) isoforms. At the molecular level, NAD^+ upregulates EVA1-C long length isoform, leading to enhanced EVA1-C-HSP70 binding; higher EVA1-C-HSP70 binding may induce autophagy for autophagic elimination of cytoplasmic cellular 'garbage', and finally mitigate AD pathologies. This study suggests aberrant AASE is a cause of AD, while NAD^+ could normalize AASEs to alleviate AD pathologies.

My third project was focused on the development of a novel AI approach for swift screening of novel and clinically translatable mitophagy inducers. By the use of three machine-learning approaches covering vector representations of molecular structures, pharmacophore

fingerprinting, and conformer fingerprinting, an AI algorithm termed ‘Fang Lab-AI’ was built. The combined application of ‘Fang Lab-AI’ and a cross-species screening platform enabled the identification of two lead compounds, kaempferol, and rhapontigenin. kaempferol and rhapontigenin induce mitophagy in cells, worm neuronal systems, and mouse brain, majorly in a PINK1-dependent manner; importantly, they reduce Aβ and Tau pathologies and conserve memory in both *C. elegans* and mouse models of AD. This study elegantly developed and applied a novel AI algorithm for fast identification of lead mitophagy-inducing compounds as drug candidates for AD; our study may inspire the application of AI for the development of drug candidates against other neurodegenerative diseases.

In summary, data from these three projects provide new mechanisms on the aetiology of AD, highlighting the intertwined linkages of reduced NAD^+, aberrant RNA splicing, compromised mitochondrial homeostasis, and accumulated brain ‘garbage’ due to impaired autophagy/mitophagy, in the development of AD. These results underline the importance of the combination of advanced AI and classical wet laboratory approaches in mechanistic studies and drug development. Our discoveries have strong translational perspective, pointing to turning up the NAD^+-ATF5-UPR^{mt}/mitophagy axis and normalization of RNA splicing as druggable targets against AD.

Sammendrag

Demens er en av de vanligste sykdommene hos eldre, som ødelegger livskvaliteten til pasientene og skaper formidable sosioøkonomiske utfordringer. Over hele verden er mer enn 50 millioner mennesker rammet av demens, blant dem anslagsvis 70-120.000 i Norge. Alzheimers sykdom (AD) er den vanligste (70 %) formen for demens. Sykdomsdefinerende patologiske trekk inkluderer ekstracellulære Aβ-plakk og intracellulære Tau-floker. Det er fortsatt ingen kur for AD, hovedsakelig på grunn av vår begrensede forståelse av årsaken(e) til denne sykdommen.

Akkumulering av skadede mitokondrier og forstyrrelser som skyldes avvikende alternative spleisehendelser (aberrant alternative splicing events, AASEs) bidrar til progresjonen av AD. Nikotinamidadenindinukleotid (oksidert form, NAD^+) er en sentral metabolitt, nødvendig for liv, helse og beskyttelse av nervevev. NAD^+-tilskudd reduserer hukommelsestap i dyremodeller for AD, delvis via vedlikehold av mitokondriene gjennom mitofagi. Hvorvidt og hvordan NAD^+ påvirker andre mitokondrielle vedlikeholdsveier, for eksempel mitokondriell utfoldet proteinrespons (mitochondrial unfolded protein response, UPRmt), er imidlertid ukjent. Videre er det uklart om og hvordan NAD^+ påvirker AASEs i AD.

Kunstig intelligens (AI) er modellering av intelligent atferd i maskiner med lite medvirkning fra mennesker. Bruken av AI i den medisinske industrien øker stadig, for eksempel til datainnsamling, analyse, prediksjon av mekanismer, klinisk sykdomsdiagnose og oppdagelse av nye medisiner. I dette doktorgradsprogrammet utførte mine kolleger og jeg grundig forskning under to synsvinkler innen AD-feltet ved å kombinere banebrytende AI og tradisjonelle våtlaboratoriemetoder. Vi har (1) klarlagt nye mekanismer for NAD^+-avhengig hemming av AD; og (2) utviklet og anvendt nye AI-baserte tilnærminger til å finne mekanismer og nye medikamenter mot AD.

Mitt første prosjekt viste at de to mitokondrielle kvalitetskontrollveiene, UPR^{mt} og mitofagi, er skadet i AD, delvis på grunn av utarmet NAD^+, som leder til redusert aktiverende transkripsjonsfaktor 5 (activating transcription factor 5, ATF5) og derav følgende redusert UPR^{mt} og svekket mitofagi. Mens nivået av NAD^+ er redusert i AD, motvirker økning av NAD^+ AD-patologier. Mekanistisk formidler NAD^+ nukleær translokasjon av ATF5 (kjerne proteinet i UPR^{mt}) via fosforylering av eiF2α, α-subenhet av eukaryotisk initieringsfaktor 2; høyere ATF5 i cellekjernen oppregulerer uttrykket av gener involvert i UPR^{mt}, noe som fører til økt motstandsdyktighet av glutamaterge og kolinerge nevroner, forbedret hukommelse, reduserte Tau-patologier og forbedret mitokondriell homeostase. Interessant nok regulerer UPR^{mt}-proteinet ATF5 også mitofagi (hovedsakelig PINK1/Parkin-avhengig mitofagi), noe som tyder på en ny rolle for ATF5 i å regulere mitokondriell homeostase via koordinering av både UPR^{mt} og mitofagi. Våre funn peker på en ny medikamentell strategi mot AD ved å finjustere NAD^+-ATF5-UPR^{mt}/mitofagi-aksen og derved bevare mitokondriell kvalitet og minimere Tau-patologi.

Mitt andre prosjekt undersøkte effekten av NAD^+ på AASEs i AD-musemodeller og humane AD-cellemodeller. Eva-1 homolog C (EVA1-C) er et protein som uttrykkes av aksoner i den utviklende ryggmargen, forhjernen og andre områder av nervesystemet. Det spiller en rolle i dannelsen av nevrale kretsløp gjennom sin vekselvirkning med Slit- og Robo-proteiner, som regulerer veiledning og stifinning hos nervefibre når de vokser ut. EVA1-C ser ut til å ha både Robo-avhengige og Robo-uavhengige funksjoner i disse prosessene, noe som tyder på at det spiller en mangefasettert rolle i utviklingen av nervesystemet. NAD^+ normaliserer AASEs i Tauopati, for eksempel ved reguleringen av isoformer av EVA1-C. På molekylært nivå oppregulerer NAD^+ EVA1-Cs lang lengde isoform, noe som fører til forbedret EVA1-C-HSP70-binding; høyere EVA1-C-HSP70-binding kan indusere autofagi for autofagisk eliminering av cytoplasmatisk "søppel" i cellene, og til slutt dempe AD-patologier. Denne studien antyder at

avvikende AASEs er en årsak til AD, mens NAD^+ kan normalisere AASEs og derved lindre AD-patologier.

Mitt tredje prosjekt var fokusert på utviklingen av en ny AI-tilnærming for rask screening av nye mitofagi-induserende stoff som kan brukes klinisk. Ved bruk av tre maskinlæringsmetoder som dekker vektorrepresentasjoner av molekylære strukturer, såkalt farmakofor 10-fingeravtrykk og konformer-fingeravtrykk, ble en AI-algoritme kalt "Fang Lab-AI" satt opp. Ved kombinert bruk av 'Fang Lab-AI' og en screeningplattform i flere arter identifiserte vi to 'lead compounds', kaempferol og rhapontigenin. Begge disse stoffene induserer mitofagi i cellekulturer, i nervesystemet hos nematoden C. elegans og i musehjerne, hovedsakelig på en PINK1-avhengig måte, og fremfor alt, de reduserer Aβ- og Tau-patologier og bevarer hukommelsen i både C. elegans og musemodeller av AD. Denne studien utviklet og brukte elegant en ny AI-algoritme for rask identifisering av mitofagi-induserende forbindelser som medikament-kandidater for AD. Vår studie kan inspirere til bruk av AI for utvikling av medikamentkandidater mot andre nevrodegenerative sykdommer.

I korthet viser data fra disse tre prosjektene nye mekanismer i ADs etiologi, med vekt på de mangslungne sammenhengene mellom redusert NAD^+, avvikende mRNA-splicing, forstyrret mitokondriell homeostase, og opphoping av avfallsstoffer i hjernen på grunn av svekket autofagi og/eller mitofagi. Disse resultatene understreker betydningen av å kombinere avansert AI med klassisk våtlabarbeid for å klarlegge sykdomsmekanismer og finne nye medikamenter. Våre oppdagelser har sterkt translasjonspotensial. De viser til oppregulering av NAD^+-ATF5-UPR^{mt}/mitofagi-aksen og normalisering av RNA-splicing som mulige mål for mediakmentell behandling av AD.

1. Introduction

I am interested in the mechanistic exploration of Alzheimer's disease (AD) aetiologies as well as in the development of drug candidates against AD. It requires extensive background knowledge on a variety of topics, including recent progress in understanding the mechanisms of AD, NAD^+ metabolism and its roles in neuronal protection, and the use of artificial intelligence (AI) in drug development. Details of these topics are elaborated below.

1.1 Alzheimer's disease

Around 50 million people worldwide suffer from dementia, about 70% due to AD. There is no known cure for AD at present (Organization WH, 2022). Extracellular amyloid-beta (Aβ) plaques and intracellular neurofibrillary tangles (NFTs) caused by hyperphosphorylation of Tau (pTau) are the disease-defining characteristics of AD (Canter RG et al., 2016). The causes of AD are still poorly understood despite decades of research. Clinical trials on anti-AD drug candidates have consistently failed over the past 20 years (Canter RG et al., 2016), indicating that additional research into processes by which AD develops is required for the development of novel medications. While it is encouraging that new anti-Aβ antibodies (such as Aduhelm/ Aducanumab in 2021 and Lecanemab in 2022) (Sevigny J et al., 2016;van Dyck CH et al.,

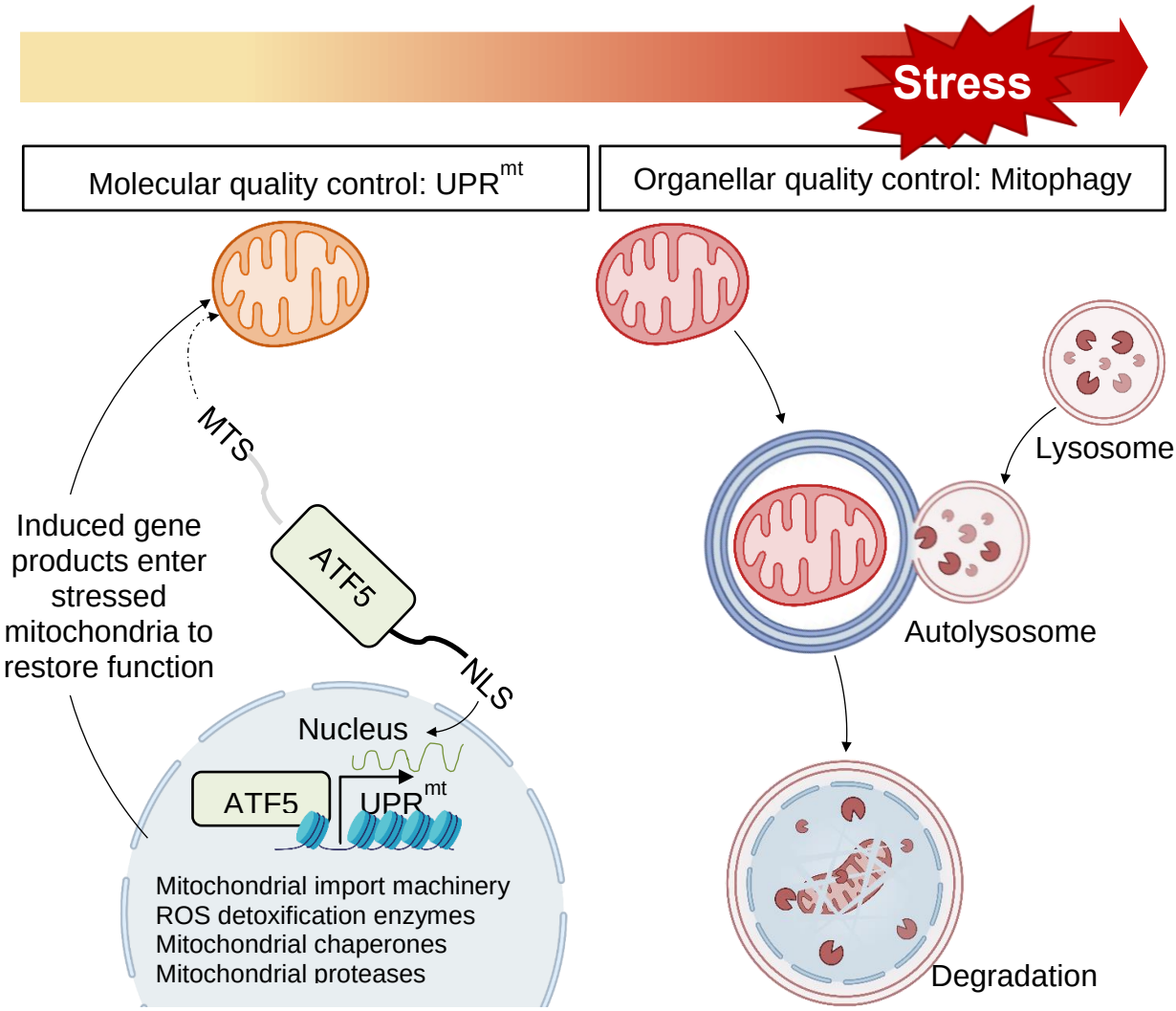

Figure 1. The organizational structure of the mitochondrial quality control systems. An intra-organellar quality control system makes up the first line. A transcriptional pathway known as the mitochondrial unfolded protein response is responsible for inducing mitochondrial chaperone proteins and proteases under stressful circumstances (UPR^{mt}). The organellar quality control system, which includes mitophagy and fusion and fission events, serves as the second line of defence. Mild mitochondrial stress may cause fusion and fission events. However, mitophagy is triggered by mitochondrial malfunction [Figure was drawn using bioRener with reference from (Rugarli EI and Langer T, 2012)].

2023), are showing limited/partial benefits, although with severe side effects for some patients, the failure to control the disease fully highlights the necessity to develop more effective and safe anti-AD drugs.

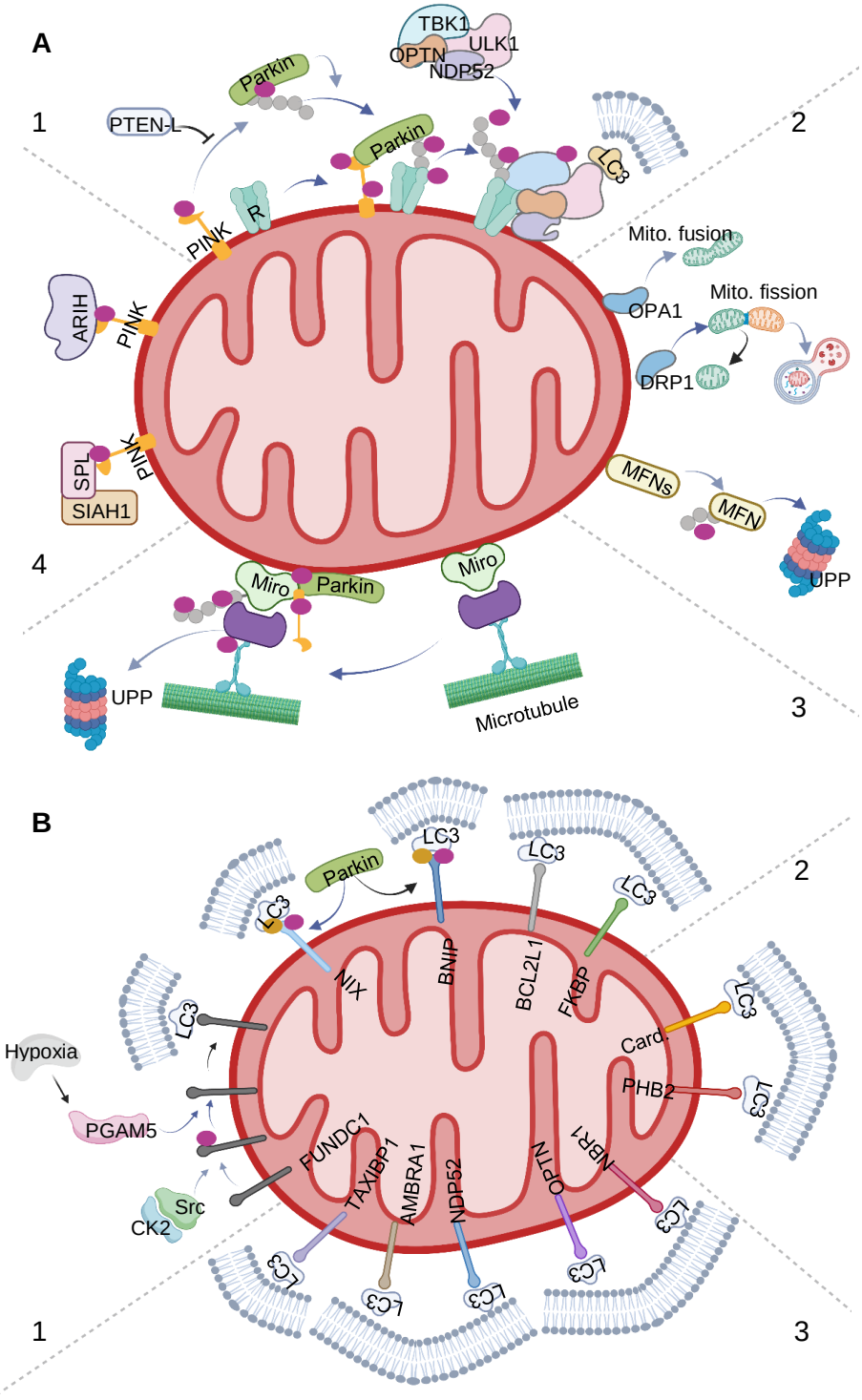

Figure 2. Overview of the several mitophagy pathways. (A) Mitophagy routes that are Parkin-(in)dependent and PINK1-dependent descending clockwise: (1) Reduced mitochondrial membrane potential enables the stability of full-length PINK1 at the outer mitochondrial membrane (OMM) for the PINK1 and Parkin-dependent mitophagy pathway. Full-length autophosphorylated PINK1 phosphorylates ubiquitin, enabling the binding of Parkin to phosphoubiquitin and the recruitment and binding of OMM receptors. Parkin, phosphorylated by PINK1, ubiquitinates several known receptors, including mitochondrial outer membrane protein porin of 36 kDa like (VDAC), mitofusins (MFN1 and MFN2), and the mammalian mitochondrial Rho (Miro). (2) Because smaller mitochondria are more quickly ingested and destroyed, mitophagy is facilitated by mitochondrial fission. (3) PINK1 and Parkin arrest mitochondrial motility through degradation of Miro. (4) PINK1-dependent, Parkin-independent mitophagy pathway. In addition to Parkin, alternative E3 ubiquitin ligases like SIAH1 and ARIH1 participate in PINK1-dependent, Parkin-independent mitophagy. (B) Receptor-mediated mitophagy pathways. Here, receptor-mediated mitophagy pathways are divided into three groups. (1): Group 1 comprises OMM proteins, including FUNDC1, NIX (BNIP3L), BNIP3, FKBP8, and BCL2L13 (the mammalian orthologue of the yeast Atg32). (2): Group 2 contains mitophagy receptors that are inner mitochondrial membrane (IMM) components, including prohibitin 2 (PHB2) and cardiolipin (Card.). (3) Group 3 comprises autophagy receptors that are also involved in mitophagy, including AMBRA1, NDP52, TAXIBP1, NBR1, OPTN, and p62 [(Figure was drawn using bioRener with reference from (Lou G et al., 2020)].

1.1.1 The AD Mitochondrial cascade hypothesis

The "powerhouses of the cell", mitochondria, produce the energy necessary for neurons to survive and operate. A healthy mitochondrial pool is essential for life and health. There is mounting evidence that AD is characterized by damaged mitochondria (Fang EF et al.,

2019;Kerr JS et al., 2017). In 2004 (Swerdlow RH et al., 2014;Swerdlow RH and Khan SM, 2004), the "AD mitochondrial cascade hypothesis" was proposed, which highlighted the significance of mitochondrial quality control in AD. Cells have developed complex and interrelated processes to preserve the quality of their mitochondria, such as mitophagy, fusion, and the mitochondrial unfolded protein response (UPR^{mt}) (Figure 1). We will be concentrating on mitophagy and UPR^{mt} in this research, so I will introduce these two pathways.

1.1.1.1 Defective mitophagy in AD

Similar to the "brain cleaning system", mitophagy (the word for mitochondrial autophagy) aims to eliminate defective mitochondria. Parkin-(in)dependent, PINK1-dependent, and receptor-mediated mitophagy are the three routes currently recognized as mitophagy mechanisms (Figure 2). In 3xTg AD and APP/PS1 mice models, AD-induced pluripotent stem cell (iPSC)-derived cortical neurons, as well as post-mortem hippocampus tissue from AD patients, mitophagy has been shown to substantially decrease at the basal level (Fang EF et al., 2019). Unc-51 like autophagy activating kinase 1 (ULK-1, low phosphorylated serine 555 sites) and TANK binding kinase 1 (TBK1, low phosphorylated serine 172 sites) are the two proteins that make up the autophagic/mitophagic initiator machinery (Fang EF et al., 2019). However, pTau- or Abeta-expressing nematodes exhibit a reduced capacity for stress-induced mitophagy (Fang EF et al., 2019). These show that impaired mitophagy is a prevalent symptom of AD, suggesting a potential new therapeutic target.

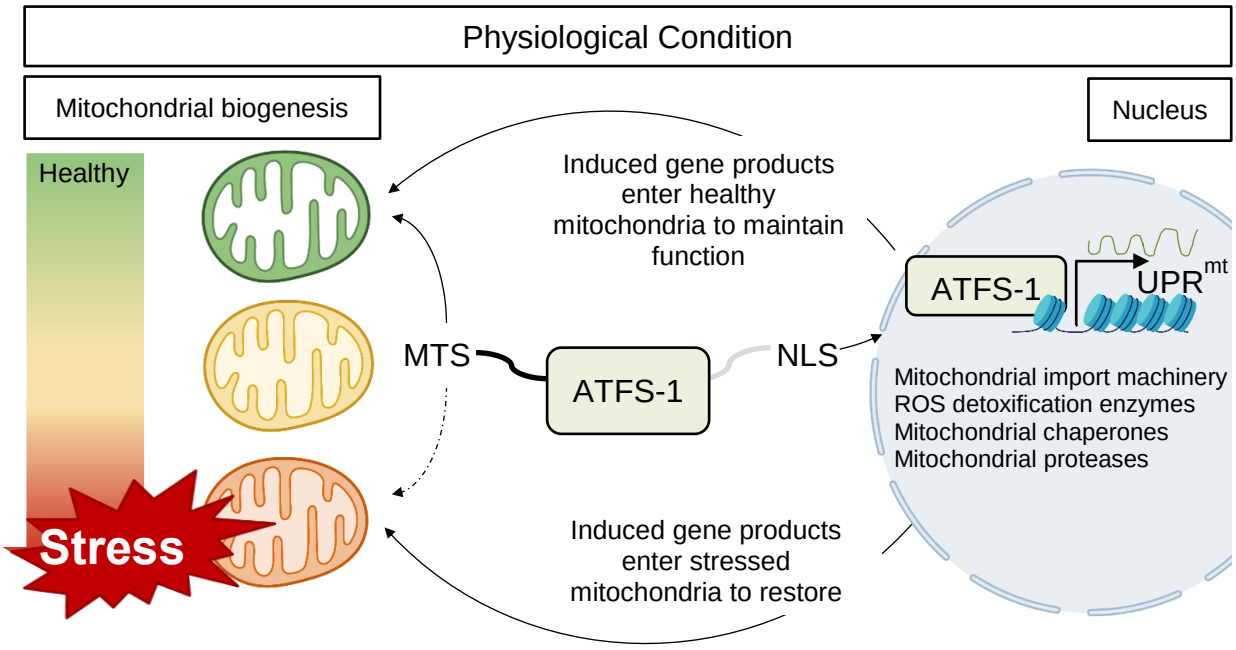

Figure 3. The effectiveness of ATFS-1 mitochondrial import in *C. elegans* under various mitochondrial stress conditions. ATFS-1 has a mitochondrial targeting sequence (MTS) as well as a nuclear localization sequence (NLS). ATFS-1 is efficiently imported into healthy mitochondria; however, OXPHOS or mitochondrial proteostasis alterations that produce mitochondrial dysfunction impair import efficiency (red). If ATFS-1 is not imported into mitochondria, it is transported to the nucleus, where it triggers transcription of mitochondrial protective genes such as mitochondrial chaperones and proteases, antioxidants, and mitochondrial protein import components. In turn, the import of protective gene products into mitochondria promotes organelle stabilization and recovery. Thus, mitochondrial import efficiency is likely used as a measure of overall mitochondrial function by cells, with ATFS-1 acting as both a sensor and a mitochondria-to-nucleus signalling mechanism. [Figure was drawn using bioRener with reference from (Melber A and Haynes CM, 2018)].

1.1.1.2 Altered UPR^{mt} in AD

Although mitophagy might be a mitochondrion's last option, the UPR^{mt} is already in place to help with the recovery of salvageable mitochondria and to reduce the harm in defective organelles (Melber A and Haynes CM, 2018). The mitochondrial unfolded protein response (UPR^{mt}) is a transcriptional response and synthesizes the mitochondrial proteome, importing it into the mitochondria (Shpilka T and Haynes CM, 2018). Cytosolic protein synthesis can be regulated during mitochondrial stress by the phosphorylation of eiF2α (Palam LR et al.,

2011;Teske BF et al., 2013;Walter P and Ron D, 2011;Watatani Y et al., 2008), which can be regulated by mitochondrial import efficiency of the transcription factor (ATFS-1) in *C. elegans* (Figure 3) (Nargund AM et al., 2012). The orthologous transcription factors (activating transcription factor 4 (ATF4), activating transcription factor 5 (ATF5), DNA damage-inducible transcript 3 (CHOP)) of ATFS-1 in mammals may act as potential mechanisms (Figure 4). In the frank familial, sporadic, and moderate cognitive impairment stage of AD, previous investigations demonstrated that numerous UPR^{mt} transcripts were altered (Beck JS et al., 2016;Sorrentino V et al., 2017).

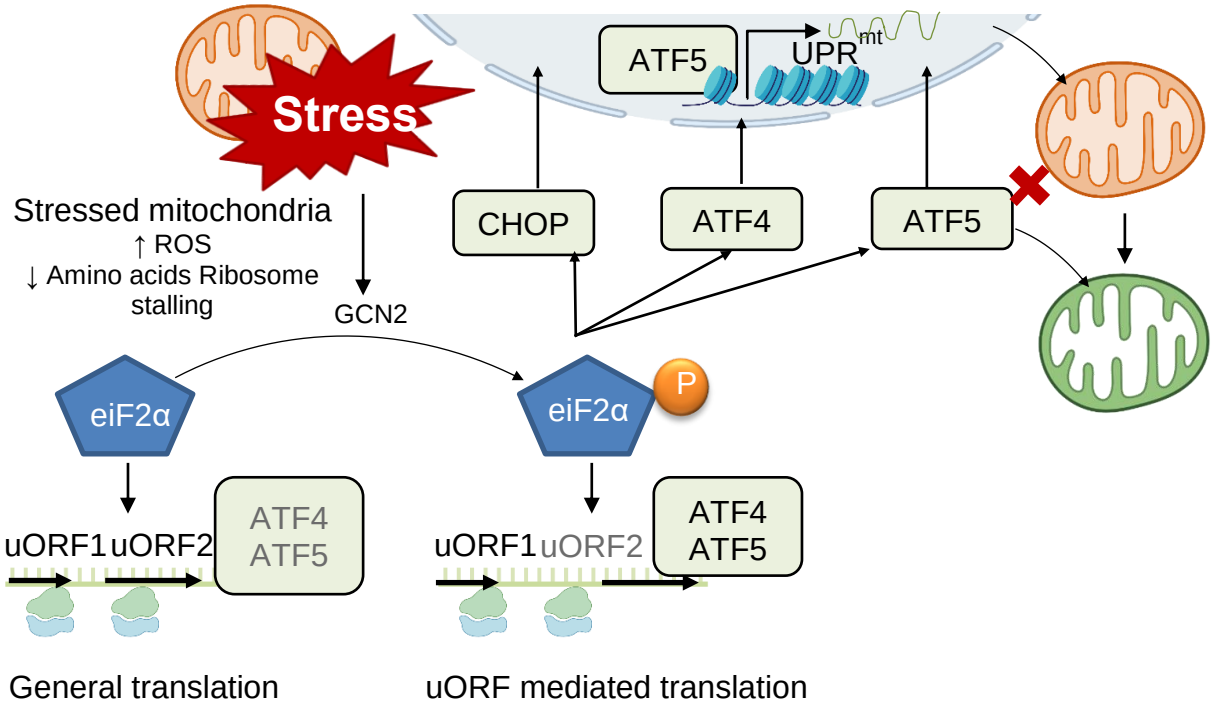

Figure 4. Molecular mechanisms inducing UPR^{mt} from stressed/damaged mitochondria. During mitochondrial dysfunction, the translation initiation factor eiF2α is phosphorylated resulting in the translation of those mRNAs harboring uORFs in the 5′ UTR. The transcription factors CHOP, ATF4, and ATF5 all have numerous uORFs and are preferentially translated during mitochondrial dysfunction (**inset**). While the precise interaction between these three transcription factors under mitochondrial stress remains unknown, all three are essential for the stimulation of genes linked with the UPR^{mt}. Atf5 transcription is induced by both CHOP and ATF4. ATF5, like ATFS-1 in *C. elegans*, has a mitochondrial targeting sequence, which may allow it to respond to mitochondrial stress by reducing mitochondrial protein import efficiency [Figure was drawn using bioRener with reference from (Melber A and Haynes CM, 2018)].

1.1.2 Dysfunction of RNA splicing in AD

Alternative splicing is a post-transcriptional regulation mechanism that impacts 92-94 percent of human genes (Wang ET et al., 2008). Alternative splicing allows for the removal of introns and the assembly of exons to create numerous RNA transcript isoforms from a single mRNA (Wright CJ et al., 2022). There are five AS types that form various transcript isoforms alternative 3′/5′ splice site (A3SS/A5SS), multiple exon skip (MES), intron retention (IR), and exon skip (ES) (Figure 5). In eukaryotes, different transcript isoforms perform related, separate, or even conflicting activities (Kornblihtt AR et al., 2013;Pan Q et al., 2008;Wang ET et al., 2008). Alternative splicing regulatory systems are numerous and conserved in the vertebrate nervous system, resulting in distinct phenotypes within and between individuals (Barbosa-Morais NL et al., 2012). AD is associated with disrupted RNA metabolism, particularly mRNA splicing (Bai B et al., 2013;Buee L et al., 2000;Raj T et al., 2018;Rockenstein EM et al., 1995;Trabzuni D et al., 2012). A transcriptomic study suggested that mRNA splicing is a characteristic of AD (Raj T et al., 2018).

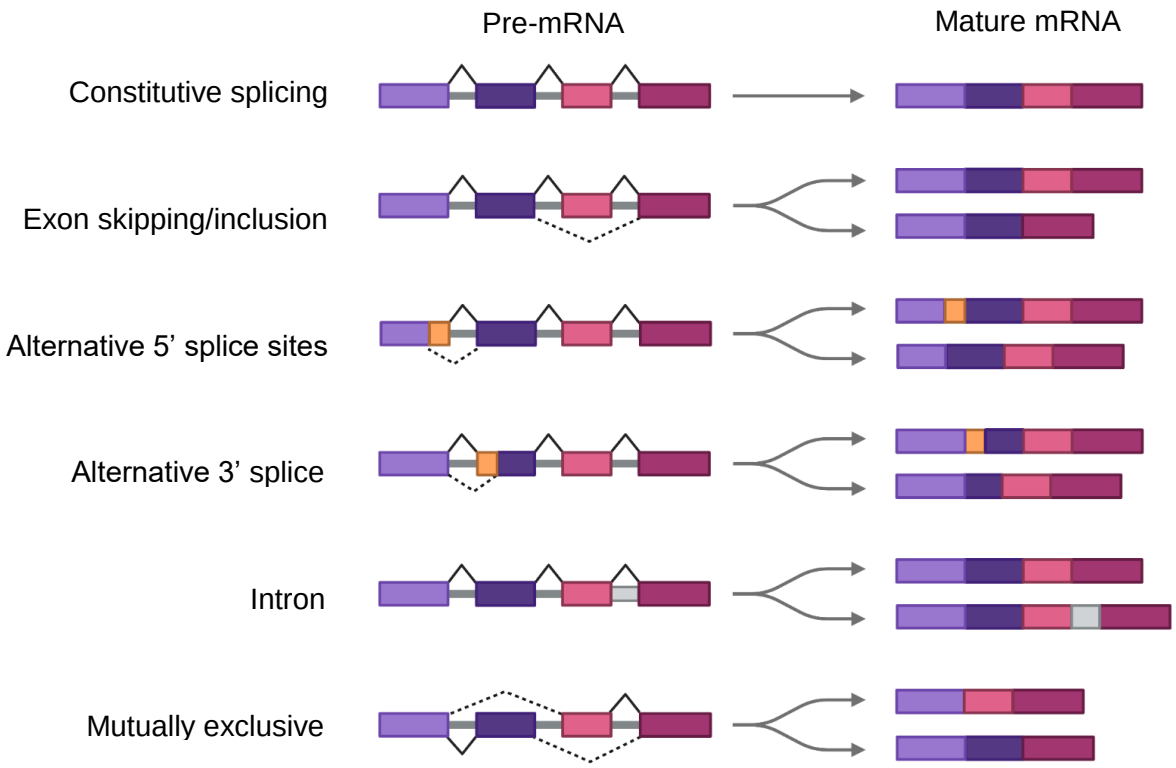

Figure 5. The diagram depicts various types of alternative splicing: ES, A3SS/A5SS, MES, and IR. Different alternative exons for the same pre-mRNA frequently exhibit distinct alternative-splicing patterns (Figures made in BioRender software).

1.2 Compromised NAD^+ metabolism and depleted downstream pathways contribute to AD

NAD^+ is an essential metabolite for survival, health, and neuroprotection (Figure 6). There is accumulating evidence that NAD^+ deficiency and impairment of NAD^+-dependent pathways contribute to AD pathogenesis. NAD^+-depletion and related metabolic abnormalities were observed in the brains of early-onset familial AD animal models (Dong Y and Brewer GJ, 2019;Hou Y et al., 2018). In the meantime, an NAD^+ booster inhibited Tau phosphorylation and cognitive impairment in a cross-species platform that included a neuronal Tau (pro-aggregate F3K280 Tau fragment) transgenic *C. elegans* model (Fang EF et al., 2019), 3xTgAD/Pol$^+$/ mice (Hou Y et al., 2018), and 3xTgAD mice (Hou Y et al., 2018).

According to research, NAD^+ upregulation of mitophagy leads to mitochondrial function recovery, reduced Tau pathologies, and memory retention (Fang EF et al., 2019). NAD^+ has been shown to promote UPR^{mt}, which improves mitochondrial proteostasis and protects against amyloid-induced proteotoxicity (Sorrentino V et al., 2017). However, it is unclear if NAD^+ reduces Tau pathologies via UPR^{mt}, how NAD^+ inhibits AD via UPR^{mt} and mitophagy, and what the connections are between UPR^{mt} and mitophagy in AD. Aside from these questions, there have been a few studies on RNA splicing dysregulation in Tauopathies (Andorfer C et al., 2003;Apicco DJ et al., 2019;Avale ME et al., 2013;Hinrich AJ et al., 2016;Lisowiec J et al., 2015;Liu F and Gong CX, 2008;Park SA et al., 2016;Peacey E et al., 2012;Schoch KM et al., 2016;Wobst HJ et al., 2017). However, a detailed mechanistic analysis of NAD^+ augmentation to demonstrate that it affects alternative splicing in Tauopathies is absent.

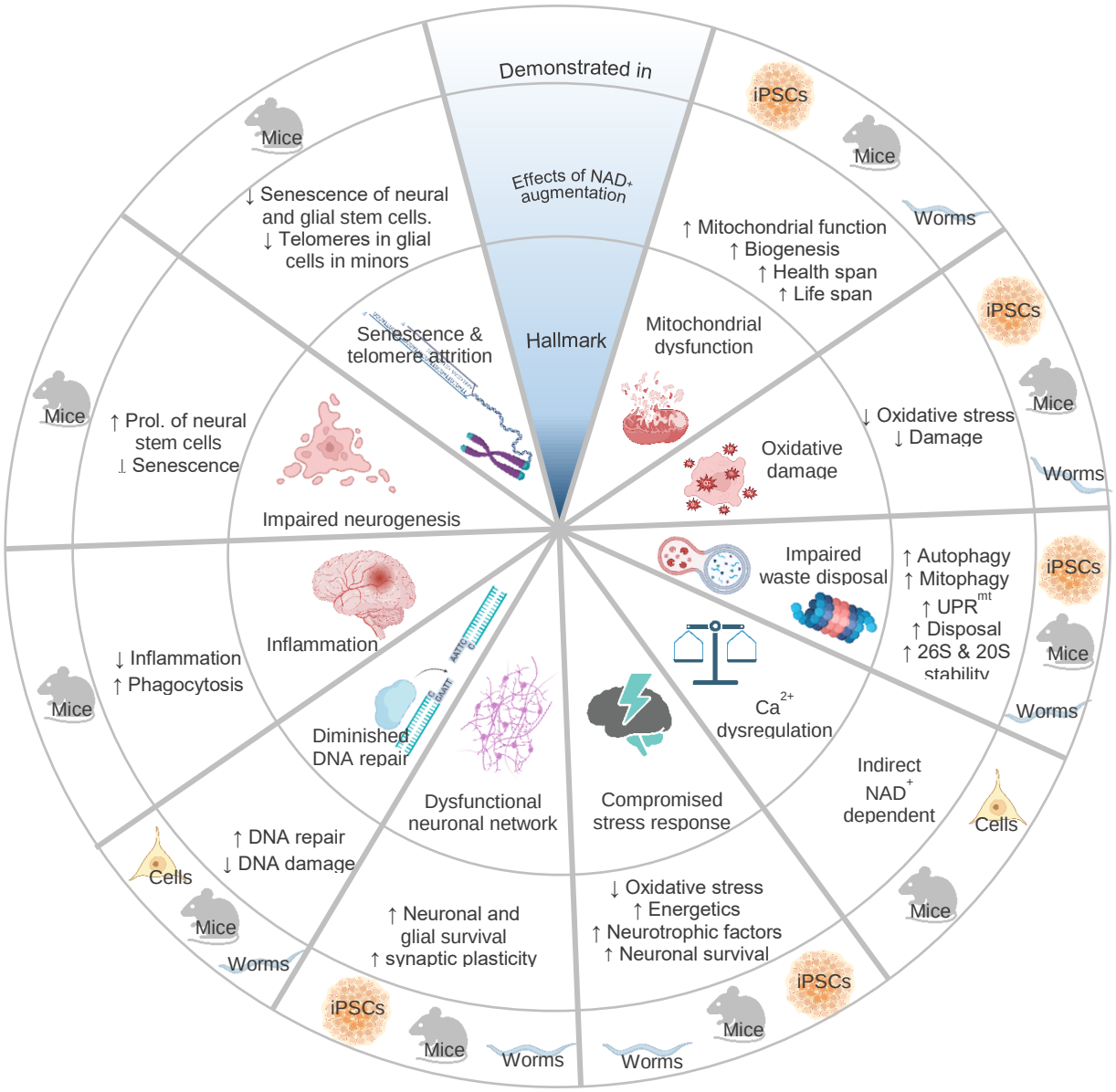

Figure 6. Reduced NAD⁺ links to the 10 hallmarks of brain aging. The 10 hallmarks of brain aging are listed. Evidence from cell culture, *C. elegans,* and mouse studies show that NAD⁺ augmentation counteracts the adversities of the hallmarks of brain aging [Figure was drawn using bioRener with reference from (Lautrup S et al., 2019)].

1.3 Artificial intelligence in medical research

AI is a broad term that refers to the use of a machine to model intelligent actions with minimal human intervention. It covers a wide range of research studies, including machine intelligence for computer vision, robotics, natural language processing, and more theoretical machine learning algorithm design, as well as the recent development of "deep learning." In general, AI is thought to have started with the invention of robotics in the 1920s. Funding for both AI-based research studies and industrial innovation projects has accelerated progress and development. AI research in medicine is advancing rapidly, with numerous applications (Figure 7). In 2016, healthcare AI projects received more investment than AI projects in other sectors of the global economy (CBINSIGHTS, 2017). In addition to traditional mathematical and statistical methodologies, AI techniques, particularly machine learning and deep learning approaches, have drawn substantial interest to the analysis of medical data, as medicine is becoming a more data-centric discipline. Using patient information and a database, AI might be utilized for diagnosis, therapy, and prognosis prediction. We highlight potential AI uses in AD diagnosis

and medication development (Figure. 8). In my doctoral program, we used AI for mechanism research and medication discovery in AD

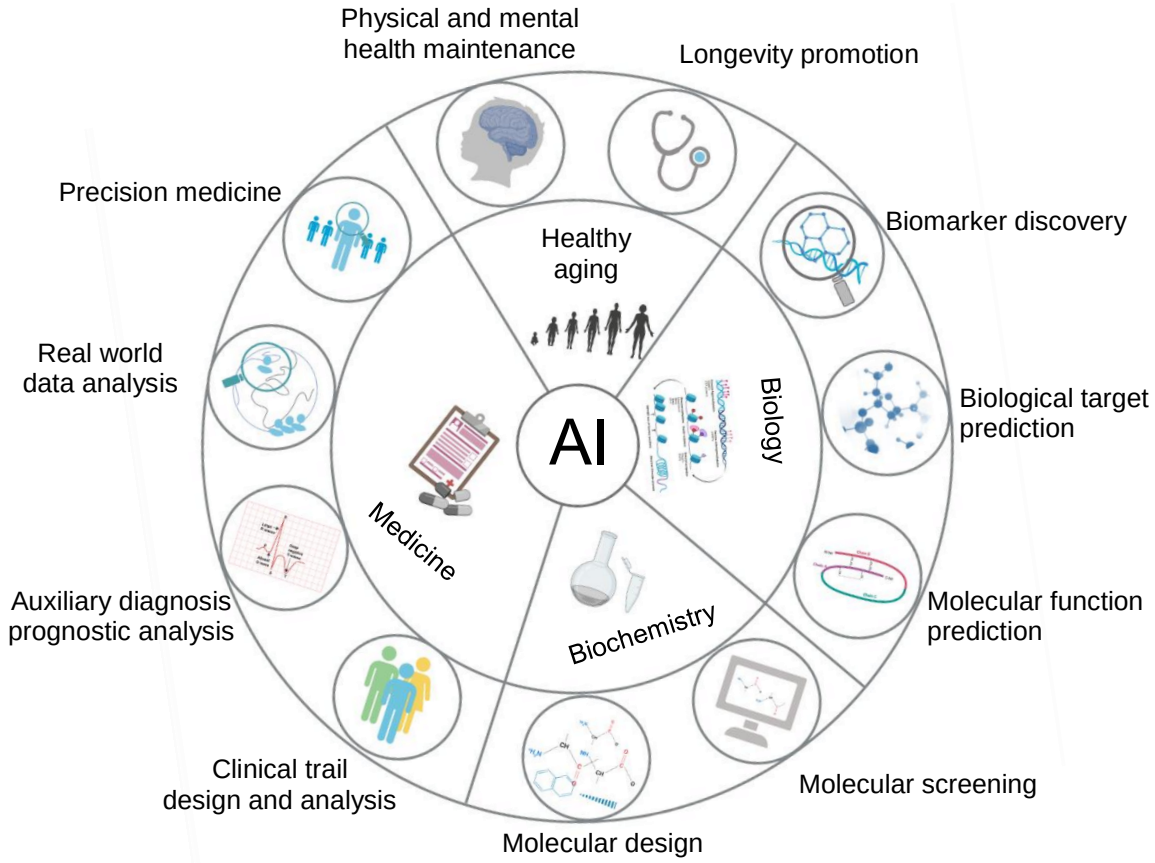

Figure 7. A summary of common applications of AI in the broad healthcare system. The broad application of AI in healthcare includes biomarker discovery, biological target prediction, molecular function prediction, molecular screening, molecular design, clinical trail design and analysis, auxiliary diagnosis, prognostic analysis, real world data analysis, precision medicine, physical and mental health maintenance, and longevity promotion (Figure adapted from the book 'Artificial Intelligence in Medicine').

1.3.1 AI in biology for mechanism study in AD

The pathogenesis of AD is currently unknown, while it is assumed to be caused by an interplay of genetic and environmental variables (Ng A et al., 2018;Ng TKS et al., 2019), with hereditary factors accounting for around 70% of the cause (Ballard C et al., 2011;Bi C et al., 2019;Freudenberg-Hua Y et al., 2018;Gatz M et al., 2006).

Aetiological studies seek to identify the environmental and genetic variables that cause disease, which can provide hints for future study into both the prevention and treatment of AD. Recently, the advancement of AI technology has made it possible to achieve this goal by utilizing huge data and ultra-complex models that outperform the processing capabilities of the human brain (Rajkomar A et al., 2019;Webb S, 2018;Zitnik M et al., 2019). Because genetic variables account for over 70% of AD cases, they have been the primary focus of AD pathogenesis research. The widespread use of microarray and next-generation sequencing (NGS)-based technologies in recent years has accelerated genetic data research. To find genetic variants in the human genome, four methodologies have now been used in the AD area, including genetic linkage analysis, candidate gene/pathway association studies, genome-wide association studies (GWAS), and next-generation sequencing (NGS)-based association studies (Fenoglio C et al., 2018).

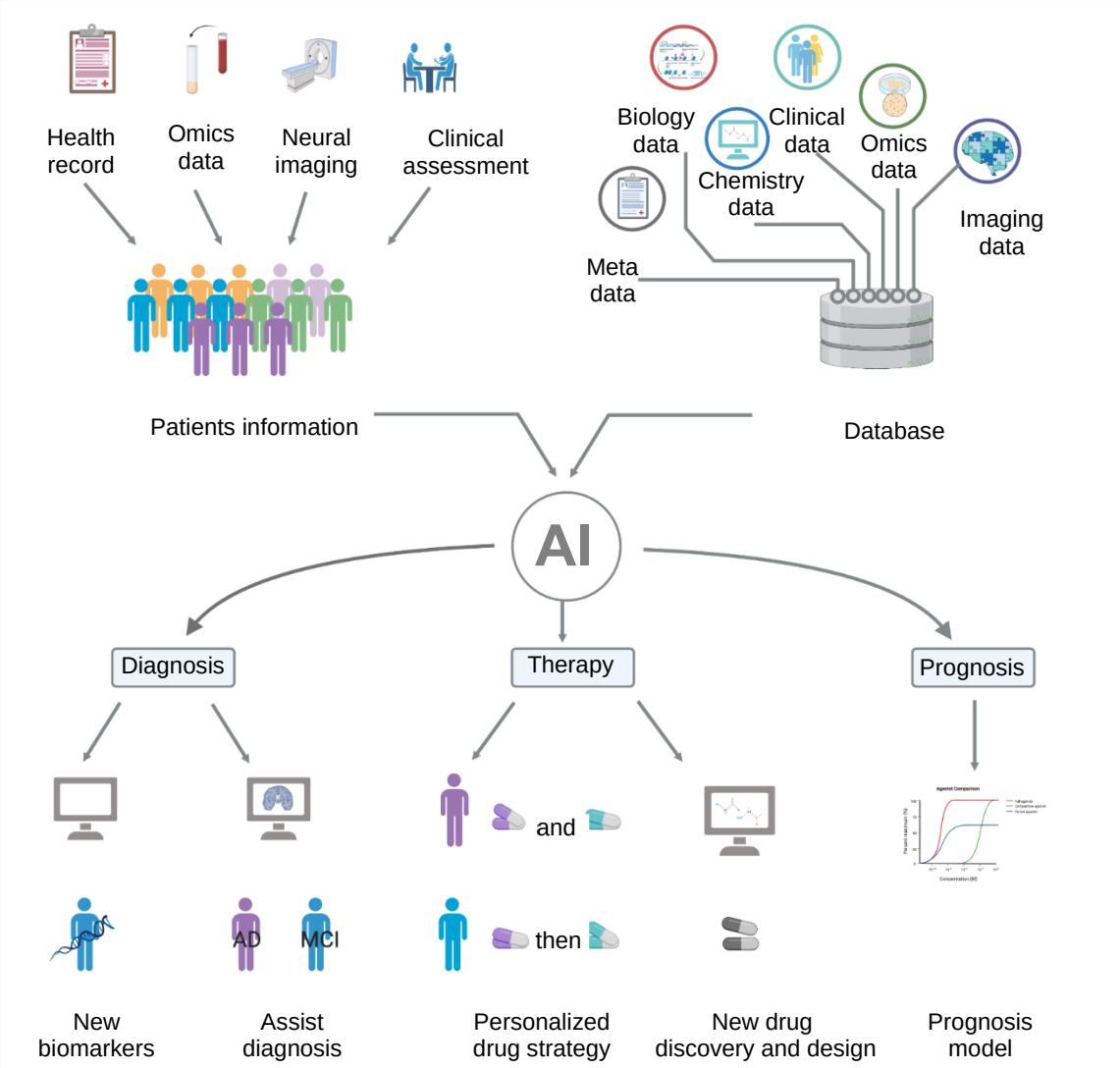

Figure 8. Prospective applications of AI technologies in the AD fields, such as in AD diagnosis, drug development, and prognosis. AI could improve diagnosis, therapy, and prognosis prediction by utilizing patient information and large datasets (Figure adapted from the book 'Artificial Intelligence in Medicine').

A protein's function is heavily dependent on its structure and predicting the spatial structure of a given amino acid sequence is critical in protein design and drug screening (Kuhlman B and Bradley P, 2019). A multi-centre effort has currently measured almost 170,000 protein structures; nonetheless, actually measuring the structure is a time-consuming and expensive technique. Using Deep Learning to anticipate structure may save costs and speed up related research (Wen B et al., 2020). Recently, AI was used to greatly increase the efficacy of protein structural predictive models, particularly in predictions with no previously known homologous structures (Abriata LA et al., 2019). The most recent version, ColabFold, combines the quick homology search of MMseqs2 (GitHub, 2023;Steinegger M and Soding J, 2017) with AlphaFold2 or RoseTTAFold. MMseqs2 (Many-against-Many sequence searching) is a software suite for searching and clustering massive protein and nucleotide sequence collections (Steinegger M and Soding J, 2017). AlphaFold2 and RoseTTAFold are deep-learning algorithms can further predict a protein's 3D shape from its linear sequence (Eisenstein M, 2021). ColabFold provides expedited prediction of protein structures and interactions. The 40-60 times faster search and optimized model use of ColabFold over AlphaFold2 or RoseTTAFold permits the prediction of nearly 1,000 structures per day on a server with one graphics processing unit. Now, ColabFold has become a free and accessible platform for protein folding research (Mirdita M et al., 2022).

In order to better understand AD aetiology, we created a pipeline platform using NGS-based technologies to detect RNA variations, and ColabFold to predict protein 3D structure and function.

1.3.2 AI for drug discovery in AD

There are no viable treatments for AD; due to the high failure rate of clinical trials, prominent pharmaceutical corporations have paused their work in this sector (Cummings J, 2018;Hay M et al., 2014;Zwierzyna M et al., 2018). For example, more than 400 clinical studies for AD were conducted between 2002 and 2012, but only one medicine was authorized, namely memantine (Cummings JL et al., 2014). This emphasizes the complexities of building customized drug strategies and opens up the possibility of using novel ways to design and find new drugs.

AI could be a new technique to create and discover new treatments for AD. As previously stated, AD pathogenesis involves a diverse set of pathways. Understanding AD requires an efficient, holistic, and detailed exploration of the data associated to these pathways. Individual researchers, however, may find this difficult. AI can assist in making sense of, and perhaps anticipate or design new medications. Knowledge graphs, which connect genes, diseases, and medications, are created by combining several data types such as ChEMBL, Ensembl, OmniPath, KEGG, and PubMed (Xie T and Grossman JC, 2018;Zitnik M et al., 2018). This approach can highlight the less-obvious links between drug targets and AD. However, the downside is the lack of granularity in biological relationships, which leads to reductions in specific predictions (Palop JJ et al., 2006). To overcome this limitation, we proposed creating a workflow that combines machine learning with a cross-species platform to fast, cost-effectively and accurately uncover novel candidate medicines for AD.

2. Aims of the study

In 2019, our team proposed and verified defective mitophagy as a new driver of AD and so far this study has received effusive and very positive responses from the community (Fang EF et al., 2019). The findings extend the 'AD mitochondrial cascade hypotheses' (Kerr JS et al., 2017;Swerdlow RH et al., 2014) by linking defective mitophagy to damaged mitochondria. In my doctoral projects, we further discussed the role of NAD^+ precursors on UPR^{mt}, the crosstalk of UPR^{mt}, and mitophagy to maintain mitochondria homeostasis in AD. At the same time, we involved AI in the mechanism study and drug discovery in AD.

In Project 1, we further asked whether NAD^+ precursors have other mechanisms on mitochondrial quality control pathways, such as UPR^{mt}. In Project 2, we try to combine new technology, namely the next-generation RNAseq and novel deep learning guided framework, forming a pipeline to discover the effects of NAD^+ on the landscape and biological relevance of alternative splicing events in Tauopathies. In Project 3, we use AI to rapidly identify mitophagy-inducing drugs for AD to further follow up our previous work.

Hence, the aims of the projects were:

2.1 Novel mechanisms of NAD^+-dependent inhibition of AD

- New mechanisms of NAD^+ precursor on mitochondrial quality control pathways in Tauopathy. (Project 1)
- New mechanisms of NAD^+ precursor on alternative RNA splicing in Tauopathy. (Project 2)

2.2 AI-based development in drug discovery and mechanistic studies

- Apply AI in mechanistic studies in AD (Project 2)
- Apply AI in the drug discovery in AD (Project 3)

3. Summary of papers

3.1 Project 1

NAD⁺ replenishment improves life span and health span in Alzheimer's disease via mitophagy and mitochondrial unfolded protein response (UPR^{mt})

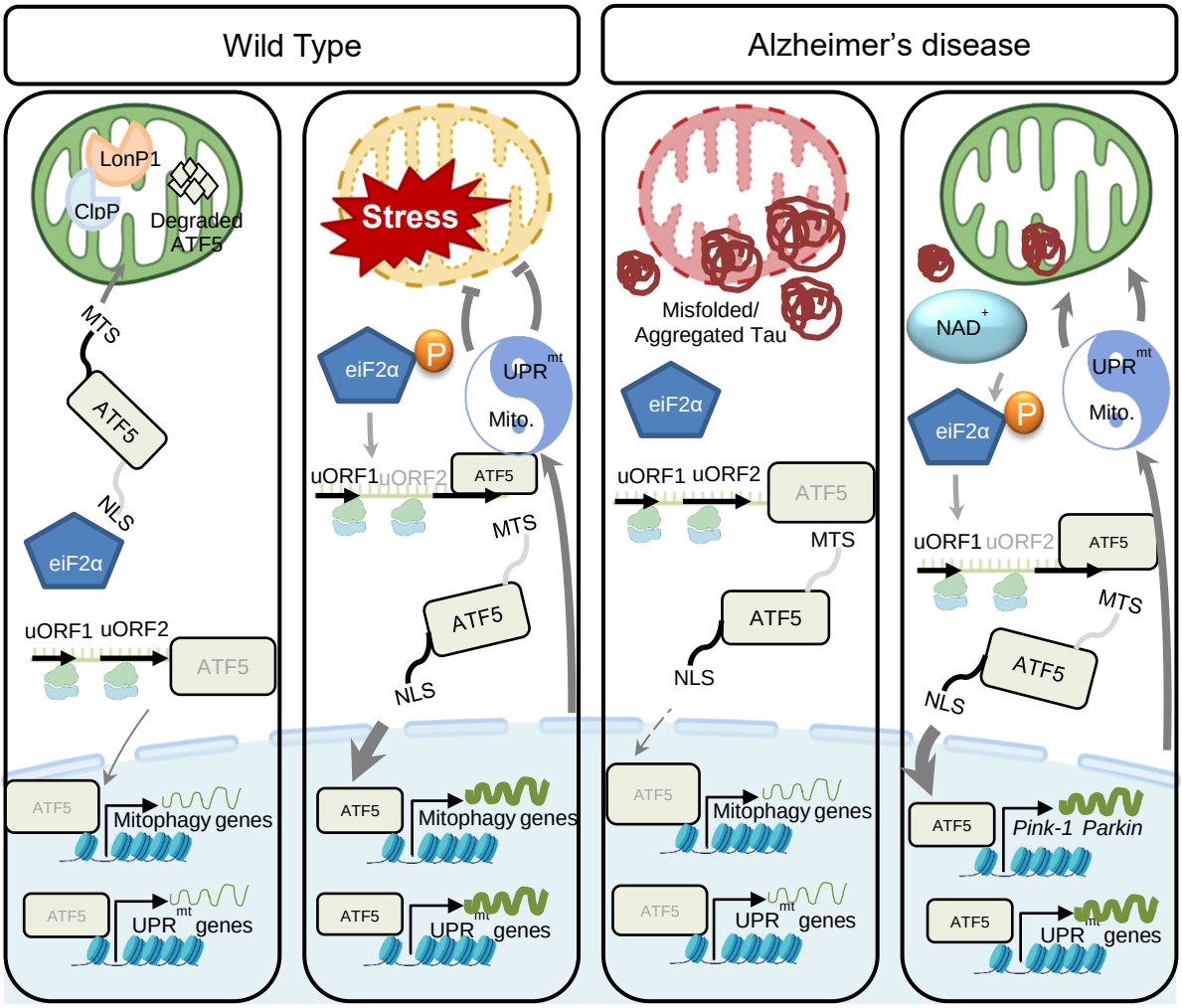

Figure 9. Description of graphical abstract (Based on literature review and experiments data): The transcription factor ATFS1 in *C. elegans* and ATF5 in mammals (ATFS1/ATF5) contains both a mitochondrial target sequence (MTS) and a nuclear localization signal (NLS) (Melber A and Haynes CM, 2018;Nargund AM et al., 2012). Under basal conditions, the mitochondrial transport system functions optimally. ATFS1/ATF5 preferentially enters the mitochondria and is degraded by mitochondrial proteases, including lon peptidase 1 (LonP1) and caseinolytic mitochondrial matrix peptidase proteolytic subunit (ClpP) (Alam S et al., 2020). Under stress and early aging conditions, mitochondrial entry systems are mildly compromised, making conditions favourable for ATFS1/ATF5 to enter the nucleus and trigger the array of gene transcription for UPR^{mt} and mitophagy. This integrated stress response (ISR) controls mRNA translation initiation. Mitochondrial stress activates the eiF2 kinases leading to eiF2α phosphorylation at Ser51. p-eiF2α leads to ternary complex depletion, decreasing cap-dependent translation and elevating the selective translation of uORF-regulated transcripts, such as ATF5. Transcription of UPR^{mt} and mitophagy-related genes will further improve mitochondria homeostasis (Deng P and Haynes CM, 2017). Under Tau-induced stress and late aging conditions, we did not observe eiF2α phosphorylation, and there is barely any ATF5 translocating to the nucleus. When an NAD⁺ precursor was used, eiF2α phosphorylation was increased leading to the ATF5 nuclear translocation effect. Transcription of UPR^{mt} and mitophagy-related genes will further ameliorate mitochondrial homeostasis (Figures made in BioRender software).

In our previous work, we tied Tau phosphorylation and amyloid pathology to mitochondrial dysfunction and defective mitophagy. These findings shed light on the underlying mechanisms of mitophagy and emphasize the importance of developing new therapeutic strategies to maintain mitochondrial homeostasis in AD and other neurodegenerative diseases. NAD⁺

precursors as a mitophagy inducer are beginning to be evaluated in neurodegeneration, especially AD, and other conditions (Fang EF et al,. 2019). Encouraged by the discovery, we went further to test what function NAD^+ precursors have in other mitochondrial maintenance pathways, namely UPR^{mt}, and what the linkages are between UPR^{mt} and mitophagy in AD.

In this project, we found that ATF5 expression and nuclear translocation is required for mitochondrial homeostasis in AD brain tissue. NAD^+ precursors promote ATF5 nuclear translocation in Tauopathy via eiF2α phosphorylation. The ATF5 nuclear translocation effect is negatively correlated with p-Tau expression, with the main underlying mechanisms being activating UPR^{mt} and mitophagy. There is crosstalk between UPR^{mt} and mitophagy in Tauopathy: (1). The NAD^+ precursor, nicotinamide mononucleotide (NMN), can balance UPR^{mt} and mitophagy in a dose-dependent way. (2). NMN can increase UPR^{mt} via the ATF5 translocation effect, which can further activate Pink-1/Parkin-dependent mitophagy. We also found mitochondrial homeostasis maintenance pathways (UPR^{mt} and mitophagy) are impaired in Tauopathy during the aging process.

3.2 Project 2

NAD^+ affects the landscape and biological relevance of alternative splicing events in tauopathies

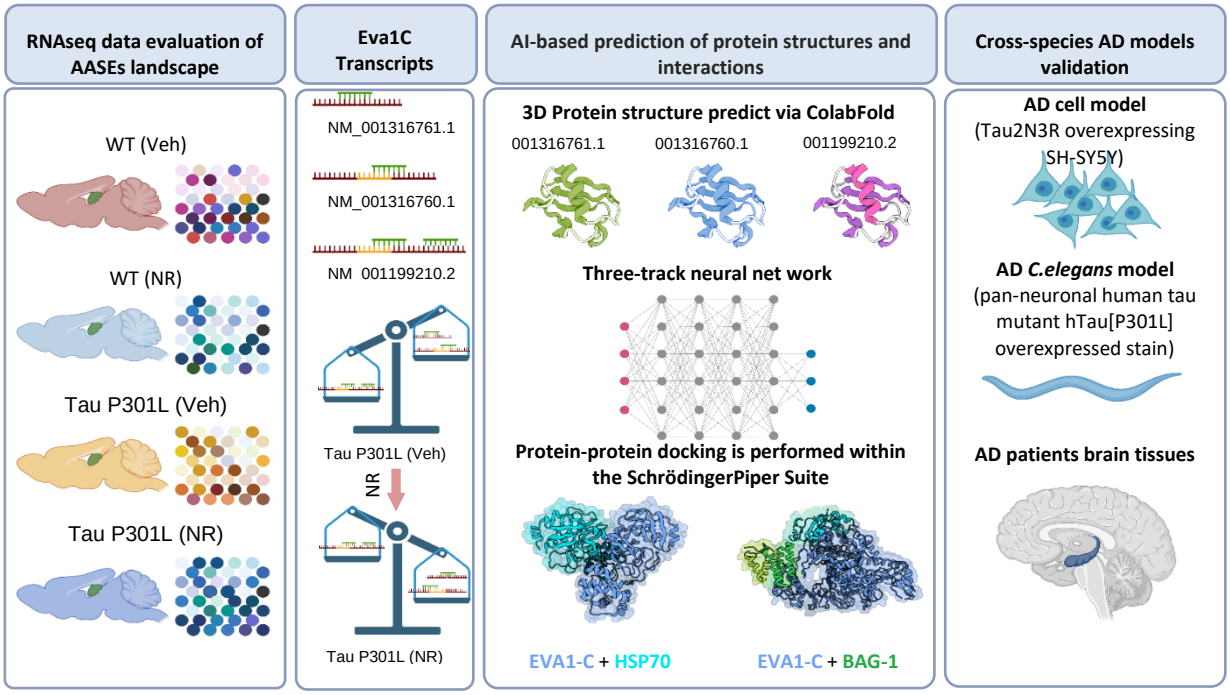

Figure 10. Description of graphical abstract: the computational pipeline combining transcriptomic analysis with AI and a validation platform to investigate the landscape and specific alternative splicing events, protein structure prediction, and the potential mechanism exploration via Protein-protein interaction (PPI) (Figures made in BioRender software).

Apart from studies that focus on the function of NAD^+ precursors on mitochondria homeostasis maintenance, disruptive RNA metabolism, especially mRNA splicing associated with AD (Buee L et al., 2000;Rockenstein EM et al., 1995), is emerging as a new hallmark of AD. There have been few investigations of dysregulation of RNA splicing in Tauopathies (Apicco DJ et al., 2019). However, a comprehensive mechanistic study of NAD^+ augmentation that shows that it regulates alternative splicing in Tauopathies is lacking. Therefore, we aimed to test the effects of NAD^+ precursors on the landscape and the biological relevance of alternative splicing events in Tauopathies.

In this project, we found RNA splicing is dysregulated in hTau.P301S transgenic mice. Alternative splicing, A5SS, and ES, in hTau.P301S transgenic mice disfavours transcripts encoding mitochondrial and synaptic proteins. Genes, the regulation of which is sensitive to NR treatment, are involved in alternative splicing processed in hTau.P301S brain. NR favours transcripts encoding proteins involved in axon development, oxygen metabolism, mitochondrion localization, and autophagy in Tauopathy. NR modifies A5SS, A3SS, and ES of genes covering multiple functions in hTau.P301S transgenic mice. NR increases the EVA1-C expression at protein level and induces long-length sequence expression with higher HSP70 binding efficacy in Tauopathy. Inhibition of eva1-c reverses the memory restoration, life span extension, and health span improvement delivered by NR in *C. elegans*. NR increases BAG co-chaperone 1 (bag-1) gene expression in an eva1-c-dependent manner. The workflow went from gene AASEs detection, protein structure definition, and interactive predictions, to cross-species validation.

3.3 Project 3

Amelioration of Alzheimer's disease pathology by mitophagy inducers identified via machine learning and a cross-species workflow

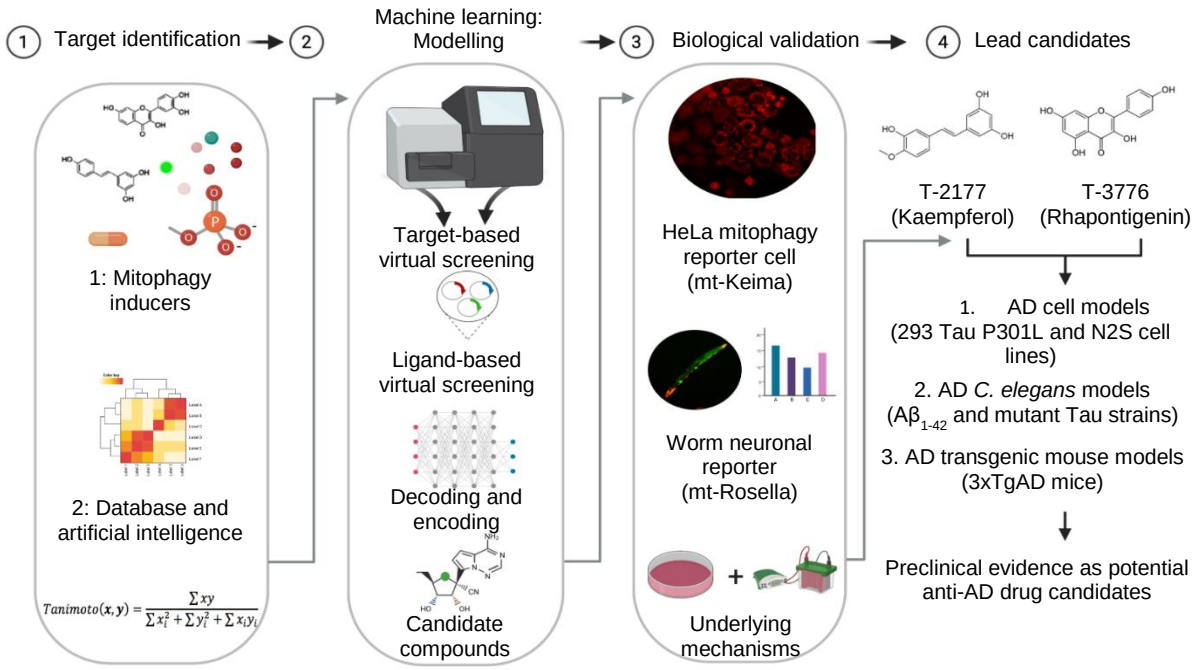

Figure 11. Description of graphical abstract: The screening workflow combining advanced AI and classical wet laboratory approaches to identify novel mitophagy modulators as potential drug candidates for AD treatment (Xie C et al., 2022).

Failed recognition and clearance of damaged mitochondria contributes to memory loss as well as Aβ and MAPT/Tau pathologies in AD, for which there is an unmet therapeutic need. Restoring mitophagy to eliminate damaged mitochondria could abrogate metabolic dysfunction, and neurodegeneration and may subsequently inhibit or slow down cognitive decline in AD models, which has been shown in our previous work (Fang EF et al., 2019). We, therefore, developed a high-throughput machine-learning approach combined with a cross-species screening platform to discover novel mitophagy-inducing compounds from a natural product library and further experimentally validated the potential candidates. Two lead compounds, kaempferol and rhapontigenin, induce neuronal mitophagy and reduce Aβ and MAPT/Tau pathologies in a PINK1-dependent manner in both *C. elegans* and mouse models of AD. Our combinational approach provides a fast, cost-effective, and highly accurate method for identification of potent mitophagy inducers to maintain brain health.

4. Discussions: project novelties, drawbacks, and future perspectives

In 1906, Alois Alzheimer first presented the signature case of AD and its pathological features. Over the past 116 years, studies on the pathological features, mechanisms, and drug treatments for AD have been intensively explored (Hardy J, 2006); however, the exact cause of AD is still without general consensus. As a result, various hypotheses regarding the causes of AD have been descripted including the amyloid, neurotransmitter, Tau propagation, mitochondrial cascade, neurovascular, exercise, inflammatory, and virus hypotheses, as well as others like the RNA splicing hypothesis (Liu PP et al., 2019). While each of the factors may provide partial contribution to the heterogeneous AD population, we focus on mitochondria. Previous studies from the Evandro Fei Fang laboratory show that accumulation of damaged mitochondria due to impaired NAD^+-mitophagy capacity plays a pivotal role in AD progression (Fang EF et al., 2017). Additionally, recent advancements and achievements in AI and deep generative models have demonstrated their utility in medical applications. In my doctoral training, I aimed to combine AI and wet lab techniques with novel mechanistic studies to propel the development of potential drug candidates against AD.

My study unveils NAD^+ mediates multiple mechanisms that could counteract AD (Project 1 & 2 & 3). Results from our previous work (Fang EF et al., 2019) and my doctoral projects highlight novel key roles of NAD^+ precursors in inhibiting AD. The first project identified that UPR^{mt}, another mitochondrial maintenance pathway, is activated by NAD^+ precursors via ATF5 nuclear translocation. Excessive UPR^{mt}, therefore, activated the downstream PINK-1/Parkin-dependent-mitophagy pathway. The NAD^+ precursor NMN regulates UPR^{mt} /mitophagy balance in a dose-dependent way. These results are in line with a previous study, which reported UPR^{mt} activation by NAD^+ precursors was able to reduce amyloid-β proteotoxicity (Sorrentino V et al., 2017). Our study provides previously unknown information around how NAD^+ precursors balance UPR^{mt}/mitophagy and the crosstalk between UPR^{mt} and mitophagy. The second project pointed out the role of NAD^+ on mRNA splicing in Tauopathy. NAD^+ switched mRNA isoform, such as EVA1-C, to possibly further mediate HSP70-autophagy. In project three, NAD^+ precursors that induce mitophagy can be used in machine learning algorithms to identify the structural features of NAD^+ that are relevant for drug development and screening. Apparently, NAD^+ precursors are deeply involved in the diverse and profound biological effects in AD. Despite these proving to be important, NAD^+ precursors as pivotal metabolite products may also target other AD hypotheses as well, such as the neurotransmitter, neurovascular, exercise, inflammatory, and virus hypotheses. Multiple control layers affected by NAD^+ precursors may collectively shape the final biological effects in AD. As an essential part of these regulatory networks, NAD^+ precursors-dependent AD inhibition should be considered in future studies.

AI provides a promising approach to mechanistic studies and drug discovery in AD (Projects 2 & 3). These two doctoral projects representatively showed the power of AI for resolving mechanisms behind complex biological effects (Project 2) and discovering drugs for AD (Project 3); the AI approach provides the skeleton of these two studies. In Project 2, it was the AI that enabled us to predict the protein structure and PPI for an unreported protein. In Project 3, it was the AI that led to the identification of new mitophagy inducers to ameliorate AD pathology. Obviously, along with the advantage of time- and money-saving, AI also enables uncovering of details that could otherwise be overlooked by regular approaches. However, these AI-predicted results still need solid validation in the wet lab. Given the different benefits of the newly developed AI approach and traditional wet-lab approaches, the machine learning plus cross-species wet-lab validation approach has been established for application in AD research including the mechanistic studies and drug discovery described in this doctoral thesis. Indeed, AI is a broad field, and we used limited approaches in my doctoral project. There are still many connections that need to be explored.

However, aside from the above mentioned implications, there are still questions that need to be answered. First, it should be determined whether NAD^+ precursors have any effects on other mitochondria maintenance pathways since we have seen that NAD^+ precursors induced UPR^{mt} and mitophagy in AD in Projects 2 and 3. Second, besides ATF5 which was shown in Project 1, how NAD^+ precursors regulate the other bZIP transcription factors, such as CHOP and ATF4, could be researched. The Basic Leucine Zipper Domain (bZIP) transcription factors have been reported to also be associated with the integrated stress response (ISR) resulting in transcriptional response to mitochondrial dysfunction in AD (Shpilka T and Haynes CM, 2018). Also, in Project 2 we found that NAD^+ can regulate alternative RNA splicing, and we do not yet know whether this RNA metabolism process can further influence mitochondria function in AD. As well, because of the low numbers of reference compounds available, that is, mitophagy inducers, in Project 3 we were not able to identify candidate compounds using machine learning approaches that need large numbers of reference compounds (e.g., between 100 to 1,000) (Mamoshina P et al., 2016;Stokes JM et al., 2020). Moreover, sex differences may affect NAD^+ precursors in AD, and this is an area that still needs to be addressed, with human longitudinal studies to provide insight. Taken together, much work remains to be done and the journey to fully understanding the mechanisms of NAD^+-dependent inhibition of AD and applying AI in the AD field has just begun.

To move forward toward a better understanding of how NAD^+ regulates a wide spectrum of biological processes in AD, further studies may potentially take the following perspectives into account. Mechanistically, further studies could help to explore the effects of NAD^+ in the other AD hypotheses. Conventionally, NAD^+ has emerged as an essential mitophagy inducer (Fang EF et al., 2019), which emphasizes its important role in the ¨mitochondrial cascade hypothesis¨. Our findings further provide evidence for the ¨mitochondrial cascade hypothesis¨ in AD (Kerr JS et al., 2017;Swerdlow RH et al., 2014) via NAD^+ precursors. We also found that NAD^+ can regulate RNA splicing processes in AD. It would be interesting to further investigate what the role of NAD^+ is in other AD hypotheses, which is ultimately beneficial for constructing a more comprehensive atlas of this NAD^+-dependent inhibition of AD. Technically, although AI-driven interventions can help to address emerging health challenges, AI is developing based on digitizing data from around the world. Global data sharing and management will greatly improve the AI approaches. With the development of AI as well as the wet lab, novel mechanisms of NAD^+-dependent inhibition of AD might be discovered.

In summary, my doctoral projects highlight the essential role of NAD^+ deficit in AD progression through reduced mitochondrial homeostasis and compromised RNA splicing, among other mechanisms. The AI approaches enable us to unveil new mechanisms and apply the new knowledge to drug discovery against AD.

5. Experimental contributions

Paper I

- Project design and coordination *
- Worm experiments *
- Cell experiments *
- Mice experiments
- Bio-information
- Publication figures edition *
- Manuscript written *

Paper II

- Project design and coordination *
- Worm experiments *
- Cell experiments *
- Mice experiments
- Human tissue experiments *
- Bio-information and AI
- Publication figures edition *
- Manuscript written *

Paper III

- Project design and coordination *
- Worm experiments *
- Cell experiments *
- Mice experiments
- Bio-information and AI
- Publication figures edition *
- Manuscript written *

The other authors also contributed to the corresponding projects; here I have just summarized my contributions to the projects which are marked with a *.

References

Abriata LA, Tamo GE, Dal Peraro M (2019), A further leap of improvement in tertiary structur e prediction in CASP13 prompts new routes for future assessments. Proteins 87:1100-111 2.

Alam S, Abdullah CS, Aishwarya R, Morshed M, Bhuiyan MS (2020), Molecular Perspectives of Mitochondrial Adaptations and Their Role in Cardiac Proteostasis. Front Physiol 11:10 54.

Andorfer C, Kress Y, Espinoza M, de Silva R, Tucker KL, Barde YA, Duff K, Davies P (2003), Hyperphosphorylation and aggregation of tau in mice expressing normal human tau isofor ms. J Neurochem 86:582-590.

Apicco DJ, Zhang C, Maziuk B, Jiang L, Ballance HI, Boudeau S, Ung C, Li H, et al. (2019), Dysregulation of RNA Splicing in Tauopathies. Cell Rep 29:4377-4388 e4374.

Avale ME, Rodriguez-Martin T, Gallo JM (2013), Trans-splicing correction of tau isoform imb alance in a mouse model of tau mis-splicing. Hum Mol Genet 22:2603-2611.

Bai B, Hales CM, Chen PC, Gozal Y, Dammer EB, Fritz JJ, Wang X, Xia Q, et al. (2013), U1 small nuclear ribonucleoprotein complex and RNA splicing alterations in Alzheimer's disea se. Proc Natl Acad Sci U S A 110:16562-16567.

Ballard C, Gauthier S, Corbett A, Brayne C, Aarsland D, Jones E (2011), Alzheimer's diseas e. Lancet 377:1019-1031.

Barbosa-Morais NL, Irimia M, Pan Q, Xiong HY, Gueroussov S, Lee LJ, Slobodeniuc V, Kutt er C, et al. (2012), The evolutionary landscape of alternative splicing in vertebrate specie s. Science 338:1587-1593.

Beck JS, Mufson EJ, Counts SE (2016), Evidence for Mitochondrial UPR Gene Activation in Familial and Sporadic Alzheimer's Disease. Curr Alzheimer Res 13:610-614.

Bi C, Bi S, Li B (2019), Processing of Mutant beta-Amyloid Precursor Protein and the Clinico pathological Features of Familial Alzheimer's Disease. Aging Dis 10:383-403.

Buee L, Bussiere T, Buee-Scherrer V, Delacourte A, Hof PR (2000), Tau protein isoforms, ph osphorylation and role in neurodegenerative disorders. Brain Res Brain Res Rev 33:95-13 0.

Canter RG, Penney J, Tsai LH (2016), The road to restoring neural circuits for the treatment of Alzheimer's disease. Nature 539:187-196.

CBINSIGHTS (2017), Healthcare Remains The Hottest AI Category For Deals. https://wwwc binsightscom/research/artificial-intelligence-healthcare-startups-investors/.

Cummings J (2018), Lessons Learned from Alzheimer Disease: Clinical Trials with Negative Outcomes. Clin Transl Sci 11:147-152.

Cummings JL, Morstorf T, Zhong K (2014), Alzheimer's disease drug-development pipeline: f ew candidates, frequent failures. Alzheimers Res Ther 6:37.

Deng P, Haynes CM (2017), Mitochondrial dysfunction in cancer: Potential roles of ATF5 and the mitochondrial UPR. Semin Cancer Biol 47:43-49.

Dong Y, Brewer GJ (2019), Global Metabolic Shifts in Age and Alzheimer's Disease Mouse B rains Pivot at NAD+/NADH Redox Sites. J Alzheimers Dis 71:119-140.

Eisenstein M (2021), Artificial intelligence powers protein-folding predictions. Nature https://w ww.nature.com/articles/d41586-021-03499-y.

Fang EF, Hou Y, Palikaras K, Adriaanse BA, Kerr JS, Yang B, Lautrup S, Hasan-Olive MM, e t al. (2019), Mitophagy inhibits amyloid-beta and tau pathology and reverses cognitive defi cits in models of Alzheimer's disease. Nat Neurosci 22:401-412.

Fenoglio C, Scarpini E, Serpente M, Galimberti D (2018), Role of Genetics and Epigenetics i n the Pathogenesis of Alzheimer's Disease and Frontotemporal Dementia. J Alzheimers D is 62:913-932.

Freudenberg-Hua Y, Li W, Davies P (2018), The Role of Genetics in Advancing Precision Me dicine for Alzheimer's Disease-A Narrative Review. Front Med (Lausanne) 5:108.

Gatz M, Reynolds CA, Fratiglioni L, Johansson B, Mortimer JA, Berg S, Fiske A, Pedersen N L (2006), Role of genes and environments for explaining Alzheimer disease. Arch Gen Ps ychiatry 63:168-174.
GitHub (2023), MMseqs2. https://githubcom/soedinglab/mmseqs2.
Hardy J (2006), A hundred years of Alzheimer's disease research. Neuron 52:3-13.
Hay M, Thomas DW, Craighead JL, Economides C, Rosenthal J (2014), Clinical developmen t success rates for investigational drugs. Nat Biotechnol 32:40-51.
Hinrich AJ, Jodelka FM, Chang JL, Brutman D, Bruno AM, Briggs CA, James BD, Stutzmann GE, et al. (2016), Therapeutic correction of ApoER2 splicing in Alzheimer's disease mice using antisense oligonucleotides. Embo Mol Med 8:328-345.
Hou Y, Lautrup S, Cordonnier S, Wang Y, Croteau DL, Zavala E, Zhang Y, Moritoh K, et al. (2018), NAD(+) supplementation normalizes key Alzheimer's features and DNA damage r esponses in a new AD mouse model with introduced DNA repair deficiency. Proc Natl Aca d Sci U S A 115:E1876-E1885.
James G, Foster SR, Key B, Beverdam A (2013), The expression pattern of EVA1C, a novel Slit receptor, is consistent with an axon guidance role in the mouse nervous system. PLoS One 8:e74115.
Kerr JS, Adriaanse BA, Greig NH, Mattson MP, Cader MZ, Bohr VA, Fang EF (2017), Mitoph agy and Alzheimer's Disease: Cellular and Molecular Mechanisms. Trends Neurosci 40:15 1-166.
Kornblihtt AR, Schor IE, Allo M, Dujardin G, Petrillo E, Munoz MJ (2013), Alternative splicing: a pivotal step between eukaryotic transcription and translation. Nat Rev Mol Cell Biol 14:1 53-165.
Kuhlman B, Bradley P (2019), Advances in protein structure prediction and design. Nat Rev Mol Cell Biol 20:681-697.
Lautrup S, Sinclair DA, Mattson MP, Fang EF (2019), NAD(+) in Brain Aging and Neurodege nerative Disorders. Cell Metab 30:630-655.
Lisowiec J, Magner D, Kierzek E, Lenartowicz E, Kierzek R (2015), Structural determinants f or alternative splicing regulation of the MAPT pre-mRNA. RNA Biol 12:330-342.
Liu F, Gong CX (2008), Tau exon 10 alternative splicing and tauopathies. Mol Neurodegener 3:8.
Liu PP, Xie Y, Meng XY, Kang JS (2019), History and progress of hypotheses and clinical tri als for Alzheimer's disease. Signal Transduct Target Ther 4:29.
Lou G, Palikaras K, Lautrup S, Scheibye-Knudsen M, Tavernarakis N, Fang EF (2020), Mitop hagy and Neuroprotection. Trends Mol Med 26:8-20.
Mamoshina P, Vieira A, Putin E, Zhavoronkov A (2016), Applications of Deep Learning in Bio medicine. Mol Pharm 13:1445-1454.
Melber A, Haynes CM (2018), UPR(mt) regulation and output: a stress response mediated b y mitochondrial-nuclear communication. Cell Res 28:281-295.
Mirdita M, Schutze K, Moriwaki Y, Heo L, Ovchinnikov S, Steinegger M (2022), ColabFold: m aking protein folding accessible to all. Nat Methods 19:679-682.
Nargund AM, Pellegrino MW, Fiorese CJ, Baker BM, Haynes CM (2012), Mitochondrial impor t efficiency of ATFS-1 regulates mitochondrial UPR activation. Science 337:587-590.
Ng A, Tam WW, Zhang MW, Ho CS, Husain SF, McIntyre RS, Ho RC (2018), IL-1beta, IL-6, TNF- alpha and CRP in Elderly Patients with Depression or Alzheimer's disease: Systema tic Review and Meta-Analysis. Sci Rep 8:12050.
Ng TKS, Ho CSH, Tam WWS, Kua EH, Ho RC (2019), Decreased Serum Brain-Derived Neu rotrophic Factor (BDNF) Levels in Patients with Alzheimer's Disease (AD): A Systematic R eview and Meta-Analysis. Int J Mol Sci 20.
Organization WH (2022), Dementia. https://wwwwhoint/news-room/fact-sheets/detail/dementi a.
Palam LR, Baird TD, Wek RC (2011), Phosphorylation of eIF2 facilitates ribosomal bypass of an inhibitory upstream ORF to enhance CHOP translation. J Biol Chem 286:10939-1094 9.

Palop JJ, Chin J, Mucke L (2006), A network dysfunction perspective on neurodegenerative diseases. Nature 443:768-773.
Pan Q, Shai O, Lee LJ, Frey BJ, Blencowe BJ (2008), Deep surveying of alternative splicing complexity in the human transcriptome by high-throughput sequencing. Nat Genet 40:1413-1415.
Park SA, Ahn SI, Gallo JM (2016), Tau mis-splicing in the pathogenesis of neurodegenerative disorders. Bmb Rep 49:405-413.
Peacey E, Rodriguez L, Liu Y, Wolfe MS (2012), Targeting a pre-mRNA structure with bipartite antisense molecules modulates tau alternative splicing. Nucleic Acids Res 40:9836-9849.
Raj T, Li YI, Wong G, Humphrey J, Wang M, Ramdhani S, Wang YC, Ng B, et al. (2018), Integrative transcriptome analyses of the aging brain implicate altered splicing in Alzheimer's disease susceptibility. Nat Genet 50:1584-1592.
Rajkomar A, Dean J, Kohane I (2019), Machine Learning in Medicine. N Engl J Med 380:1347-1358.
Rockenstein EM, McConlogue L, Tan H, Power M, Masliah E, Mucke L (1995), Levels and alternative splicing of amyloid beta protein precursor (APP) transcripts in brains of APP transgenic mice and humans with Alzheimer's disease. J Biol Chem 270:28257-28267.
Rugarli EI, Langer T (2012), Mitochondrial quality control: a matter of life and death for neurons. EMBO J 31:1336-1349.
Schoch KM, DeVos SL, Miller RL, Chun SJ, Norrbom M, Wozniak DF, Dawson HN, Bennett CF, et al. (2016), Increased 4R-Tau Induces Pathological Changes in a Human-Tau Mouse Model. Neuron 90:941-947.
Sevigny J, Chiao P, Bussiere T, Weinreb PH, Williams L, Maier M, Dunstan R, Salloway S, et al. (2016), The antibody aducanumab reduces Abeta plaques in Alzheimer's disease. Nature 537:50-56.
Shpilka T, Haynes CM (2018), The mitochondrial UPR: mechanisms, physiological functions and implications in ageing. Nat Rev Mol Cell Biol 19:109-120.
Sorrentino V, Romani M, Mouchiroud L, Beck JS, Zhang H, D'Amico D, Moullan N, Potenza F, et al. (2017), Enhancing mitochondrial proteostasis reduces amyloid-beta proteotoxicity. Nature 552:187-193.
Steinegger M, Soding J (2017), MMseqs2 enables sensitive protein sequence searching for the analysis of massive data sets. Nat Biotechnol 35:1026-1028.
Stokes JM, Yang K, Swanson K, Jin W, Cubillos-Ruiz A, Donghia NM, MacNair CR, French S, et al. (2020), A Deep Learning Approach to Antibiotic Discovery. Cell 180:688-702 e613.
Swerdlow RH, Burns JM, Khan SM (2014), The Alzheimer's disease mitochondrial cascade hypothesis: progress and perspectives. Biochim Biophys Acta 1842:1219-1231.
Swerdlow RH, Khan SM (2004), A "mitochondrial cascade hypothesis" for sporadic Alzheimer's disease. Med Hypotheses 63:8-20.
Stimulus package. Nat Med 24:247.
Teske BF, Fusakio ME, Zhou D, Shan J, McClintick JN, Kilberg MS, Wek RC (2013), CHOP induces activating transcription factor 5 (ATF5) to trigger apoptosis in response to perturbations in protein homeostasis. Mol Biol Cell 24:2477-2490.
Trabzuni D, Wray S, Vandrovcova J, Ramasamy A, Walker R, Smith C, Luk C, Gibbs JR, et al. (2012), MAPT expression and splicing is differentially regulated by brain region: relation to genotype and implication for tauopathies. Hum Mol Genet 21:4094-4103.
van Dyck CH, Swanson CJ, Aisen P, Bateman RJ, Chen C, Gee M, Kanekiyo M, Li D, et al. (2023), Lecanemab in Early Alzheimer's Disease. N Engl J Med 388:9-21.
Walter P, Ron D (2011), The unfolded protein response: from stress pathway to homeostatic regulation. Science 334:1081-1086.
Wang ET, Sandberg R, Luo S, Khrebtukova I, Zhang L, Mayr C, Kingsmore SF, Schroth GP, et al. (2008), Alternative isoform regulation in human tissue transcriptomes. Nature 456:470-476.

Watatani Y, Ichikawa K, Nakanishi N, Fujimoto M, Takeda H, Kimura N, Hirose H, Takahashi S, et al. (2008), Stress-induced translation of ATF5 mRNA is regulated by the 5'-untranslated region. J Biol Chem 283:2543-2553.
Webb S (2018), Deep learning for biology. Nature 554:555-557.
Wen B, Zeng WF, Liao Y, Shi Z, Savage SR, Jiang W, Zhang B (2020), Deep Learning in Proteomics. Proteomics 20:e1900335.
Wobst HJ, Denk F, Oliver PL, Livieratos A, Taylor TN, Knudsen MH, Bengoa-Vergniory N, Bannerman D, et al. (2017), Increased 4R tau expression and behavioural changes in a novel MAPT-N296H genomic mouse model of tauopathy. Sci Rep 7:43198.
Wright CJ, Smith CWJ, Jiggins CD (2022), Alternative splicing as a source of phenotypic diversity. Nat Rev Genet 23:697-710.
Xie C, Zhuang XX, Niu Z, Ai R, Lautrup S, Zheng S, Jiang Y, Han R, et al. (2022), Amelioration of Alzheimer's disease pathology by mitophagy inducers identified via machine learning and a cross-species workflow. Nat Biomed Eng 6:76-93.
Xie T, Grossman JC (2018), Crystal Graph Convolutional Neural Networks for an Accurate and Interpretable Prediction of Material Properties. Phys Rev Lett 120:145301.
Zitnik M, Agrawal M, Leskovec J (2018), Modeling polypharmacy side effects with graph convolutional networks. Bioinformatics 34:i457-i466.
Zitnik M, Nguyen F, Wang B, Leskovec J, Goldenberg A, Hoffman MM (2019), Machine Learning for Integrating Data in Biology and Medicine: Principles, Practice, and Opportunities. Inf Fusion 50:71-91.
Zwierzyna M, Davies M, Hingorani AD, Hunter J (2018), Clinical trial design and dissemination: comprehensive analysis of clinicaltrials.gov and PubMed data since 2005. BMJ 361:k2130.

Appendix

Paper I, II and III

I

II

III

ARTICLES
https://doi.org/10.1038/s41551-021-00819-5

nature biomedical engineering

Check for updates

OPEN

Amelioration of Alzheimer's disease pathology by mitophagy inducers identified via machine learning and a cross-species workflow

Chenglong Xie[1,2,3,4,5,21], Xu-Xu Zhuang[6,21], Zhangming Niu[7,8,21], Ruixue Ai[2,21], Sofie Lautrup[2], Shuangjia Zheng[9], Yinghui Jiang[8], Ruiyu Han[2], Tanima Sen Gupta[2], Shuqin Cao[2], Maria Jose Lagartos-Donate[2], Cui-Zan Cai[6], Li-Ming Xie[6], Domenica Caponio[2], Wen-Wen Wang[10], Tomas Schmauck-Medina[2], Jianying Zhang[2], He-ling Wang[2], Guofeng Lou[2], Xianglu Xiao[8], Wenhua Zheng[11], Konstantinos Palikaras[12], Guang Yang[13,14], Kim A. Caldwell[15,16], Guy A. Caldwell[15,16], Han-Ming Shen[17,18], Hilde Nilsen[2,19], Jia-Hong Lu[6]✉ and Evandro F. Fang[2,19,20]✉

A reduced removal of dysfunctional mitochondria is common to aging and age-related neurodegenerative pathologies such as Alzheimer's disease (AD). Strategies for treating such impaired mitophagy would benefit from the identification of mitophagy modulators. Here we report the combined use of unsupervised machine learning (involving vector representations of molecular structures, pharmacophore fingerprinting and conformer fingerprinting) and a cross-species approach for the screening and experimental validation of new mitophagy-inducing compounds. From a library of naturally occurring compounds, the workflow allowed us to identify 18 small molecules, and among them two potent mitophagy inducers (Kaempferol and Rhapontigenin). In nematode and rodent models of AD, we show that both mitophagy inducers increased the survival and functionality of glutamatergic and cholinergic neurons, abrogated amyloid-β and tau pathologies, and improved the animals' memory. Our findings suggest the existence of a conserved mechanism of memory loss across the AD models, this mechanism being mediated by defective mitophagy. The computational–experimental screening and validation workflow might help uncover potent mitophagy modulators that stimulate neuronal health and brain homeostasis.

Accumulation of damaged mitochondria in the brain is a hallmark of brain aging and related neurodegenerative diseases, including Alzheimer's disease (AD)[1–5]. As the most common form of dementia, AD affects around 50 million individuals worldwide without an available cure[6]. Accumulation of amyloid β (Aβ) and neurofibrillary tangles (majorly p-Tau aggregates) are the disease-defining pathological features of AD. However, clinical drug developments targeting Aβ and Tau have struggled to produce positive results[7], highlighting the urgent need for discovery and development of novel therapeutic interventions. Mitochondria are fundamental subcellular organelles that generate adenosine triphosphate (ATP), which is essential for the excitability and survival of neurons. In addition, they are at the centre of signalling pathways regulating Ca^{2+}, oxidative stress, developmental and synaptic plasticity, as well as neuronal fate determination[8]. Mitochondria constantly experience endogenous (for example, DNA damage and oxidative toxicants) and exogenous (for example, environmental exposure) stresses, which cause structural and/or functional damage to these essential organelles[9]. In a normal physiological environment, damaged mitochondria are efficiently cleared by mitophagy, a subtype of selective macroautophagy (hereafter referred to as autophagy)[10]. However, in elderly individuals or people with common neurodegenerative diseases such as AD, Parkinson's disease, Amyotrophic lateral sclerosis and Huntington's disease in which accumulation of defective mitochondria is a common feature, and possibly a driving force of memory impairment and dementia, autophagic processes may be disrupted[1,5,10]. Emerging evidence highlights that mitophagy impairment mediates the accrual of

[1]Department of Neurology, The First Affiliated Hospital of Wenzhou Medical University, Wenzhou, China. [2]Department of Clinical Molecular Biology, University of Oslo and Akershus University Hospital, Lørenskog, Norway. [3]Institute of Aging, Wenzhou Medical University, Wenzhou, China. [4]Oujiang Laboratory, Wenzhou, Zhejiang, China. [5]Key Laboratory of Alzheimer's Disease of Zhejiang Province, Wenzhou, China. [6]State Key Laboratory of Quality Research in Chinese Medicine, Institute of Chinese Medical Sciences, University of Macau, Macau, China. [7]Aladdin Healthcare Technologies Ltd., London, UK. [8]MindRank AI Ltd., Hangzhou, Zhejiang, China. [9]School of Data and Computer Science, Sun Yat-sen University, Guangzhou, China. [10]Center of Traditional Chinese Medicine, The Second Affiliated Hospital and Yuying Children's Hospital of Wenzhou Medical University, Wenzhou, China. [11]Faculty of Health Sciences, University of Macau, Taipa, Macau, China. [12]Department of Physiology, School of Medicine, National and Kapodistrian University of Athens, Athens, Greece. [13]Cardiovascular Research Centre, Royal Brompton Hospital, London, UK. [14]National Heart and Lung Institute, Imperial College London, London, UK. [15]Department of Biological Sciences, The University of Alabama, Tuscaloosa, AL, USA. [16]Departments of Neurology and Neurobiology, Center for Neurodegeneration and Experimental Therapeutics, Nathan Shock Center for Research on the Basic Biology of Aging, University of Alabama at Birmingham School of Medicine, Birmingham, AL, USA. [17]Department of Physiology, Yong Loo Lin School of Medicine, National University of Singapore, Singapore, Singapore. [18]Faculty of Health Sciences, University of Macau, Macau, China. [19]The Norwegian Centre on Healthy Ageing (NO-Age), Oslo, Norway. [20]Department of Geriatrics, The First Affiliated Hospital, Zhengzhou University, Zhengzhou, China. [21]These authors contributed equally: Chenglong Xie, Xu-Xu Zhuang, Zhangming Niu and Ruixue Ai. ✉e-mail: jiahonglu@um.edu.mo; e.f.fang@medisin.uio.no

dysfunctional mitochondria in the AD brain[11]. Indeed, the basal levels of mitophagy are less than 50% in AD patient brain tissue compared with healthy controls[11]. Moreover, several regulators of autophagy and mitophagy pathways, such as phosphatidylinositol-binding clathrin assembly protein (PICALM)[12], presenilin 1 (PS1)[13], phosphatase and tensin homologue (PTEN)-induced kinase1 (PINK1), TANK-binding kinase 1 (TBK1), Unc-51-like kinase-1 (ULK1)[11] and Bcl-2 associated athanogene 3 (BAG-3)[14] are lowly expressed or impaired in AD patients. Genetic and/or pharmacologic restoration of mitophagy inhibits disease progression in preclinical AD models[11,15]. Given the continued failures in anti-AD drug development, approaches targeting the broader aspects of AD pathologies, such as defective mitophagy, may hold a therapeutic potential.

Bioavailable neuronal mitophagy inducers are scarce. Thus, we set out to develop a screening workflow combining advanced artificial intelligence (AI) and classical wet laboratory approaches to identify novel mitophagy modulators as potential drug candidates for AD treatment. The application of traditional chemistry or high-throughput approaches for drug discovery is time-consuming and also carry a high failure rate[16]. Machine learning is emerging as a powerful, fast, reliable and cost-effective approach to drug development, which can accelerate discovery and decision making for predefined questions with precise data[17–20]. Machine learning has been used in pharmaceutical development, bioactivity prediction, de novo molecular design, synthesis prediction and biological image analysis, among other applications[19,21,22]. It is a popular tool in drug discovery when using a large arsenal of compounds; however, the limitation of broad application is the necessity for a sizeable number of labelled data points to ensure model generalizability and avoid overfitting[19,22]. In view of the scarcity of known mitophagy inducers, an alternative machine learning approach is the use of 'biological fingerprints', which are representations of chemical structures originally designed to assist in chemical database substructure searching[23]. Here we outline the development of an AI-aided high-throughput screen workflow that combines AI, mammalian cells, nematodes and mice to create an approach for identifying potent mitophagy modulators.

Results

An AI-aided model for screening of mitophagy inducers. A combinational molecular representation approach, including Mol2vec, pharmacophore fingerprint and 3D conformers fingerprint, was used for modelling (Fig. 1a,b). We first compiled a dataset that was large-scale, structurally diverse and task related. The ChEMBL[24] and ZINC natural product databases[25] were filtered using procedures outlined elsewhere[26], producing a dataset with 19.9 million compounds (that is, the pre-training dataset). This pre-training dataset was used to train the multi-representations model, which translated a molecule into an information-enriched structure vector in an unsupervised manner, without the need for numerous annotated data. The model followed a natural language processing strategy[26], wherein molecules were considered as sentences and substructures as words. By iteratively learning the relative position of each substructure in a molecule, the model could finally capture the global structural information of each substructure in the chemical space. New molecules could be described by summing the substructure vectors retrieved from a pre-trained Mol2vec model. The obtained compound feature vectors could then be used to calculate the structural distance of any two compounds in the projected chemical space. Further, to fill in the blanks of 2D pharmacophore and 3D conformer information, the pharmacophore and shape fingerprinting techniques were introduced to augment the representation of molecules (Fig. 1a). A total of 14 known mitophagy inducers were used as reference (Supplementary Table 1).

After model development and augmentation, we subsequently applied it to identify potential mitophagy inducers from a natural product library (named Macau Library), which contained 3,274 natural compounds isolated mainly from a series of traditional Chinese medicinal plants that have been used to treat neurodegenerative diseases and other diseases[27,28]. Similarity scores for each compound against each of the 14 known mitophagy inducers were determined, compounds were ranked on the basis of their structural (Mol2vec score), pharmacophore fingerprint and shape distance (3D conformers fingerprint) against the known inducers (Supplementary Table 1). We identified a total of 18 molecules in the Macau Library that were most similar to the existing (known) mitophagy inducers, with a threshold of 0.75. We set the threshold to 0.75 on the basis of published works[29,30] and our in-house justification of the workload for wet-lab validation. Detailed information of the 18 in silico-selected molecules is documented (Supplementary Fig. 1 and Table 2). We further performed chemical similarity analysis of the top 18 molecules: while 1D similarities are lower than 40% between any two compounds, there are some compounds with high scores in 2D (for example, 91% for T2174 and T0579) and 3D (for example, 71% for T3S1068 and T2177) similarity analyses (Additional Supplementary Table). More details on the AI procedures can be found in Methods.

In vitro and in vivo validation of mitophagy candidates. The 18 AI-selected molecules were then subjected to experimental verification in both human cells (HeLa cells) and the soil-dwelling nematode *Caenorhabditis elegans*. HeLa cells co-expressing the E3 ubiquitin ligase Parkin and the mitochondria-targeted form of monomeric Keima fluorescent reporter (mt-Keima)[31] were used. Keima is a coral-derived, lysosomal degradation-resistant, dual-excitation ratio-metric fluorescent protein that is pH-sensitive; it shows shorter-wavelength excitation (green) in healthy mitochondria normally with neutral pH, while it turns to longer-wavelength excitation (red) in damaged mitochondria undergoing acidic lysosomal degradation (Fig. 2a)[31]. These features of the mt-Keima reporter allow qualitative assessment of mitophagic flux in both cells and mouse models[31–33]. To ensure high translational potential, we started with a series of doses covering 0.1, 1.0 and 10 μM, with 10 μM as the cut-off threshold. In a first-pass study of the 18 AI-selected compounds, 8 molecules (Quercetin (Macau Library ID: T-2174), Quercetin dihydrate (T-6630), Tacrolimus (T-2144), Ascomycin (T-2481), Isorhamnetin (T-2836), Pinostilbene (T-3755), Kaempferol (Kaem, T-2177) and Rhapontigenin (Rhap, T-3776)) induced mitophagy at 10 μM; the remaining 10 molecules did not induce detectable mitophagy up to 10 μM and were excluded from the study at this

Fig. 1 | The use of combined machine learning strategies to identify novel mitophagy inducers. a, The workflow for model pre-training: (i) Molecules within the pre-training dataset were transferred into SMILES sequences, molecular interaction features and 3D conformers fingerprint in the data preparation stage; (ii) Three encoders (for 1D, 2D and 3D representations) were then designed to embed the input data, and these representational embeddings were aggregated into the encoder model of the multi-representation; (iii) The multi-representational embeddings were then passed to the representation decoder to pre-train the multi-representation molecule model. 'F' and 'G' stand for 'Functional encoder' and 'Generator' respectively. **b**, The workflow for the virtual screening process: (i) The virtual screening library contained 3,274 molecules from a traditional Chinese medicine dataset, named Macau Library; (ii) The 1D, 2D and 3D molecular representations for each compound were generated on the basis of the pre-trained molecule representation models; (iii) The representations were then aggregated and clustered, and a hyper-space filter was applied to the representations to filter out outliers; (iv) The similarity scores for each compound were calculated to generate the top N candidate compounds.

point (Fig. 2b,c and Supplementary Fig. 2a,c,d). It was noted that Quercetin dihydrate and Quercetin exhibited very similar results, likely due to their structural and functional similarities, thus Quercetin dihydrate was eliminated from the study at this point. To confirm whether the 7 remaining molecules trigger mitophagy in a dose-dependent manner, we administered higher doses of each compound (20, 50 and 100 μM) to the same HeLa mt-Keima cells. We were unable to observe any dose-dependent mitophagic upregulation in response to Quercetin, Tacrolimus and Ascomycin supplementation past 10 μM. However, Isorhamnetin, Pinostilbene, Kaem and Rhap administration triggered mitophagy in a dose-dependent manner (Fig. 2b,c). Therefore collectively, among the 18 AI-selected molecules, 8 showed an ability to stimulate mitophagy in vitro, with 4 of them inducing mitophagy in a dose-dependent manner.

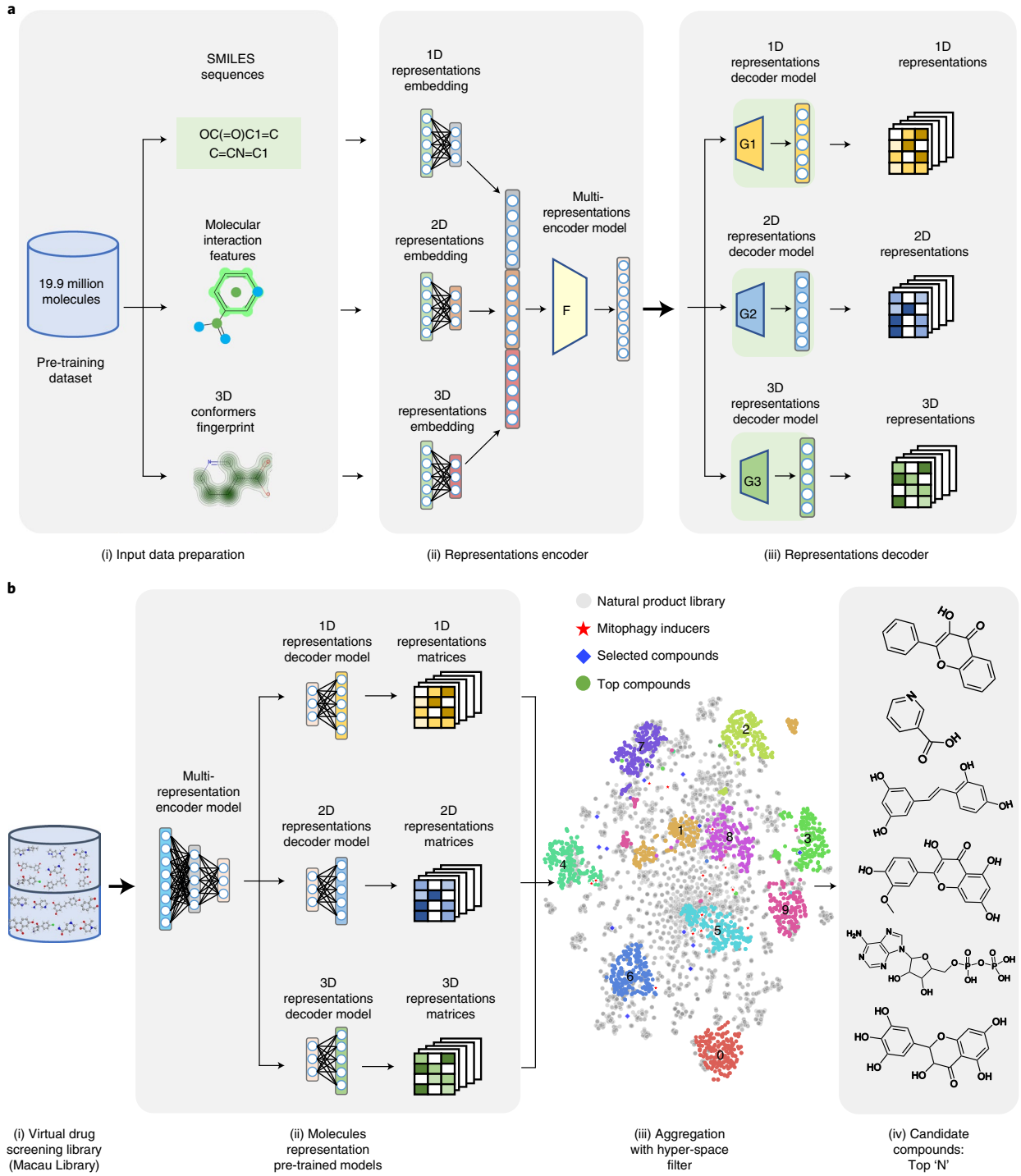

To investigate whether the aforementioned mitophagy inducers could mediate neuronal mitophagy in vivo, we used transgenic nematodes with pan-neuronal expression of mitochondria-targeted Rosella (mt-Rosella, a dual colour-emission biosensor). The mt-Rosella biosensor comprises a green fluorescent protein (GFP) variant sensitive to the acidic environment of the lysosomal lumen, which is fused to the fast-maturing pH-insensitive DsRed. Mitophagy index is assessed by monitoring the GFP/DsRed ratio, with reduced values signifying mitophagy induction[11] (Supplementary Fig. 4a). We supplemented 0.2 mM and 1.0 mM of each mitophagy-inducing compound to mt-Rosella-expressing animals from eggs onwards and analysed mitophagy levels in 1-day-old adults. Rotenone, a mitochondrial complex I inhibitor, was used as positive control to trigger mitophagy. Quercetin (at 1 mM), Kaem (at 0.2 mM) and Rhap (at both 0.2 mM and 1 mM) were able to induce neuronal mitophagy in worms, while Tacrolimus, Ascomycin, Isorhamnetin and Pinostilbene were negative for neuronal mitophagy induction (Fig. 2d and Supplementary Fig. 4b). In summary, among the 18 AI-selected candidates, 3 – Quercetin, Kaem and Rhap – stimulated mitophagy in both human cells and *C. elegans* neurons.

In addition to using HeLa mt-Keima cells and mt-Rosella-expressing animals to quantify mitophagy by Kaem and Rhap, we further validated the robust mitophagy induction capacities of Kaem and Rhap. Firstly, immunoblot data indicate that both Kaem and Rhap dose-independently (20, 40 and 80 μM for 24 h) reduced the expression of the mitochondrial outer membrane protein MFN2 and mitochondrial inner membrane protein Tim23 in both YFP-Parkin-expressing HeLa cells and Mito-GFP- and mCherry-Parkin-expressing HeLa cells (Fig. 3a–h). Secondly, Kaem and Rhap (20 μM, 24 h) enhanced co-localization of mitochondria (Mito-GFP) with the LAMP1-antibody-labelled lysosome, indicating increased lysosomal degradation of mitochondria via mitophagy (Fig. 3i,j). Thirdly, Kaem and Rhap at 0.2 mM stimulated neuronal mitophagy in *C. elegans* as evidenced by increased LGG-1/Atg-8 to DCT-1/NIX co-localization, and increased mitochondria in the lysosomes as shown by reduced GFP/DsRed (Fig. 3k,l). Fourthly, data from electron microscopy (EM) showed that Kaem and Rhap induced mitophagosome-like events in HeLa cells (Fig. 3m and Extended Data Fig. 1a), as well as in hippocampal brain tissues from wild-type (WT) and AD-like 3xTg mice (Fig. 3n and Extended Data Fig. 1b; details on the mouse studies are shown below). To note, lower doses of either Kaem or Rhap were unable to induce mitophagy in HeLa mt-Keima cells (2.5 and 5 μM, 24 h; Supplementary Fig. 2b) or the nematode neurons (0.01, 0.05, 0.1 mM; Fig. 3k,l). Collectively, these data unequivocally point to robust mitophagy stimulation capacity of both Kaem and Rhap in cell culture system, nematodes and mice.

Additionally, we compared our combinational AI model (Fig. 1a) with other machine learning approaches (1D, 2D or 3D) to determine their accuracy in identifying mitophagy inducers. We selected the top 5 scored compounds from each of the independent approaches for validation in HeLa mt-Keima cells. Compounds in the 1D- and 3D-selected lists, at 10 μM, were unable to induce detectable mitophagy in HeLa mt-Keima cells (Supplementary Fig. 3). All top 5 compounds recommended by the 2D approach were in the top 18 list selected by our combinational AI model: 3 compounds (T0879, T2812, T2144 at 10 μM) were unable to induce mitophagy, the remaining 2 (Ascomycin (T2481) and Pinostilbene (T3755)) were able to induce mitophagy in cells, but were unable to induce neuronal mitophagy in nematodes (Fig. 2). Additionally, we reviewed and listed the hit rate for experimental high-throughput screening and other AI drug discovery projects for a comprehensive comparison study. Overall, the hit rate of our model (in vitro validation) is higher than the experimental high-throughput screening (44% vs 0.14%) and substantially outperforms other machine learning, quantitative structure–activity relationship (QSAR) and computer-aided approaches (Supplementary Table 3). Collectively, these in silico, in vitro and in vivo data indicate that our combinational AI approach is more accurate in predicting molecules with mitophagy induction and neuroprotection activities both in vitro and in vivo, than the individual 1D, 2D or 3D approaches.

Kaem and Rhap inhibit memory loss in Aβ_{1-42} *C. elegans*. Recent evidence underlies the likely causative role of compromised mitophagy in AD pathogenesis[11,34]. Thus, we examined the impact of the newly identified mitophagy stimulators on memory improvement in both Aβ and Tau nematode models. To investigate whether pharmacological upregulation of mitophagy restores memory deficits, we evaluated learned behaviour in transgenic nematodes, whereby they have pan-neuronal expression of human Aβ_{1-42} (hAβ_{1-42})[35], via aversive olfactory learning chemotaxis assay (where a negative value correlates with chemotaxis-related memory)[11]. hAβ_{1-42} nematodes treated with Kaem or Rhap displayed improved learned behavioural performance, while Quercetin did not appear to restore associative memory deficits (Fig. 4a and Supplementary Fig. 5a). Thus, among the 18 AI-selected candidates, Kaem and Rhap demonstrated the capacity to stimulate mitophagy in both human cells and *C. elegans* neurons, and improved an established measure of simple associative memory in these transgenic hAβ_{1-42} worms.

We then investigated the underlying molecular mechanisms to identify how Kaem and Rhap improve memory, focusing on mitophagy/autophagy-related pathways. While none of the compounds had any effect on the mRNA levels of *pink-1*, *pdr-1* (orthologue of human *PARK2/Parkin)*, *bec-1* (orthologue of human *BECN1/Beclin-1*), *vps-34* and *skn-1* (a stress response gene also involved in mitophagy[36]), they both increased transcriptional levels of *dct-1* and *sqst-1* (*SQSTM1* gene in humans) in transgenic hAβ_{1-42} worms (Fig. 4b). To consider translational and post-translational modifications, and due to limitations in available antibodies for *C. elegans* studies, we extended our mechanistic studies to human HeLa cells and scrutinized the mitophagy-inducing capacity of the molecules by checking them against a list of mitophagy/autophagy proteins that are known to be critical in mitochondrial metabolism or that are altered in AD[11]. In most cases, Kaem increased levels of PINK1, Parkin, Beclin-1, LC3B-II and AMBRA1, and reduced p62 in a dose-dependent manner; a very similar pattern was seen in the Rhap-treated human cells (Extended Data Fig. 2). Moreover, Rhap treatment increased the phosphorylation levels of the autophagy

Fig. 2 | Evaluation of mitophagy stimulation capacity of the AI top-scored molecules in vitro (mt-Keima) and in animals (mt-Rosella). a, A schematic representation showing mechanisms of how the mt-Keima protein can be used as a mitophagy reporter. For confocal microscopy, dual-excitation ratio imaging was carried out with two sequential excitation lasers (458 nm and 561 nm). Representative confocal images are of HeLa cells expressing mt-Keima treated with vehicle (DMSO) or Carbonyl cyanide m-chlorophenyl hydrazone (CCCP) (15 μM, 3 h). **b**,**c**, Effects of Quercetin, Tacrolimus, Ascomycin, Isorhamnetin, Pinostilbene, Kaem and Rhap (from 0.1 μM to 100 μM, 24 h) on mitophagy induction. **d**, Effects of in vitro-positive mitophagy inducers on the induction of neuronal mitophagy in worms expressing mt-Rosella reporter. Rotenone (5 μM and 10 μM, 4 h) was used as positive control. Data were pooled from 2 biological replicates (total $n = 20$–35 nematodes per group), with results shown as mean ± s.e.m. Two-way ANOVA followed by Tukey's multiple comparisons test; NS, no significance; $^{*}P < 0.05$, $^{**}P < 0.01$, $^{***}P < 0.001$. A set of representative images of cellular positive (related to Fig. 2b,c) and negative mitophagy inducers (with quantifications) is included in Supplementary Fig. 2. Mechanisms of the mt-Rosella sensor as well as a set of representative images (related to Fig. 2d) are shown in Supplementary Fig. 4.

factor ULK1 at Ser555, which is essential for mitophagy initiation[37] (Extended Data Fig. 2). In addition, to increase the expression of multiple mitophagy-related proteins, Kaem or Rhap supplementation resulted in reduced protein levels of Mitofusin-2 (MFN2) and elevated the ratio of p-DRP1 (Ser616)/DRP1 (Extended Data Fig. 2). These findings suggest that mitochondrial fission is

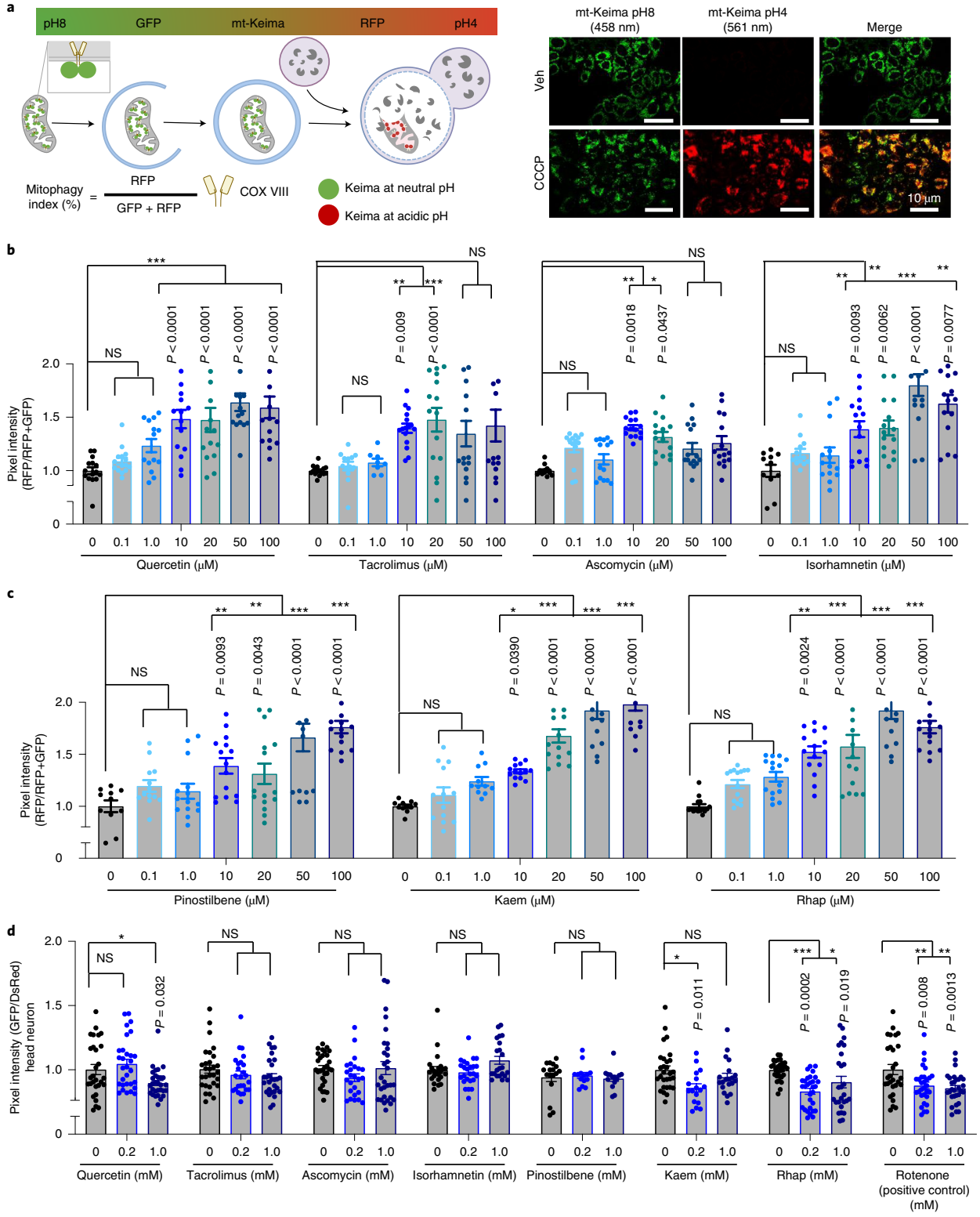

triggered upon Kaem and Rhap treatment, leading to the generation of smaller and fragmented organelles that can be easily engulfed by autophagosomes[38]. To further investigate whether Kaem- and Rhap-dependent memory improvement in the $hA\beta_{1-42}$ worms is due to mitophagy induction (rather than any off-target effects), we introduced loss-of-function mutations (*pink-1*, *pdr-1*, *dct-1*) or knocked down selected genes (*sqst-1*, *bec-1*, via RNAi) on the basis of PCR and immunoblot data. Depletion of *pdr-1* and *dct-1* abrogated Kaem-dependent memory improvement in the $hA\beta_{1-42}$ worms, whereas Rhap-induced memory improvement was dependent on the *pink-1* pathway (Fig. 4c(left) and Supplementary Fig. 5f). Collectively, Kaem and Rhap appear to trigger mitophagy through the upregulation and/or activation of specific mitophagy components and via the modulation of mitochondrial dynamics.

To uncover the mechanisms of memory retention mediated by Kaem and Rhap at a cellular level, we asked whether these compounds act through the glutamatergic or cholinergic neurons, which are both impaired in AD[39]. Overexpression of $hA\beta_{1-42}$ specifically in the glutamatergic neurons in worms ($hA\beta_{1-42}^{Glu}$) has been shown to induce neurodegeneration[36,40]. We examined whether Kaem and Rhap could alleviate neurodegeneration and improve associative learning in these $hA\beta_{1-42}^{Glu}$ worms. Both Kaem and Rhap administered at 0.2 mM improved memory deficits observed in $hA\beta_{1-42}^{Glu}$; $hApoE4^{Glu}$ worms, as evidenced by the restoration of the chemotactic index to a level even surpassing that of $hA\beta_{1-42}^{Glu}$; $hApoE-3^{Glu}$ control animals (Fig. 4c(right)). As previously described[35,36], five specific glutamatergic neurons in the tail region of *C. elegans* hermaphrodites (LUA (R), LUA (L), PVR, PLM (R) and PLM (L)) (Supplementary Fig. 5g(left) and Video) afford a means of robust quantification of neurodegeneration in vivo. These anatomically isolated neurons facilitate unparalleled accuracy in scoring loss of neuronal processes and cell bodies at the single-neuron level, as they reproducibly degenerate in response to constitutive hAβ expression, and this occurs progressively with age[40,41]. Kaem inhibited glutamatergic neurodegeneration in adult Day 3 $hA\beta_{1-42}^{Glu}$; $hApoE4^{Glu}$ worms (Fig. 4d(left)). There was a trend towards glutamatergic neuroprotection by Rhap as a small percentage of worms reached 5 neurons, with fewer worms in the 1–2 neurons groups (Fig. 4d(left); $P=0.0714$). Indeed, in addition to inhibiting neuronal loss, administration of either Kaem or Rhap improved neuronal health as evidenced by increased GFP intensity (for example, in PVR neurons, Fig. 4d(right)) and also improved neuronal morphology (Supplementary Fig. 5g). Impairment of the cholinergic system plays an important role in the pathophysiology of AD, and cholinergic therapies serve as a standard pharmacological approach in AD[42]. To investigate the effect of Kaem or Rhap on synaptic transmission of acetylcholine, pan-neuronal $hA\beta_{1-42}$ worms were exposed to an acetylcholinesterase inhibitor, aldicarb, and the time-course of paralyzing effects was scored[43]. While Kaem had no detectable effect on aldicarb-induced paralysis, Rhap greatly improved resistance of the $hA\beta_{1-42}$ worms to aldicarb-induced paralysis, indicating possible cholinergic protection by Rhap (Fig. 4e and Supplementary Fig. 6a,b). The aldicarb-hypersensitive strain VC223 and the aldicarb-resistant NM204 were used as controls (Supplementary Fig. 6g).

We further asked whether Kaem and Rhap could reduce $hA\beta_{1-42}$ production by using N2a mouse neuroblastoma cells expressing the Swedish K595N and M596L mutations in Amyloid-beta precursor protein/APP (APPSwe). Both Kaem and Rhap reduced full-length APP, CTF-α (non-amyloidogenic pathway via α-secretase) and CTF-β (amyloidogenic pathway via β-secretase) in these mouse neuroblastoma cells in a dose-dependent manner, suggesting a possibility of reduction in amounts of CTF-β available to be cleaved to $hA\beta_{1-42}$ via γ-secretase (Extended Data Fig. 1c–f, and further verified in mouse brain detailed below). In summary, Kaem and Rhap improve the function or survival of glutamatergic and cholinergic neurons and reduce $hA\beta_{1-42}$ production.

Kaem and Rhap improve memory by reducing Tau pathologies. In addition to alleviating Aβ pathology, we asked whether Kaem and Rhap protect against tauopathies by using the well-characterized CK12 (hTau4R1N(P301L)[44], pan-neuronal expression) and BR5270 (with pro-aggregant hTau(F3Δ280) tau fragment[45], pan-neuronal expression) strains. While the hTau(P301L) worms are known to have impaired memory[11], both Kaem and Rhap improved memory in this Tau strain (Fig. 5a,b). Tacrolimus, Ascomycin, Isorhamnetin or Pinostilbene did not show associative memory improvement to the hTau(P301L) worms at 1 mM, but Tacrolimus and Isorhamnetin improved associative memory at 0.2 mM (Supplementary Fig. 5b–e).

Kaem increased mRNA levels of *dct-1*, *pink-1*, *pdr-1* and *bec-1*, while having no effect on *sqst-1*, *vps-34* or *skn-1* in the hTau(P301L) worms (Fig. 5c). Rhap treatment resulted in increased mRNA levels of *pink-1*, *sqst-1*, *vps-34* and *skn-1* without having an effect on *dct-1*, *pdr-1* or *bec-1* (Fig. 5d). Kaem-induced memory improvement in hTau(P301L) worms was in a *pink-1*-, *dct-1*- and *bec-1*-dependent manner; Rhap-induced memory improvement in hTau(P301L) worms was in a *dct-1*-dependent manner (Fig. 5e). Furthermore, both Kaem and Rhap greatly improved the resistance of the hTau(P301L) worms against aldicarb-induced paralysis, indicating possible cholinergic protection (Supplementary Fig. 6c,d). Further investigation into the effects of Kaem and Rhap in hTau(F3Δ280) worms showed that both Kaem and Rhap improved the memory capacity in these worms[11] (Extended Data Fig. 3a). Mechanistically, although Kaem and Rhap had no or only minor changes in *pink-1* and *pdr-1* mRNA levels (Extended Data Fig. 3b), Kaem- and Rhap-induced memory improvement in the hTau(F3Δ280) worms was in a *pink-1*- and *pdr-1*-, but not *dct-1*-dependent manner (Extended Data Fig. 3c,d). Furthermore, both Kaem and Rhap greatly improved the resistance

Fig. 3 | Kaem and Rhap induce mitophagy in cells, *C. elegans* neurons and mouse brain. a, Effects of Kaem and Rhap on the protein levels of mitofusin2 (MFN2), YFP-Parkin and Tim23 in HeLa cells stably overexpressing YFP-Parkin. **b**–**d**, Semi-quantification of **a** ($n=3$ biological replicates). **e**, Effects of Kaem and Rhap on the protein levels of MFN2, YFP-Parkin and Tim23 in HeLa cells stably overexpressing Mito-GFP and mCherry-Parkin. **f**–**h**, Semi-quantification of **e** ($n=3$ biological replicates). For **a** and **e**, CCCP was used as positive control. **i**, Images showing co-localization of mitochondria (Mito-GFP) and lysosomes (LAMP1 antibody) under Kaem and Rhap (20 uM, 24 h) administration in GFP-mito-mCherry-Parkin HeLa cells. White arrows indicate mitophagy events. **j**, Quantification of **i** with data from 3 biological repeats with around 5–7 images per biological repeat. **k**, Transgenic nematodes were treated with Kaem and Rhap (both with 0.01, 0.05, 0.1 and 0.2 mM), with mitophagy events calculated by the co-localization between the autophagic marker DsRed::LGG-1 and the mitophagy receptor DCT-1::GFP in neurons. $n=18$–20 neurons from 2 biological repeats. While the left panel shows one representative set of images, quantitative data are shown in the right panel. **l**, Effects of Kaem and Rhap on the induction of neuronal mitophagy in worms with mt-Rosella reporter. Data were pooled from 2 biological replicates (total $n=20$–35 nematodes per group), with the results shown as mean ± s.e.m. **m**,**n**, Data of quantified electron microscopic images showing effects of Kaem and Rhap on mitochondrial morphology and mitophagy-like events in mt-Keima HeLa cells (**m**) (20 μM for 24 h) and mouse hippocampal brain tissues (**n**) (100 mg kg^{-1} d^{-1} via oral gavage from 12 months for 7 consecutive days; $n=3$ mice per group, with 4 random hippocampal neuronal images per mouse). Representative images are shown in Extended Data Fig. 1a,b. All quantitative data are shown as mean ± s.e.m. One-way ANOVA followed by Šidák's multiple comparisons test; $^{**}P$ 0.01, $^{***}P$ 0.001. Original unprocessed western blot gel data are in Source Data Fig. 4.

of the hTau(F3Δ280) worms against aldicarb-induced paralysis, indicating possible cholinergic protection (Supplementary Fig. 6e,f). In addition to memory benefit, Kaem and Rhap also improved healthspan measured as an enhancement of pharyngeal pumping in the hTau(P301L) worms (Extended Data Fig. 3f), although no statistical significance in improved mobility was observed (Extended Data Fig. 3g).

We then examined whether Kaem or Rhap supplementation exerts a beneficial effect by reducing pathological Tau aggregates. Phosphorylations of designated Tau sites are essential for Tau aggregation. Indeed, Kaem and Rhap diminished Tau phosphorylation levels at multiple sites such as Thr181, Ser202/Thr205 and Thr231 in mammalian HEK293-Tau P301L cells (Fig. 5f). Considering that Tau fibrils mediate transmission of neurofibrillary tangles

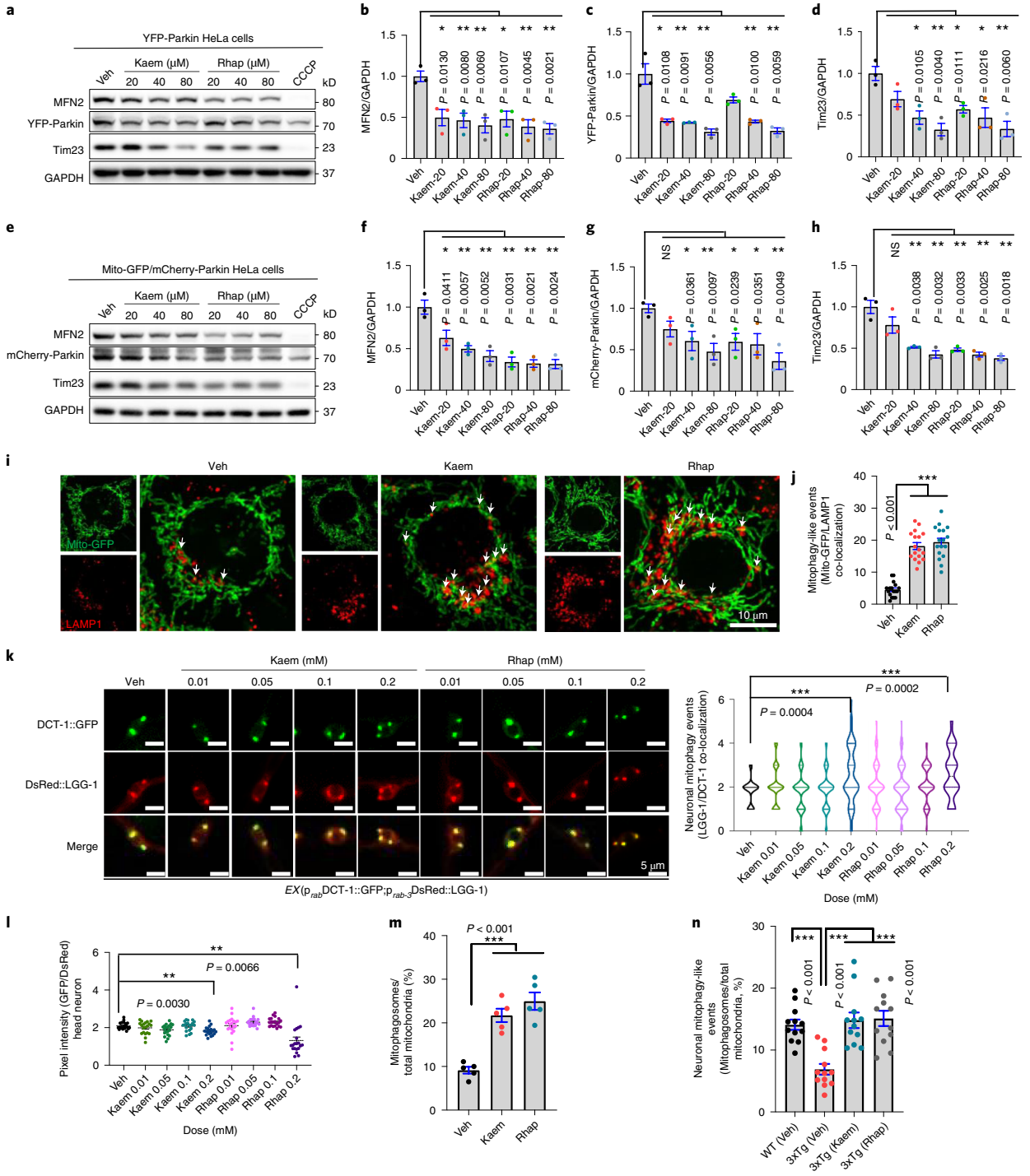

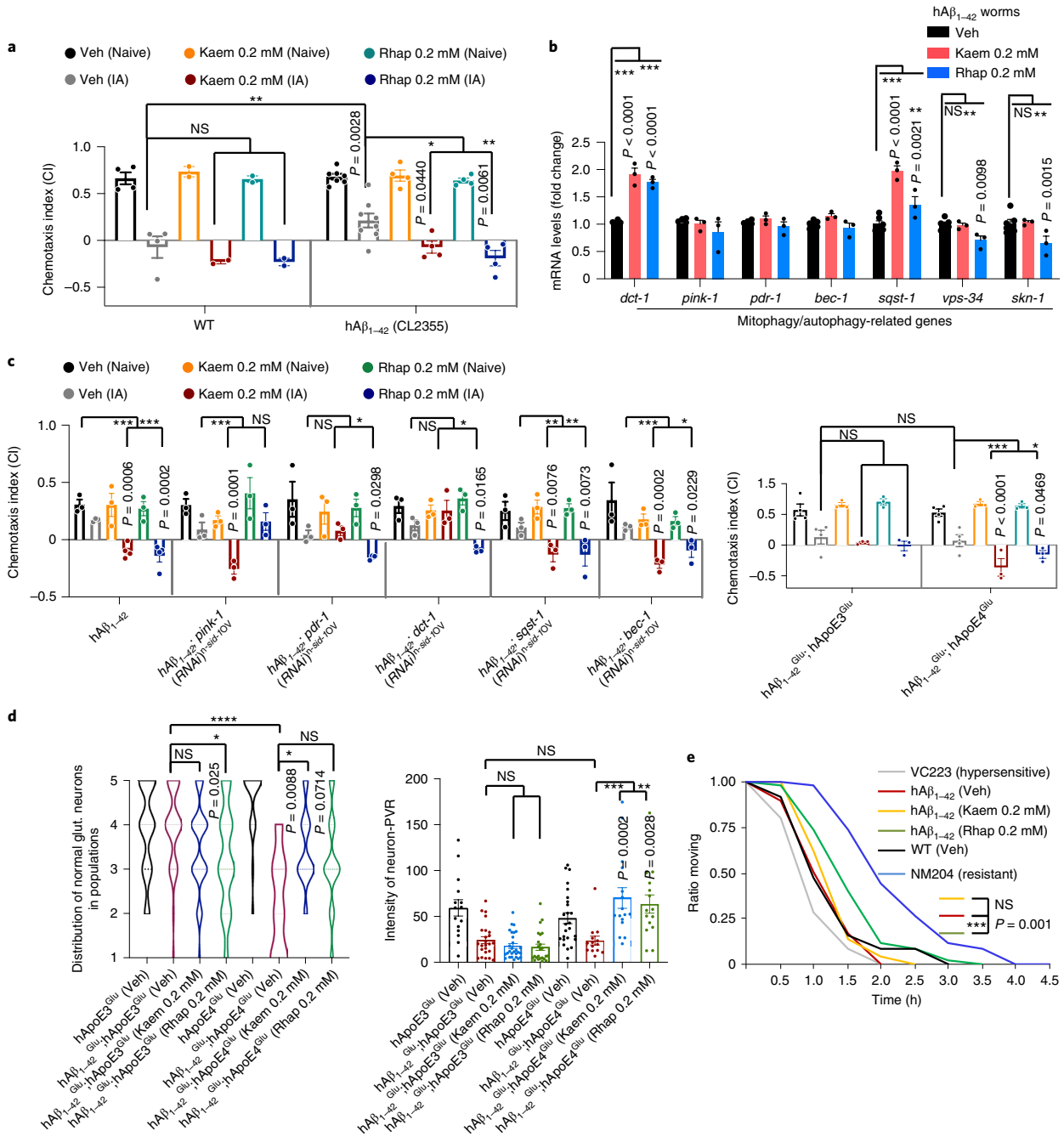

Fig. 4 | Mitophagy stimulation restores memory deficit and abrogates pathologies in AD-like Aβ worms, and regulates cellular Aβ production in mouse neuroblastoma cells. a, Effects of Kaem and Rhap on associative memory in adult day 1 WT and $hA\beta_{1-42}$ (CL2355) worms. Data were pooled from at least 4 biological replicates. **b**, Effects of Kaem and Rhap on designated gene expression in day 1 adult worms. Data are from 1 representative biological repeat (3 technical repeats) from a total of 3 biological replicates. **c**, Left: effects of *pink-1*, *pdr-1*, *dct-1*, *sqst-1* and *bec-1* on Kaem- and Rhap-dependent memory improvement in the $hA\beta_{1-42}$ (CL2355) worms. Right: effects of Kaem and Rhap on associative memory in adult day 1 $hA\beta_{1-42}{}^{Glu}$;$hApoE3^{Glu}$ (UA353) and $hA\beta_{1-42}{}^{Glu}$;$hApoE4^{Glu}$ (UA355) worms. 'Glu' denotes that either $hA\beta_{1-42}$ or hApoEs were expressed only in the glutamatergic neurons. Data were pooled from at least 4 biological replicates. **d**, Effect of Kaem or Rhap on glutamatergic neuroprotection in the $hA\beta_{1-42}{}^{Glu}$;ApoE4 worms and other worm strains. Left: distribution of worms with different numbers of 5 designated tail neurons ($n = 80$–100 from 2 biological replicates). Right: the fluorescent intensity of PVR neurons ($n = 15$ from 2 biological replicates). **e**, Effects of Kaem and Rhap on acetylcholinesterase inhibitor aldicarb-induced paralysis. VC223 (a strain hypersensitive to aldicarb-induced paralysis) and NM204 (a strain resistant to aldicarb-induced paralysis) were used as controls. All quantitative data are shown as mean ± s.e.m. Two-way ANOVA followed by Tukey's multiple comparisons test (**a**–**e**); NS, no significance; $^*P < 0.05$, $^{**}P < 0.01$, $^{***}P < 0.001$. Effects of Kaem and Rhap on Aβ generation in mouse neuroblastoma cells are shown in Extended Data Fig. 1c–f. Additional data related to **e** are in Supplementary Fig. 6.

(a possible hypothesis of age-dependent spreading of Tau pathology in AD patients[46–48]), we asked whether Kaem and Rhap could alleviate 'seeded Tau'-induced Tau pathology. To explore this angle, we employed a high-content microscopy-based assay using HEK293 cells stably expressing the 0N4R isoform of human Tau, bearing the P301S mutation with a C-terminal Venus fluorescent protein tag[49]. It has been reported that ectopic addition of recombinant heparin-assembled P301S Tau (Tau seeds with no Venus tag) promoted the generation of intracellular bright Tau foci from a disperse distribution, indicating extracellular inclusion of pathological Tau seed-induced intracellular Tau aggregation[49] (Extended Data Fig. 3h,i). While Rhap had no statistically significant effect on the reduction of Tau seed-induced intracellular Tau aggregation from a dose range between 3.125 µM to 25 µM, Kaem dramatically reduced intracellular Tau aggregation in a dose-dependent manner, with 25 µM showing over 80% reduction (Fig. 5g). Moreover, we assessed whether Kaem or Rhap affects the degradation of Tau aggregates; however, both did not reduce the numbers of Tau foci at up to 25 µM for 24 h (Extended Data Fig. 3j,k). Kaem-induced decrease of seed-induced Tau aggregation was not due to cell death, as we did not detect any side effect on cell viability even up to 50 µM of Kaem for 24 h (Extended Data Fig. 3l). To conclude, Kaem and Rhap improve memory in Tau-expressing nematodes, as well as antagonize multiple p-Tau sites and/or Tau aggregation.

Effects of combined treatment and other factors on the hTau worms. We further investigated whether a combination of Kaem and Rhap had any additive or synergistic effect to combat memory loss in the AD worms. In the transgenic hTau(P301L) worms, a dose of either 0.2 mM Kaem or Rhap was able to improve memory. When administered together, we did not observe any additive or synergistic benefit in memory improvement (Fig. 5h). Further, since population studies indicate that individuals with AD have a shorter lifespan than healthy controls[50,51], we examined whether enhanced memory (Fig. 5a,b) and healthspan (Extended Data Fig. 3f) also correlated with an increased lifespan. While the hTau(P301L) worms had a shorter lifespan compared with the WT N2 worms (Extended Data Fig. 1g), Kaem (0.2 mM) or Rhap (0.2 mM) administration extended the WT N2 nematode average lifespan by 24.5% and 32.5%, and hTau(P301L) nematode lifespan by 5.8% and 17.4%, respectively (Extended Data Fig. 1h,i and Supplementary Table 4). No synergistic effects in lifespan extension were noticed when combining Kaem (0.2 mM) and Rhap (0.2 mM) in either hTau(P301L) worms or N2 control animals (Extended Data Fig. 1h,i and Supplementary Table 4).

The changes in the biological effects (for example, chemotaxis-based memory performance) on the worms as induced by the tested compounds may also be attributable to alternate mechanisms, such as microbial metabolism (for example, dependence on the live food *Escherichia coli* (OP50) to metabolize the metabolic precursors to more bioactive ones) or changes in eating pattern due to a dietary restriction mimetic[52,53]. We performed additional analyses looking into the potential effect of microbial metabolism and eating habits on memory. Since both Kaem and Rhap were supplemented in the hTau(F3Δ280)-expressing worms fed dead OP50, memory improvements were not likely to have been affected by microbial metabolism (Extended Data Fig. 3e). Likewise, exposing the worms to Kaem and Rhap likely did not reduce short-term food intake, but rather increased it; this may be due to the increased pharyngeal pumping observed with drug treatment (Extended Data Fig. 3f), thus excluding any indirect effects arising from dietary restriction.

Kaem and Rhap forestall pathologies in the 3xTg AD mice. Encouraged by the in silico, in vitro and nematode data, we wondered whether the anti-AD effects would translate to rodents. Therefore, we decided to test this using classical 3xTg AD mice bearing both Aβ and Tau pathologies[54]. We treated the 3xTg AD mice from 12.5 months with both compounds (100 mg kg^{-1} d^{-1}) via oral gavage for 2 consecutive months and subsequently assessed memory and pathologies. In line with the results obtained using the *C. elegans* AD models, both Kaem and Rhap greatly improved spatial learning and memory in the Morris water maze test in terms of latency to the platform from days 1 to 6 (Fig. 6a,b), and in-platform frequency for the probe trial at day 7 (Fig. 6c). Similarly, Kaem and Rhap improved spatial memory in 3xTg AD mice tested using the Y maze spontaneous alternation performance test (Fig. 6d). Both molecules enhanced visual recognition memory when tested with a novel object recognition (NOR) test (Fig. 6e) compared with WT mice (Veh).

We further asked whether improved cognition in the 3xTg AD mice was due to the alleviation of Aβ and Tau pathologies. Indeed, Kaem and Rhap comparably reduced insoluble $Aβ_{1–40}$ (Fig. 6f), as well as soluble and insoluble levels of $Aβ_{1–42}$ (Fig. 6g) in the hippocampal tissue of the 3xTg AD mice; consistently, an anti-$Aβ_{1–16}$ (clone 6E10)-antibody probed immune-fluorescent evaluation showed reduced Aβ load per region of interest (ROI) (Fig. 6h,i). Mechanistically, Kaem and Rhap reduced Aβ production as supported by decreased levels of FL-APP, CTF-β and CTF-α in the hippocampal tissue of the 3xTg AD mice (Fig. 6j–l and Extended Data Fig. 4a), mirroring the results seen in the N2a mouse neuroblastoma cells (Extended Data Fig. 1c–f). While microglia use energy (generated mainly by mitochondria) to clear Aβ plaques, we recently reported over 60% reduction of microglial mitophagy in the hippocampal tissue from an APP/PS1 mouse model, which could be a cause for the reduced phagocytosis of Aβ plaques in AD; mitophagy stimulation increased microglial phagocytosis in the APP/PS1 mice[11,55]. Accordingly, we evaluated whether Kaem and Rhap influenced microglial activity and whether the increased microglial activity could enhance the removal of Aβ plaques. Indeed, Kaem and Rhap increased phagocytic engulfment of Aβ plaques by microglia from 35.4% (microglia with Aβ/total microglia, Veh Group) to 83.0% and 72.6%, respectively (Extended Data Fig. 4d,e). Kaem and Rhap also increased microglial populations in the AD hippocampus from 8.3 (number per region of interest) to 15.7 and 13.7, respectively (Extended Data Fig. 4d). Further, Kaem- and Rhap-treated mice displayed a decreased number and length of microglial processes, highlighting their shift towards a phagocytic state (Extended Data Fig. 4d).

Fig. 5 | Mitophagy stimulation restores memory deficit in the AD-like hTau(P301L) *C. elegans* model and inhibits Tau pathologies in mammalian cells. **a**,**b**, Effects of Kaem (**a**) or Rhap (**b**) on associative memory in transgenic nematodes expressing hTau(P301L) (CK12). Data were pooled from 4 biological replicates. **c**,**d**, Effects of Kaem (**c**) and Rhap (**d**) on designated gene expressions in adult day 1 worms. Data are from a total of 3 biological replicates. **e**, Effects of *pink-1*, *pdr-1*, *dct-1*, *sqst-1* and *bec-1* on Kaem- and Rhap-dependent memory improvement in the hTau(P301L) worms. **f**, Western blot data with semi-quantifications showing changes in designated phosphorylated Tau sites in the HEK 293 cells expressing pTRE3G-mcherry-BI promoter-EGFP Tau P301L (HEK 293 3G-EGFP-Tau P301L/mCherry) with 24 h treatment of Kaem or Rhap. **g**, Effects of Kaem and Rhap on seeded Tau-induced endogenous Tau aggregation in the HEK293 cells expressing 0N4R P301S Tau-Venus. Data are from 3 biological replicates. **h**, Evaluation of any synergistic effects of Kaem and Rhap on associative memory in hTau(P301L) (CK12) worms. Data were pooled from 3 biological replicates. All quantitative data are shown as mean ± s.e.m. Two-way ANOVA followed by Tukey's multiple comparisons test (**a**–**h**). NS, no significance; $^{*}P < 0.05$, $^{**}P < 0.01$, $^{***}P < 0.001$. Additional Tau seeding data are included in Extended Data Fig. 3h–k. Original western blot gels for **f** are included in Source Data Fig. 2.

We then examined aggregation levels of Tau in response to Kaem and Rhap treatment. While Kaem reduced 62.2% of AT8 (for p-Tau Ser202/Thr205)-positive cells, Rhap abrogated 73.5% of AT8-positive cells in the hippocampus of the 3xTg AD mice (Fig. 6m,n). At the molecular level, Kaem and Rhap dramatically reduced the phosphorylation levels of multiple classical p-Tau sites,

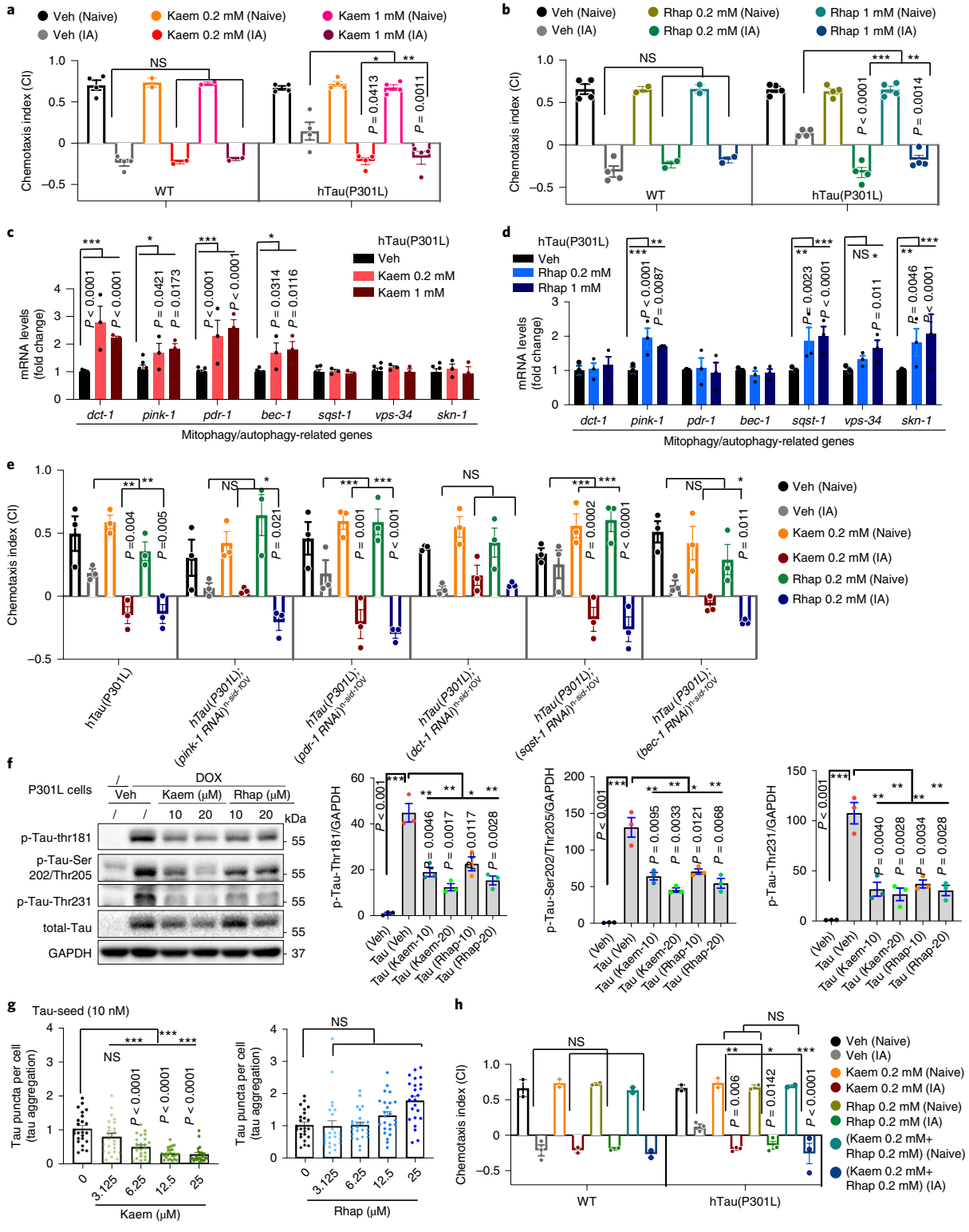

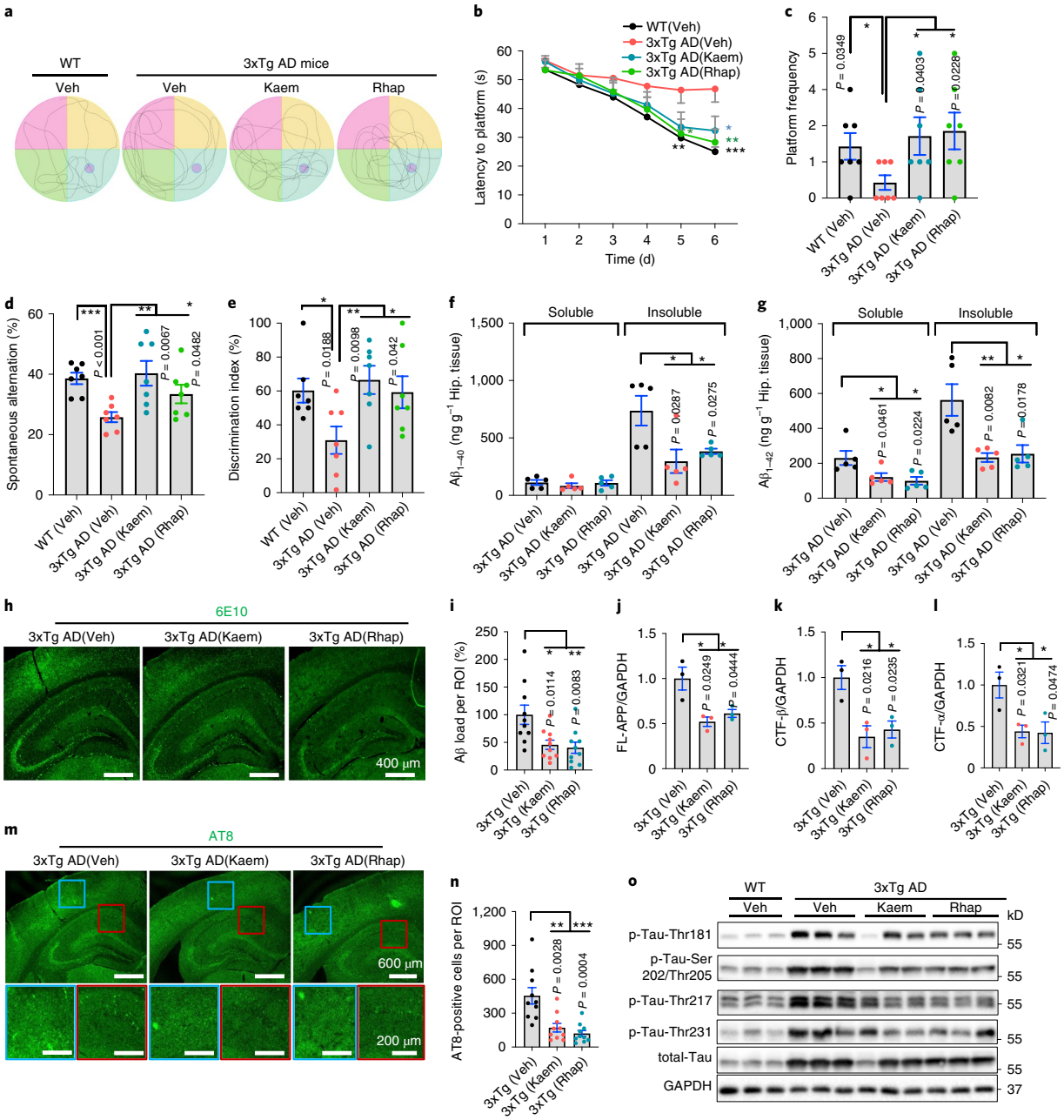

Fig. 6 | Mitophagy stimulation forestalls memory loss and ameliorates both Aβ and Tau pathologies in 3xTg AD mice. The 3xTg AD mice were treated with Kaem or Rhap (100 mg kg^{-1} d^{-1}) via oral gavage for 2 months starting from 12.5 months of age. **a**, Representative images of the swimming tracks of mice at day 7 in the Morris water maze test ($n = 6$ mice per group). **b**, Latency to the platform of mice from days 1 to 6. **c**, Platform frequency of mice in the probe trial at day 7. **d**,**e**, Effects of Kaem and Rhap on spontaneous alternation (**d**) (Y maze) and novel object recognition/NOR (**e**). **f**,**g**, Soluble and insoluble $A\beta_{1-40}$ and $A\beta_{1-42}$ levels in hippocampal tissues. $n = 5$ mice in all groups. **h**, Immunohistochemical analysis of Aβ load in 3xTg AD mice hippocampi and cortices under Kaem or Rhap treatment. Experiments were repeated twice independently, with similar results. **i**, Quantification of Aβ load per ROI in images from **h**. $n = 10$ random areas in the ROIs from 3 mice per group. **j**–**l**, Semi-quantification of western blot data showing effects of Kaem and Rhap on the levels of full-length APP (FL-APP), CTF-β and CTF-α in hippocampal tissues from the 3xTg AD mice ($n = 3$ biologically independent samples). **m**, Representative immunofluorescence staining of AT8-positive cells in the cortex and hippocampus of 3xTg AD mouse brains. Experiments were repeated twice independently, with similar results. The blue and red squares denote designated brain regions were magnified. **n**, Quantified data of **m** ($n = 10$ random areas in the ROIs from 3 mice in each group). **o**, Effects of Kaem and Rhap on the expression levels of different p-Tau sites (Thr181, Ser202/Thr205, Thr217 and Thr231) in hippocampal tissues from the 3xTg AD mice ($n = 3$ mice per group). All quantitative data are shown as mean ± s.e.m. Two-way ANOVA followed by Tukey's multiple comparisons test (**b**–**g**, **i**–**l**, **n**). NS, no significance; $^*P < 0.05$, $^{**}P < 0.01$, $^{***}P < 0.001$. Additional data on the mechanisms of mitophagy induction by Kaem and Rhap in mice are shown in Extended Data Fig. 4. Original western blot gels for **o** are included in Source Data Fig. 3.

such as Thr181, Ser202/Thr205 and Thr231, by over 50% (Fig. 6o and Extended Data Figs. 1j,k and 4b,c). Recent clinical studies point to a new p-Tau site, p-Tau217, which increases during early AD and correlates with AD with high sensitivity and discriminative accuracy[56,57]. To this end, we evaluated the effect of Kaem and Rhap on p-Tau217. Intriguingly, Kaem and Rhap caused a 57.8% and a 66.6% reduction in p-Tau217 expression, respectively (Fig. 6o and Extended Data Fig. 1l). To investigate whether the Kaem- and Rhap-induced reduction in p-Tau was dependent on mitophagy, we knocked down *PINK1 gene* in HEK 293 (with Tau P301L) cells. Immunoblotting data show that *PINK1* knockdown almost completely annulled the effect of Kaem and Rhap on the phosphorylation status of Tau, suggesting that these mitophagy inducers inhibit p-Tau (thr181) and p-Tau (thr217) via a PINK1-dependent pathway (Extended Data Fig. 1m–o).

We further checked mitophagy status in the 3xTg AD mice. Immunoblotting data from the hippocampal tissue show that major mitophagy proteins, including PINK1, Parkin, OPTN and p-ULK1 (Ser555), were reduced in the 3xTg AD mice when compared with WT mice. Meanwhile, levels of these proteins were higher in Kaem- and Rhap-fed AD mice (Extended Data Fig. 4f–j). In line with our results from cells and worms, our mouse data suggest that Kaem and Rhap restore impaired mitophagy in the 3xTg AD mice. In line with the immunoblot data, electron microscopic analysis shows accumulated mitochondria in the hippocampal tissue of the 3xTg AD mice, while this phenomenon was alleviated with Kaem or Rhap treatment accompanying increased mitophagy (Fig. 3n and Extended Data Fig. 1b). Furthermore, Kaem and Rhap increased protein expression levels of members of the mitochondrial OXPHOS complex (CV-ATP5A, CIII-UQCRC2 and CI-NDUFB8) in hippocampal tissue of 3xTg AD mice (Extended Data Fig. 4m).

While basal autophagy was lower in the hippocampal tissue of the 3xTg AD mice (lower LC3B-II/LC3B-I and higher p62) compared with WT mice, administration of Kaem and Rhap increased autophagy in the 3xTg AD mice (Extended Data Fig. 4f,k,l). Indeed, Kaem and Rhap promoted autophagy in vitro at 10 μM (Extended Data Fig. 4n–p), a dose that also triggers mitophagy in vitro (Fig. 2c). However, Kaem- and Rhap-induced memory improvement in worms is dependent on key mitophagy genes, such as *pink-1*, *pdr-1* or *dct-1/NIX* (Figs. 4c(left) and 5e, and Extended Data Fig. 3c). In addition, Kaem- or Rhap-induced inhibition of multiple p-Tau sites (Thr181 and Thr217) was dependent on the mitophagy gene *PINK-1* (Extended Data Fig. 1m–o). Given the intertwined linkage between mitophagy and autophagy, we do not exclude the possibility of a Kaem- and Rhap-induced non-mitophagy-related autophagy in the contribution to the multiple behavioural and pathological benefits reported here. Collectively, these combined behavioural, histological and molecular data indicate the bioavailability and strong capacity of Kaem and Rhap to retard memory loss, while simultaneously decreasing both Aβ and Tau pathologies in the 3xTg AD mouse model.

Discussion

Aiming to unveil additional AD aetiologies and support the development of novel anti-AD drug candidates, we have established an in silico-in vitro-worm-mouse screening technology and validation approach to identify novel mitophagy modulators. Our method revealed two bioavailable neuronal mitophagy inducers with anti-AD potential, as they showed conserved memory retention capacity in one Aβ nematode model, two Tau nematode models and the 3xTg AD rodent model. Compared with most clinical-trial-stage anti-AD drug candidates, which target only Aβ or Tau pathology[7], these mitophagy inducers work on both. Mechanistically, they inhibit Aβ pathology via production inhibition and microglial phagocytic clearance, abrogate Tau pathology via inhibition of multiple p-Tau sites (including p-Tau181, Ser202/Thr205, Thr231 and Thr217) and reduce spreading of pathological Tau. Kaem and Rhap are likely biological safe as the doses used for *C. elegans* and mice did not show detectable side effects (Extended Data Fig. 5 and Fig. 6). E.g., based on the toxicity assay results, treatments with Kaem or Rhap at concentrations ranging from 0.01 to 1 mM did not influence worm development (Extended Data Fig. 5a–d).

Over the past years, the scope of AI has moved from sheer theoretical knowledge to real-world applications, including drug development for aging and various diseases[17,19,22,58]. Our AI-driven virtual screening recommendation has achieved a 44% (8/18) success rate, which is much higher than traditional screening methods for small compounds. For instance, typical rates from experimental high-throughput screening have ranged between 0.01% to 0.5%, while typical hit rates for prospective virtual screening have been reported at 1%–10%[59,60]. Due to the low numbers of reference compounds, that is, mitophagy inducers (Supplementary Table 1), we have not been able to identify candidate compounds using machine learning approaches that may require large numbers of reference compounds (typically requiring between 100 to over 1,000 compounds)[19,22]. To overcome the shortage of reference compounds, we have chosen to use a combinational approach, combining simplified molecular-input line-entry system (SMILES) sequences, molecular interaction features and 3D conformers fingerprint, which can represent the molecule as a fixed bit-string on the basis of expert-encoded substructures, but do not require big training datasets[23]. However, since the fingerprint techniques rely heavily on the manually designed functional groups in the local chemical environment, they cannot capture global structural and pharmacophore information, and thus usually underperform in the context of complicated biological systems[61]. More recently, several fingerprint-inspired unsupervised machine learning approaches (for example, Mol2vec[26] and N-gram[26]) have rapidly advanced to utilizing larger compound datasets such as ChEMBL and ZINC for the comprehensive representation of molecules[24,25], yielding gains in property prediction performance over manually crafted fingerprints and preliminary machine learning methods. Compared to the sparse fingerprint vectors, our method has provided an efficient and information-enriched molecular embedding technique via learning the global relationship and 'semantic similarity' of each component. This has encouraged us to bypass the large dataset required by an unsupervised machine learning regime and has established a pipeline for virtual screening in complicated biological systems on the basis of only a few data points. Our machine learning approach could be applied to the screening of additional new mitophagy stimulators in larger drug libraries. Advanced AI technologies, such as a trained deep neural network[62], could be used to predict mitophagy induction activity in molecules that are structurally different from known mitophagy inducers in the future, when larger numbers of reference compounds become available.

Our findings reveal a conserved mechanism for memory loss that is at least partially mediated by defective mitophagy, while our in silico, high-accuracy screening technology paves the way for identifying exploitable mitophagy stimulators to improve healthspan and cognition in humans. Since mitochondria are essential for neuronal plasticity and survival, we have postulated that defective mitophagy driven by genetics, aging and/or other environmental factors, displays a causative role ahead of Aβ and Tau pathologies in AD development and progression[1,2,11]. The current study further consolidates this hypothesis since key mitophagy pathways, including the PINK1/Parkin pathway, possess a central role in memory improvement upon supplementation with mitophagy-inducing compounds. Kaem is a natural flavanol available in a variety of plants including beans, tea, kale and broccoli[63]. Rhap is a stilbenoid/phytoalexin, an antimicrobial compound produced by plants, such as *Vitis* species (grapes), etc. A well-known natural analogue of Rhap is resveratrol, which shows anti-aging and neuroprotective activi-

ties in cross-species animal studies and clinical trials[64,65]. Preclinical studies have shown that the anti-AD potential of Kaem may lie in its anti-oxidative and anti-inflammatory activities[66,67]. Indeed, a recent ongoing community-based prospective cohort study with a total of 921 participants, suggests that taking flavonols, including Kaem, reduces the risk of AD[63]. The current study verifies the anti-AD potential of Kaem using both nematode and rodent models of AD, and shows that mitophagy induction is a major molecular mechanism of neuroprotection for AD. We also identified Rhap as a robust mitophagy inducer able to potentially inhibit Aβ and Tau pathologies in both worm and mouse models of AD, in a largely mitophagy-dependent manner. The pharmacokinetic data for both Kaem and Rhap are available. Kaem can cross the blood–brain barrier;[68–70] whether Rhap is able to cross the blood–brain barrier has yet to be determined. Future clinical studies should address the appropriate dose range, delivery routes and any potential side effects. To note, our mitophagy-targeting drug screening strategy also reduces the risk of eliminating potential anti-AD drug candidates that may have little or no capacity to induce mitophagy. Among the 18 AI-selected molecules, Tacrolimus was able to induce mitophagy in HeLa cells but not in worm neurons. However, Tacrolimus was able to improve memory in the hTau(P301L) *C. elegans* model at a concentration of 0.2 mM (but not at 1 mM) (Supplementary Fig. 5b). Tacrolimus, a calcineurin inhibitor and an immunosuppressant, inhibited Aβ-induced dendritic spine loss[71] and is scheduled for a pilot open-labelled clinical trial (NCT04263519).

Efficacy and safety determine clinical success in drug development[72]. A challenge in virtual screening and computer-aided drug design is the existence of 'pan-assay interference compounds' (PAINS), which are chemical compounds that normally cause false-positive results in high-throughput screens[73–76]. The application of carefully selected PAINS-related filters into machine learning/AI-based drug screening[75], including the one we generated here, should be used. While we do not exclude the possibility that Rhap and Kaem could be hydroxylated, our strategy involving sophisticated in vitro analyses and multiple bioassays across two distinct in vivo experimental systems consistently shows the specificity and efficacy of the two lead compounds. Furthermore, the value of the effective dose of a drug candidate is a pivotal indicator of the potential of clinical studies. While the in vitro cell culture-based effective doses for many of the promising drug candidates are in the nM to 10 μM range[7,77], there are drug candidates with effective doses in the mM range. For example, while nicotinamide adenine dinucleotide (oxidized form, NAD^+) is reduced in aging and AD, there are many clinical trials on the application of NAD^+ precursors, such as nicotinamide riboside and nicotinamide mononucleotide, in treating neurodegenerative diseases and multiple age-related diseases[5]. The effective doses for nicotinamide riboside/nicotinamide mononucleotide in cell culture are between 0.5 to 3.0 mM; the doses used in clinical trials range from 250 to 2,000 mg d^{-1} without detectable toxicity[5,78]. For Kaem and Rhap, no detectable toxicity was observed at 50 μM in cells (effective dose = 10 μM) (Extended Data Fig. 3l), at 0.5 mM in *C. elegans* (effective dose = 0.2 mM) (Extended Data Fig. 5a–d) or at (100 mg kg^{-1} d^{-1}) in mice (Fig. 6). These data strongly indicate that Kaem and Rhap are effective and safe in both cells and animals.

It is intriguing that aging and defective mitophagy converge with AD-defining Aβ and Tau pathologies to inflict synaptic loss and neuronal death leading to subsequent cognitive dysfunction and brain homeostatic collapse. Although hyperactivation of mitophagy may not be without detrimental consequences for health, targeted mitophagic restoration is able to alleviate memory loss in a diverse set of nematode and rodent models of AD[11,15,79]. The broader impacts of mitophagy in targeting multiple aspects of AD pathogenesis, such as impaired proteostasis, inflammation, neuronal death, glial dysfunction and energy metabolism[1,11,80], support the potential value of examining mitophagy inducers for AD mitigation in a clinical setting.

Methods

Machine learning-based screening of mitophagy inducers. Multi-representation models (1D, 2D and 3D) were first pre-trained to generate representations for compounds. The goal of the pre-training process is to generate comprehensive molecular representations for different molecules. The pre-training models can generate vector representations for molecules that are not included in the initial pre-training dataset. The compounds from the ChEMBL and ZINC database were filtered using the parameters noted in Jaeger et al[26]. We transformed the compounds into SMILES representations using RDKit[81], which simplified multi-dimensional molecular structures into ordered text chains. In total, 19.9 million molecules were included in all further processes (hereafter called the pre-training dataset). A Mol2vec model was pre-trained on the basis of the pre-training dataset and new molecules could be described by summing the substructure vectors retrieved from a pre-trained Mol2vec model. The 2D pharmacophore fingerprint was implemented to introduce the fragment graph relationship between different molecules. Ehrlich[82] defined a pharmacophore as "a molecular framework that carries (phoros) the essential features responsible for the biological activity of a drug (pharmakon)". Therefore, the structural similarity between different molecules could be captured on the derived distance between the topological distributions of the various atoms that were inherent in the function of the molecules themselves. The 2D pharmacophore fingerprint was obtained using RDKit[81], producing a vectorized prioritization of molecules based on the 2D topological similarity (that is, the fingerprint). The 3D conformers fingerprint method, initially described by Landrum et al., was introduced to augment the 3D information[83]. The original dataset (with an initial 19.9 million compounds) was again run through RDKit using the 3D conformer fingerprint module. This technique used information about the features (chemically active areas) on a molecule, producing a 'feature-map vector' that captured information around the projected biological activity of molecules.

We applied the 1D, 2D and 3D fingerprints to identify potential mitophagy inducers within the screening process. The similarity score for each of the 3,724 compounds with the filtered molecules was calculated, with a higher score indicating a higher degree of similarity. We defined the strength of the relationship from the three models trained by different information, that is, 1D—molecules semantic information, 2D—fragments graph relationship and 3D—atomic bonds, spatial angle and length as the similarity. The similarity score was calculated as:

$$s = v * w, \tag{1}$$

where s is the similarity score, * is the vector dot product, and v (the inductor vector) and w (the compound vector) are high-dimensional vector representations from the pre-trained model.

We clustered the representation based on the 14 mitophagy inducers scored by the similarity function (equation 1). We then filtered the outliers and ranked the low-score compounds on the basis of filter function (equation 2).

$$\text{filter function} = \begin{cases} 0 & s = 1 \\ s \;\; \theta \le s < 1 \\ 0 & s < \theta \end{cases}, \tag{2}$$

where s is the similarity score and θ stands for the cut-off value (=0.75). The molecules with a similarity ranking score ≥0.75 were selected. In total, the selection method described here produced 18 novel analogue compounds for validation (Supplementary Table 2).

Small compounds in the Macau Library. All AI-selected compounds were from the State Key Laboratory of Quality Research in Chinese Medicine, Institute of Chinese Medical Sciences, University of Macau, Macau SAR, China (J.-H.L.). All molecules were of at least 98% purity and dissolved in dimethylsulfoxide (DMSO) for experiments. For the in vitro and in vivo experiments, Kaem (HY-14590) and Rhap (HY-N2229) were purchased from MedChemExpress, with 99.62% and 99.66% purity, respectively.

C. elegans strains and genetics. A list of strains used in this study is shown in Supplementary Table 6.

Drug treatment of C. elegans. All the *C. elegans* strains were maintained at 20 °C in standard nematode growth medium (NGM) plates with OP50 as a food resource[84]. All the experiments were performed at 20 °C, unless specified elsewhere. DMSO-dissolved compounds (Kaem, Rhap, Quercetin, Ascomycin, Tacrolimus, Isorhamnetin and Pinostilbene) were added just before pouring the NGM plates. Worms were treated with designated drugs from either egg hatching or L4 stage, or other time points as specified elsewhere.

mRNA quantification using *C. elegans* tissue. Real-time PCR was performed as previously described[85]. Worms of designated age were collected, washed with M9

buffer, followed by isolation of total RNA using TRIzol (Thermo Fisher, Catalog no. 15596026). For complementary DNA synthesis, messenger RNA was reversely transcribed using an iScript cDNA Synthesis Kit (catalog no. 1708890, Bio-Rad) for 5 min at 25 °C, 20 min at 46 °C, 1 min at 95 °C and finally at 4 °C for storage. cDNA samples were then used for standard real-time quantitative reverse transcription PCR (real-time qRT-PCR) to quantify mRNA levels of *dct-1*, *pink-1*, *pdr-1*, *bec-1*, *sqst-1*, *vps-34*, *skn-1* and *rheb-1* mRNA using the following primers:

dct-1: 5′-GGCTCCAACCTTACCACTCC-3′ and 5′-GCAAATCCTACT GCTGCTCC-3′;

pink-1: 5-AGCATATCGAATCGCAAATGAGTTAG-3′ and 5′-TCGACCGTGGCGAGTTACAAG-3′;

pdr-1: 5′-AGCCACCGAGCGATTGATTGC-3′ and 5′-GTGGCATTTTGGGCATCTTCTTG-3′;

bec-1: 5′-CTGTCAGCATCCGTTGAGGT-3′ and 5′-AGAGCGTCAGAGCAATCATTACA-3′;

sqst-1: 5′-ATCCGCTCCTCACCAAATGC-3′ and 5′-TGTTGGACGAAGGGGAACAG-3′;

vps-34: 5′-ATGATTCCAGGTATGCGGGC-3′ and 5′-CTGACGAGCAAGTTGAGAGGA-3′;

skn-1: ACAGTGCTTCTCTTCGGTAGC-3′ and 5′-GAGACCCATTGGACGGTTGA-3′; and

rheb-1: 5′-ACAAGACGGATCTCAGCACG-3′ and 5′-TCGAACACCTCATGCACTCG-3′.

Quantitative PCR was performed in triplicates, and the real-time PCR reactions were performed using QuantStudio 7 Flex System v1.1 (Applied Biosystems by Life Technologies) by heating to 95 °C for 10 min, cycling 40 times between 95 °C for 15 s, 60 °C for 1 min, and taking a melt-curve analysis between 95 °C for 15 s and 60 °C for 1 min.

Evaluation of neuronal mitophagy inducers using a *C. elegans* mitophagy reporter strain. A *C. elegans* neuronal mitophagy reporter strain (neuronal mt-Rosella) was used to quantify neuronal mitophagy in worms as previously described:[11] transgenic animals expressing a pan-neuronal mt-Rosella biosensor that combines a GFP variant sensitive to the acidic environment of the lysosomal lumen, fused to the pH-insensitive *Discosoma* red fluorescent protein (DsRed). Mitophagy was calculated as GFP/DsRed. Thus, the lower the ratio of pixel intensity, the higher the level of mitophagy. For all nematode experiments, compounds (0.01–1 mM) were administered from egg stage onwards. Unless specified, adult day 1 (the day after the L4 stage) nematodes were used for the experiments. Moreover, transgenic nematodes expressing the DCT-1::GFP mitophagy reporter, together with the autophagosomal marker LGG-1::DsRed in neurons were used to quantify mitophagy as previously reported[11]. Kaem and Rhap (0.01–1 mM) were administered from egg hatching onwards. Images of adult day 1 worms were taken using confocal microscopy, with co-localization between LGG-1 and DCT-1 serving to quantify the number of mitophagy events.

***C. elegans* short-term memory assay.** Chemotaxis to soluble and volatile compounds (isoamyl alcohol, IA) was performed at 20 °C on 10 cm agar plates as previously described[11,86]. In step 1, synchronized worms (around 200 worms per group) were collected and washed 5 times with M9 buffer, followed by placement in plain NGM plates (with no OP50) with/without IA for 90 min. In this step, for the IA conditioning plate, a droplet of 10 µl pure IA was placed on the middle of the lid. In step 2, to prepare assay plates, 20 µl 20 mM NaN_3 was added on 'IA' and trap 'T' points, respectively. Assay plates were left at room temperature (20–22 °C) for 30 min to dry before testing. A 0.5 × 0.5 cm Parafilm was placed over the 'IA' area of each plate. In step 3, worms from step 1 were collected via washing with M9 buffer, followed by placing the rinsed worms on the source point 'S' area (additional M9 buffer was quickly dried with tissue paper). Four µl diluted IA (1/50) was added on the Parafilm placed on the 'IA' area. The worms were left at room temperature for 2 h. For step 4, the number of worms in different regions were counted, including the 'S', 'IA' and 'T' areas. The chemotaxis index was calculated as (#'IA' − #'T')/(#'IA' + #'T' + #'S'), where '#' denotes numbers[87]. A smaller score correlates with better memory performance. Three to six biological replications were performed for all nematode experiments. The memory assay was performed using adult day 1 worms, unless specified elsewhere.

***C. elegans* lifespan assay, pharyngeal pumping rate, mobility and toxicity assays.** Lifespan analysis was performed at 20 °C as previously described[88], using 3.5 cm NGM plates with *E. coli* OP50 seeded 3 d ahead of experiments. Drugs (final concentrations were 0.2 mM Rhap, and 0.2 mM Kaem) were added during pouring of the NGM plates. Synchronous animal populations were generated via a 6 h egg lay by gravid adults to obtain tightly synchronized embryos that were allowed to develop into adulthood under defined conditions. Around 35–40 L4 stage worms (day 0) were transferred to 3.5 cm plates to obtain synchronous populations of at least 100 animals per condition. Animals were scored as dead or alive and transferred every 2–3 d to fresh plates seeded with OP50 during the fertile period, and then every 5 d until death. Worms were examined every day and were considered dead when they had stopped pharyngeal pumping and were unresponsive to touch. Worms that died due to internal bagging, crawling on the edge of the plates or gonad extrusion were scored as censored. These animals were included in lifespan analyses up to the point of censorship and were weighted by '0' in mortality calculations. Parameters like mean, standard deviation of the mean and *P* value were calculated using the log-rank test (Mantel–Cox) from a pooled population of animals. Kaplan–Meier (K–M) survival curves were used for lifespan presentation. We used the GraphPad Prism software package for statistical analysis and to determine lifespan values. For evaluations of pharyngeal pumping rates, worms were synchronized and raised to adults as mentioned in the lifespan assay methodology. At designated ages, pharynx contractions were manually counted for 30 s[88]. *C. elegans* movement analysis was performed as described[89]. Briefly, worms were exposed to designated concentrations of Kaem (0. 2 mM) and Rhap (0. 2 mM) beginning at egg stage and the maximum velocity of movement was determined at adult day 1. Fifty to 100 nematodes were placed in one plate and recorded for 1 h and 30 min using the Movement Tracker system (Nemamtrix) to assess mobility. Three biological repeats were carried out. A double-blinded approach was used to ensure objectivity. Toxicity experiments, including fecundity (3 h egg-lay), egg hatching and larval development, were conducted using N2 *C. elegans* at 20 °C as detailed elsewhere[90]. Briefly, synchronized eggs were placed on NGM plates seeded with *E. coli* (OP50). L4 larvae were subsequently transferred onto fresh OP50-seeded NGM plates and allowed to grow to adulthood. Ten adult day 1 worms were transferred onto assay NGM plates with OP50 and containing either Kaem (0.01, 0.05, 0.1, 0.2, 1 mM), Rhap (0.01, 0.05, 0.1, 0.2, 1 mM) or vehicle control. Three plates of worms for each group were set up to achieve an $n = 30$ per experimental condition. The gravid worms were subjected to a 3 h egg-lay followed by removal of worms from the plates. The number of eggs laid was quantified as a measure of the reproductive capacity of the worms. The following day, the number of unhatched eggs and L1 larvae were counted to determine the efficiency of egg hatching. Development to L4 larvae was assessed 36 h later after egg laying as a measure of larval growth. Finally, the growth of L4 larvae to adulthood was quantified 16 h after the L4 larval stage.

Evaluation of neuronal activity and neurodegeneration in *C. elegans*. Glutamatergic neurodegeneration was analysed using a well-established method reported elsewhere[40,91]. In brief, adult day 3 animals were prepared for confocal imaging. While there are around 15 glutamatergic neurons in the worm tail region[92], 5 were the focus of this analysis: LUA (R), LUA (L), PVR, PLM (R) and PLM (L). An animal was scored as normal if all 5 neurons were present and without malformations such as axon breaks, swelling, distension or separation of the soma. In addition, GFP intensity of the PVR neurons was quantified using the software ImageJ-1.50, with data from 30 worms randomly selected in each group from 2 biological replicates. Only PVR neurons with no clear malformations such as axon breaks, swelling, distension or abnormal location in the tail, were used for intensity quantification. The experiments were repeated 2 times with 40–50 worms per group per experiment.

Cholinergic synaptic transmission assay was performed as previously described[43]. This assay evaluates the sensitivity of worms to the synaptic transmission of acetylcholine at the neuromuscular junction via monitoring the paralyzing effect of an acetylcholinesterase inhibitor, aldicarb. In the presence of aldicarb, breakdown of acetylcholine is inhibited, resulting in the accumulation of acetylcholine in the synaptic cleft. This build-up of acetylcholine results in over-activation of cholinergic receptors, followed by muscle hyper-contraction, paralysis and finally death. Briefly, synchronized adult day 1 worms, achieved via a 5 h egg-lay, were incubated in the presence of aldicarb at different concentrations and scored every 30 min for the time course of the aldicarb-induced paralysis. While a series of doses were used (vehicle, 0.25, 0.5 and 1 mM) for optimization, 0.5 mM was chosen for further rescue experiments (±0.2 mM Kaem or 0.2 mM Rhap, or as described elsewhere). Thirty worms per group were used for the experiments, with finalized data from 2–4 biological repeats. VC223 (a strain hypersensitive to aldicarb-induced paralysis) and NM204 (a strain resistant to aldicarb-induced paralysis) were used as controls. Data were analysed and presented using Prism 8.0 (GraphPad Software).

Detection of in vitro mitophagy using mt-Keima fluorescent reporter. Imaging of mt-Keima HeLa cells was performed as reported elsewhere[31], using different settings for GFP and red fluorescent protein (RFP). mt-Keima is a ratiometric pH-sensitive fluorescent protein that exhibits green fluorescence (excitation 458 nm) in basic or neutral conditions and red fluorescence (excitation 561 nm) in acidic conditions[33]. For our experiments, the settings used were green channel (excitation 458 nm, emission 570–695 nm) to visualize normal mitochondria, and red channel (excitation 561 nm, emission 570–695 nm) to visualize mitochondria undergoing mitophagy. The mt-Keima HeLa cells were treated with different drugs of designated doses for 24 h, followed by confocal imaging. A total of 5 randomly selected regions per sample was chosen for imaging, with a total of 3 biological repeats. Data were quantified, using ImageJ software, as the total number of red pixels divided by the total number of all pixels.

Evaluation of Tau aggregation and degradation in HEK293 cells expressed with P301S Tau-Venus. HEK293 cells stably expressing the 0N4R isoform of human Tau, bearing P301S mutation with a C-terminal Venus tag treated with exogenous recombinant heparin-assembled P301S Tau (tau seeds) were used for the experiments. Exogenous Tau seeds promote the conversion of endogenous

Tau Venus from a dispersed distribution to bright foci[49]. Both the HEK293 P301S Tau-Venus cell line and the Tau seeds were a gift from the Dr William A. McEwan Lab at the University of Cambridge. The HEK293 P301S Tau-Venus cells were cultured in DMEM (with 10% fetal bovine serum (FBS) and 1% penicillin–streptomycin (P&S)) in a humidified incubator at 37 °C with 5% CO_2. On the day of the experiment, cells were trypsinized and seeded in Opti-MEM (Gibco, no FBS, no antibiotics) at a density of 5,000 cells per well per 50 µl in a 96-well plate (precoated with Poly d-lysine/PDL) and incubated for 24 h. To induce endogenous Tau aggregation, 50 µl Tau-containing Opti-MEM lacking FBS and antibiotics (20 nM Tau + 1% Lipofectamine 2000) was pre-incubated at room temperature for 10 min, then added to each well for 1.5 h incubation at 37 °C. Two types of experiments were performed: one to evaluate Tau aggregation and the other to quantify degradation of aggregated Tau. Experiment one was to evaluate how drugs affected seeded Tau-induced endogenous Tau aggregation: 50 µl DMEM (with 20% FBS and 1% P&S) containing vehicle (DMSO), Kaem (3.125, 6.25, 12.5, 25 µM) or Rhap (3.125, 6.25, 12.5, 25 µM) were added to respective wells, then incubated for 72 h. Cells were then fixed with 4% formaldehyde solution in 1× PBS for 10 min at room temperature. Cells were then stained with DAPI (1 µg ml^{-1}) in 1× PBS for 10 min before imaging. For experiment two, to evaluate how drugs affect degradation of aggregated Tau, 50 µl DMEM (with 20% FBS and 1% P&S) was added, followed by 48 h incubation. The medium was replaced with 150 µl DMEM (with 10% FBS and 1% P&S) and vehicle (DMSO), or Kaem (3.125, 6.25, 12.5, 25 µM) or Rhap (3.125, 6.25, 12.5, 25 µM) for 24 h. Cells were fixed with 4% formaldehyde solution in PBS for 10 min at room temperature. Cells were stained with DAPI (1 µg ml^{-1}) in PBS for 10 min before imaging. A fluorescent microscope (ZEISS Axio Zoom.V16) was used for imaging. One image per well was taken, with a total of 8 technical repeats per biological repeat. Data were analysed using ImageJ, from images from 3 biological repeats.

Cell culture for mechanistic studies. The N2a, YFP-Parkin HeLa, Mito-GFP/mCherry-Parkin Hela, HEK 293 and GFP-LC3 HeLa cells were cultured in DMEM containing 10% FBS and 1% P&S. N2S (N2a cells expressing human Swedish mutant APP695) and HEK 293 cells expressing pTRE3G-mcherry-BI promoter-EGFP Tau P301L were maintained in DMEM supplemented with 10% FBS, 1% P&S and 200 µg ml^{-1} G418. A high concentration (approximately 1,000 µg ml^{-1}) G418 was used for selection, and a low concentration (200 µg ml^{-1}) was used for maintenance. The expression of EGFP-Tau P301L is controlled by the addition of doxycycline (DOX) to the culture medium before indicated treatments. All the cell lines were maintained in the incubator at 37 °C with 5% CO_2. After designated treatments, cells were subjected to imaging (autophagy) or collected for western blot analysis. For the autophagy imaging, GFP-LC3 HeLa cells were fixed and stained with DAPI. The images were acquired using a confocal microscope (TCS SP8, Leica).

Transgenic mice, behavioural, pathological and mechanistic studies. Mice homozygous for all three mutant alleles (3xTg AD; homozygous for the Psen1 mutation and homozygous for the co-injected APPSwe and tauP301L transgenes (Tg(APPSwe,tauP301L)1Lfa)) were obtained from the Jackson Laboratory. The 3xTg AD mice and age-matched C57 mice were housed in individually ventilated cages on standardized rodent bedding. Mice were housed under constant light cycle (12 h light/dark) with free food and water available. The 12.5-month-old 3×Tg AD mice were treated with Kaem or Rhap (100 mg kg^{-1} d^{-1}) by oral gavage for 2 months, and subsequently evaluated for behavioural and molecular endpoints. All animal care and experimental procedures were approved by the Committee on the Ethics of Animal Experiments of the University of Macau (UMARE-013–2019).

Mouse behavioural studies. Several behavioural assays, including Morris Water Maze (MWM), Y maze and NOR were used to investigate changes in learning and memory. The MWM test was performed as described previously[93]. The device is a circular white pool (120 cm diameter × 50 cm depth) filled with water dyed white with TiO2, and with temperature maintained at 22 °C. A 10-cm-diameter platform was placed 1 cm below the water surface at a fixed position. Mice were trained with 4 trials per day for 6 consecutive days. Each trial lasted 60 s or until the mouse found the platform. If the mouse did not find the platform during the allocated time period, the experimenter directed the mouse to the platform. After each trial, the mouse was placed on the platform for 10 s. On the 7th day, the platform was removed for a probe trial (60 s) to assess long-term spatial memory retrieval. All parameters were recorded by a video tracking system (Labmaze V3.0, Zhongshi Technology). The Y maze spontaneous alternation performance (SAP) test measures the ability to recognize a previously explored environment[94]. The maze consists of 3 arms (30 cm length × 20 cm height × 6 cm width) with an angle of 120 ° between each arm. Mice were introduced to the centre of the Y maze and allowed to freely explore the maze for 10 min. The maze was cleaned with 75% ethanol solution between animals to eliminate odour traces. The number of entries into each arm was recorded with Labmaze video tracking system. SAP is the number of subsequent forays into a novel arm over the course of 3 entries. The spontaneous alternation (%) = number of actual alternations/(total arm entries − 2) × 100. The NOR tests were performed as described previously[95]. The device is a grey plastic box (35 cm length × 35 cm width × 25 cm height). Mice could explore two identical objects for 5 min during the training phase; 2 h later, each mouse was returned to the box, which had been modified to contain one familiar object and one novel object. The box was cleaned with 75% ethanol solution between animals to eliminate odour traces. The Labmaze video tracking system was used to monitor exploration behaviour. Exploration time was calculated as the length of time each mouse sniffed or pointed its nose or paws at the object. The 'recognition index' refers to the time spent exploring the novel object relative to the time spent exploring both objects. For the behavioural studies, 7 mice were used. No statistical methods were used to predetermine sample sizes, but our sample sizes are similar to those reported elsewhere[96].

EM. The ultrastructure of mitochondria and mitophagosomes was visualized and imaged with EM using the method reported elsewhere[11]. In brief, after killing the mice with the standard approach and a quick collection of the designated brain tissue, Veh-, Kaem- and Rhap-treated mouse hippocampal tissues were fixed in 2.5% glutaraldehyde (pH 7.4) for 2 h. After three washes with 0.1 M phosphate buffer (pH 7.2), the tissues were fixed in 1% osmic acid at 4 °C for 2 h. The samples were gradient dehydrated in a series of ethanol baths. Subsequently, the samples were embedded in Epon-Araldite resin for penetration and placed in a mold for polymerization. After the semi-thin section was used for positioning, the ultra-thin section was made and collected for microstructure analysis, followed by counter-staining with 3% uranyl acetate and 2.7% lead citrate. The samples were then observed with an HT7800 transmission electron microscope. Three mice per group were used for EM examination, with 10–20 images randomly taken. Data were analysed manually in a double-blinded manner.

Immunohistochemistry/Immunofluorescence. After the behavioural tests, anaesthetized mice were perfused with pre-cooled 1× PBS. Half brains were placed in 4% paraformaldehyde in PBS for 24 h and then equilibrated in 30% sucrose for 72 h at 4 °C; 1:8 series equidistant floating 30 µm coronal sections (240 µm interval) were prepared, including the dentate gyrus area. Approximately 9–10 slices from each mouse were incubated in blocking buffer (5% goat serum and 0.3% Triton X-100 in PBS) for 30 min at room temperature. Samples were then incubated overnight with the primary antibody at 4 °C and then incubated with the appropriate fluorescent probe-conjugated secondary antibodies for 1 h at room temperature while protected from light. Nuclei were stained with DAPI at a 1:1,000 dilution. Specific primary antibodies used included mouse anti-β-amyloid, 1–16 antibody (clone 6E10, catalog no. 803002, BioLegend), rabbit anti-iba1 antibody (019–19741, Wako) and mouse anti-AT8 antibody (cat no. MN1020, ThermoFisher). The slices were mounted with FluorSave reagent and visualized using the Leica TCS SP8 confocal microscope. Aβ plaques and AT8-positive cells per ROI were counted and quantified using ImageJ software. To assess morphological changes of microglial cells, ImageJ was used to measure numbers and length of processes per microglial cell[11,96]. To evaluate phagocytosis, numbers of iba1-positive microglia cells that were also Aβ-positive in the CA1 region were counted.

For the co-labelling analysis, rabbit anti-iba1 antibody (019–19741, FUJIFILM Wako Pure Chemical) and mouse anti-β-amyloid, 1–16 antibody (no. 803002, BioLegend) were used. Primary antibodies were visualized with Alexa-Fluor 488 and Alex-Fluor 555 secondary antibodies (ThermoFisher), and the cell nuclei visualized with DAPI. For the quantification of Aβ plaques, deposits larger than 10 µm were included. At least 3 random images per mouse from a total of 3 mice were used for quantification. To detect the co-localization of mitochondria and lysosomes after Kaem and Rhap treatments, LAMP1 antibody (no. sc-18821, Santa Cruz) was used to label lysosomes in Mito-GFP/mCherry-Parkin HeLa cells. A Leica TCS SP8 confocal microscope was used to capture pictures and ImageJ software was used to quantify the co-localization events. To detect the effects of the top 5 potential compounds on mitophagy induction, HeLa cells expressing mt-Keima were treated with designated compounds for 24 h, then imaged and quantified with a Zeiss LSM 880 Confocal System.

Enzyme-linked immunosorbent assay (ELISA) for $A\beta_{1-40}$ and $A\beta_{1-42}$. ELISA assays were performed as reported previously, with minor modifications[97]. Mouse hippocampal tissues were homogenized individually with Qiagen TissueLyser-II homogenizer in radioimmunoprecipitation assay (RIPA) buffer (R0728, Sigma) containing protease and phosphatase inhibitors. Extracts were sonicated and spun at 100,000 *g* for 20 min at 4 °C. Insoluble pellets were extracted in 70% formic acid by sonication and spun at 100,000 *g* for 20 min. Samples were neutralized in 1 M Tris buffer (pH 11, 1:12 ratio dilution) and diluted in blocking buffer before loading on ELISA. Aβ in the RIPA fraction was regarded as the detergent-soluble fraction, while Aβ in the neutralized formic acid fraction was considered as the detergent-insoluble fraction. The ELISA plates were coated overnight with 6E10 (4 µg ml^{-1}) antibody in coating buffer 0.1 M Na_2CO_3 (pH 9.6) and blocked with 4% Block Ace in PBS for 2 h. Equal amounts of the fractions were loaded in duplicate wells and incubated at room temperature for 2 h under shaking. Biotinylated 5C3 (no. 0060S, Nanotools) and 8G7 (no. 0061S, Nanotools) were used to determine $A\beta_{1-40}$ and $A\beta_{1-42}$, respectively. Secondary antibodies were diluted at 1:1,000 concentration in 1% Block Ace solution and incubated at room temperature for 2 h.

After washing the plates with PBS with 0.1% Tween20 (PBST), streptavidin-HRP was added and the plates were incubated at 37 °C for 1 h. TMB substrate (no. 555214, BD Biosciences) was then added to the plates, and plates were incubated at room temperature for 30 min. Finally, an equal volume of stop solution was added, and absorbance was measured at 450 nm.

Western blots using materials from cells and mouse brain. Western blot assay was done as previously described[88]. Samples from different cell lines and mouse brain tissues were collected and prepared using 1× RIPA buffer containing protease and phosphatase inhibitors, and the protein concentrations tested using the bovine serum albumin (BSA) method. Proteins were separated on a NuPAGE 4–12% Bis-Tris Protein Gel at 200 V running for 1 h (catalogue no. NP0336BOX, Thermo Fisher Scientific) and set transfer system at 250 mA for ~2–3 h (for all the proteins from 15 kDa to 350 kDa) on PVDF membrane and then probed with various antibodies. Chemiluminescence detection was performed using a ChemiDoc XRS System (Bio-Rad Laboratories). Gamma adjustment was used to reduce the dark background when necessary. Quantification was performed using ImageJ. Antibodies used were as follows (all from Cell Signaling Technology, unless otherwise stated): PINK1 antibody (catalog no. ab75487, Abcam; no. A7131, ABclonal), Parkin antibody (no. NB100–91921, Novus), FUNDC1 antibody (no. ab74834, Abcam), LC3B antibody (no. NB100–2220, Novus), Beclin1 antibody (no. 3495s), phospho-DRP1 antibody (no. S616), DRP1 antibody (no. 8570s), p62 antibody (no. 8025s), MFN2 antibody (no. 94823s), phospho-ULK1 antibody (no. 5869s), ULK1 antibody (no. 6439s), AMBRA1 antibody (no. 24907s), OPTN antibody (no. A1845, ABclonal), Tau antibody (no. 46687s), p-Tau-thr181 (no. 12285s), p-Tau-thr231 (no. ab151559, Abcam), p-Tau-ser202/thr205 (no. MN1020, ThermoFisher), p-Tau-thr217 (no. 44–744, ThermoFisher), beta amyloid polyclonal antibody (no. 51–2700, ThermoFisher), Parkin Rabbit pAb (no. A0968, ABclonal), Tim23 antibody (no. 611222, BD Biosciences), Total OXPHOS Rodent WB Antibody Cocktail (no. ab110413, Abcam) and β-actin antibody (no. A5441, Sigma). Secondary antibodies included anti-mouse immunoglobulin G (IgG; catalogue no. 7076s) and anti-rabbit IgG (no. 7074s). Primary antibodies were used at a 1:1,000 dilution, with secondary antibodies used at a 1:2,000–5,000 dilution.

Statistical analysis. Data are presented as mean ± s.e.m., unless otherwise specified. Two-tailed unpaired *t*-tests were used for comparisons between two groups. Group differences were analysed with one-way analysis of variance (ANOVA) followed by Šidák's multiple comparisons test or two-way ANOVA followed by Tukey's multiple comparisons test for multiple groups. Prism 8.0 (GraphPad Software) was used for the statistical analysis. *P* values <0.05 were considered statistically significant.

Reporting Summary. Further information on research design is available in the Nature Research Reporting Summary linked to this article.

Data availability

The main data supporting the findings of this study are available within the Article and its Supplementary Information. The raw wet-lab data generated in this study are available from the corresponding authors on reasonable request. Restrictions apply to the AI-related data: all requests for raw and processed data will be reviewed by Mindrank AI to verify whether the request is subject to any intellectual property or confidentiality constraints. Source data are provided with this paper.

Code availability

Custom code was specific to our computing infrastructure and mainly used for data input/output and parallelization across computers and graphics processors. The code, currently under a patent-examination process, is available from the corresponding authors on reasonable request.

Received: 20 February 2021; Accepted: 24 September 2021;
Published online: 6 January 2022

References

1. Lou, G. et al. Mitophagy and neuroprotection. *Trends Mol. Med.* **26**, 8–20 (2019).
2. Kerr, J. S. et al. Mitophagy and Alzheimer's disease: cellular and molecular mechanisms. *Trends Neurosci.* **40**, 151–166 (2017).
3. Yuan, J. et al. Two conserved epigenetic regulators prevent healthy ageing. *Nature* **579**, 118–122 (2020).
4. Kobro-Flatmoen, A. et al. Re-emphasizing early Alzheimer's disease pathology starting in select entorhinal neurons, with a special focus on mitophagy. *Ageing Res. Rev.* **67**, 101307 (2021).
5. Lautrup, S., Sinclair, D. A., Mattson, M. P. & Fang, E. F. NAD(+) in brain aging and neurodegenerative disorders. *Cell Metab.* **30**, 630–655 (2019).
6. Patterson, C. *World Alzheimer Report 2018: The State of the Art of Dementia Research: New Frontiers* (ADI, 2019).
7. Cummings, J., Lee, G., Ritter, A., Sabbagh, M. & Zhong, K. Alzheimer's disease drug development pipeline: 2019. *Alzheimers Dement.* **5**, 272–293 (2019).
8. Mattson, M. P., Gleichmann, M. & Cheng, A. Mitochondria in neuroplasticity and neurological disorders. *Neuron* **60**, 748–766 (2008).
9. Tigano, M., Vargas, D. C., Tremblay-Belzile, S., Fu, Y. & Sfeir, A. Nuclear sensing of breaks in mitochondrial DNA enhances immune surveillance. *Nature* **591**, 477–481 (2021).
10. Aman, Y. et al. Autophagy in healthy aging and disease. *Nat. Aging* **1**, 634–650 (2021).
11. Fang, E. F. et al. Mitophagy inhibits amyloid-beta and tau pathology and reverses cognitive deficits in models of Alzheimer's disease. *Nat. Neurosci.* **22**, 401–412 (2019).
12. Harold, D. et al. Genome-wide association study identifies variants at CLU and PICALM associated with Alzheimer's disease. *Nat. Genet.* **41**, 1088–1093 (2009).
13. Lee, J. H. et al. Lysosomal proteolysis and autophagy require presenilin 1 and are disrupted by Alzheimer-related PS1 mutations. *Cell* **141**, 1146–1158 (2010).
14. Fu, H. et al. A tau homeostasis signature is linked with the cellular and regional vulnerability of excitatory neurons to tau pathology. *Nat. Neurosci.* **22**, 47–56 (2019).
15. Du, F. et al. PINK1 signalling rescues amyloid pathology and mitochondrial dysfunction in Alzheimer's disease. *Brain* **140**, 3233–3251 (2017).
16. Brown, E. D. & Wright, G. D. Antibacterial drug discovery in the resistance era. *Nature* **529**, 336–343 (2016).
17. LeCun, Y., Bengio, Y. & Hinton, G. Deep learning. *Nature* **521**, 436–444 (2015).
18. Vamathevan, J. et al. Applications of machine learning in drug discovery and development. *Nat. Rev. Drug Discov.* **18**, 463–477 (2019).
19. Stokes, J. M. et al. A deep learning approach to antibiotic discovery. *Cell* **180**, 688–702 e613 (2020).
20. Mamoshina, P., Vieira, A., Putin, E. & Zhavoronkov, A. Applications of deep learning in biomedicine. *Mol. Pharm.* **13**, 1445–1454 (2016).
21. Chen, H., Engkvist, O., Wang, Y., Olivecrona, M. & Blaschke, T. The rise of deep learning in drug discovery. *Drug Discov. Today* **23**, 1241–1250 (2018).
22. Zhavoronkov, A. et al. Deep learning enables rapid identification of potent DDR1 kinase inhibitors. *Nat. Biotechnol.* **37**, 1038–1040 (2019).
23. Rogers, D. & Hahn, M. Extended-connectivity fingerprints. *J. Chem. Inf. Model.* **50**, 742–754 (2010).
24. Gaulton, A. et al. The ChEMBL database in 2017. *Nucleic Acids Res.* **45**, D945–D954 (2017).
25. Sterling, T. & Irwin, J. J. ZINC 15–ligand discovery for everyone. *J. Chem. Inf. Model.* **55**, 2324–2337 (2015).
26. Jaeger, S., Fulle, S. & Turk, S. Mol2vec: unsupervised machine learning approach with chemical intuition. *J. Chem. Inf. Model.* **58**, 27–35 (2018).
27. Yuan, N. N. et al. Canthin-6-one accelerates alpha-synuclein degradation by enhancing UPS activity: drug target identification by CRISPR-Cas9 whole genome-wide screening technology. *Front. Pharm.* **10**, 16 (2019).
28. Cai, C. Z. et al. Natural alkaloid harmine promotes degradation of alpha-synuclein via PKA-mediated ubiquitin-proteasome system activation. *Phytomedicine* **61**, 152842 (2019).
29. Yang, X., Wang, Y., Byrne, R., Schneider, G. & Yang, S. Concepts of artificial intelligence for computer-assisted drug discovery. *Chem. Rev.* **119**, 10520–10594 (2019).
30. Pham, T. H., Qiu, Y., Zeng, J., Xie, L. & Zhang, P. A deep learning framework for high-throughput mechanism-driven phenotype compound screening and its application to COVID-19 drug repurposing. *Nat. Mach. Intell.* **3**, 247–257 (2021).
31. Sun, N. et al. Measuring in vivo mitophagy. *Mol. Cell* **60**, 685–696 (2015).
32. Katayama, H., Kogure, T., Mizushima, N., Yoshimori, T. & Miyawaki, A. A sensitive and quantitative technique for detecting autophagic events based on lysosomal delivery. *Chem. Biol.* **18**, 1042–1052 (2011).
33. Fang, E. F. et al. In vitro and in vivo detection of mitophagy in human cells, *C. elegans*, and mice. *J. Vis. Exp.* **22**, 56301 (2017).
34. Kingwell, K. Turning up mitophagy in Alzheimer disease. *Nat. Rev. Drug Discov.* https://www.nature.com/articles/d41573-019-00035-6 (2019).
35. Dosanjh, L. E., Brown, M. K., Rao, G., Link, C. D. & Luo, Y. Behavioral phenotyping of a transgenic *Caenorhabditis elegans* expressing neuronal amyloid-beta. *J. Alzheimers Dis.* **19**, 681–690 (2010).
36. Fang, E. F. et al. Tomatidine enhances lifespan and healthspan in *C. elegans* through mitophagy induction via the SKN-1/Nrf2 pathway. *Sci. Rep.* **7**, 46208 (2017).
37. Lazarou, M. et al. The ubiquitin kinase PINK1 recruits autophagy receptors to induce mitophagy. *Nature* **524**, 309–314 (2015).
38. Fang, E. F. et al. Defective mitophagy in XPA via PARP-1 hyperactivation and NAD(+)/SIRT1 reduction. *Cell* **157**, 882–896 (2014).
39. Francis, P. T. The interplay of neurotransmitters in Alzheimer's disease. *CNS Spectr.* **10**, 6–9 (2005).
40. Griffin, E. F. et al. ApoE-associated modulation of neuroprotection from Abeta-mediated neurodegeneration in transgenic *Caenorhabditis elegans*. *Dis. Model Mech.* **12**, dmm037218 (2019).

41. Treusch, S. et al. Functional links between Abeta toxicity, endocytic trafficking, and Alzheimer's disease risk factors in yeast. *Science* **334**, 1241–1245 (2011).
42. Hampel, H. et al. The cholinergic system in the pathophysiology and treatment of Alzheimer's disease. *Brain* **141**, 1917–1933 (2018).
43. Mahoney, T. R., Luo, S. & Nonet, M. L. Analysis of synaptic transmission in *Caenorhabditis elegans* using an aldicarb-sensitivity assay. *Nat. Protoc.* **1**, 1772–1777 (2006).
44. Cummins, N., Tweedie, A., Zuryn, S., Bertran-Gonzalez, J. & Gotz, J. Disease-associated tau impairs mitophagy by inhibiting Parkin translocation to mitochondria. *EMBO J. e99360* (2018).
45. Fatouros, C. et al. Inhibition of tau aggregation in a novel *Caenorhabditis elegans* model of tauopathy mitigates proteotoxicity. *Hum. Mol. Genet.* **21**, 3587–3603 (2012).
46. Iba, M. et al. Synthetic tau fibrils mediate transmission of neurofibrillary tangles in a transgenic mouse model of Alzheimer's-like tauopathy. *J. Neurosci.* **33**, 1024–1037 (2013).
47. Spillantini, M. G. & Goedert, M. Tau pathology and neurodegeneration. *Lancet Neurol.* **12**, 609–622 (2013).
48. Wegmann, S. et al. Experimental evidence for the age dependence of tau protein spread in the brain. *Sci. Adv.* **5**, eaaw6404 (2019).
49. McEwan, W. A. et al. Cytosolic Fc receptor TRIM21 inhibits seeded tau aggregation. *Proc. Natl Acad. Sci. USA* **114**, 574–579 (2017).
50. Wolfson, C. et al. A reevaluation of the duration of survival after the onset of dementia. *N. Engl. J. Med.* **344**, 1111–1116 (2001).
51. Kua, E. H. et al. The natural history of dementia. *Psychogeriatrics* **14**, 196–201 (2014).
52. Cabreiro, F. et al. Metformin retards aging in *C. elegans* by altering microbial folate and methionine metabolism. *Cell* **153**, 228–239 (2013).
53. Ryu, D. et al. Urolithin A induces mitophagy and prolongs lifespan in *C. elegans* and increases muscle function in rodents. *Nat. Med.* **22**, 879–888 (2016).
54. Oddo, S. et al. Triple-transgenic model of Alzheimer's disease with plaques and tangles: intracellular Abeta and synaptic dysfunction. *Neuron* **39**, 409–421 (2003).
55. Lautrup, S. et al. Microglial mitophagy mitigates neuroinflammation in Alzheimer's disease. *Neurochem. Int.* **129**, 104469 (2019).
56. Mattsson-Carlgren, N. et al. Longitudinal plasma p-tau217 is increased in early stages of Alzheimer's disease. *Brain* **143**, 3234–3241 (2020).
57. Palmqvist, S. et al. Discriminative accuracy of plasma phospho-tau217 for Alzheimer disease vs other neurodegenerative disorders. *JAMA* **324**, 772–781 (2020).
58. Aman, Y. et al. The NAD(+)-mitophagy axis in healthy longevity and in artificial intelligence-based clinical applications. *Mech. Ageing Dev.* **185**, 111194 (2020).
59. Zhu, T. et al. Hit identification and optimization in virtual screening: practical recommendations based on a critical literature analysis. *J. Med. Chem.* **56**, 6560–6572 (2013).
60. Truchon, J. F. & Bayly, C. I. Evaluating virtual screening methods: good and bad metrics for the "early recognition" problem. *J. Chem. Inf. Model.* **47**, 488–508 (2007).
61. Chuang, K. V., Gunsalus, L. & Keiser, M. J. Learning molecular representations for medicinal chemistry. *J. Med. Chem.* **63**, 8705–8722 (2020).
62. Stokes, J. M. et al. A deep learning approach to antibiotic discovery. *Cell* **181**, 475–483 (2020).
63. Holland, T. M. et al. Dietary flavonols and risk of Alzheimer dementia. *Neurology* **94**, e1749–e1756 (2020).
64. Pollack, R. M. et al. Resveratrol improves vascular function and mitochondrial number but not glucose metabolism in older adults. *J. Gerontol. A Biol. Sci. Med Sci.* **72**, 1703–1709 (2017).
65. Bonkowski, M. S. & Sinclair, D. A. Slowing ageing by design: the rise of NAD(+) and sirtuin-activating compounds. *Nat. Rev. Mol. Cell Biol.* **17**, 679–690 (2016).
66. Kouhestani, S., Jafari, A. & Babaei, P. Kaempferol attenuates cognitive deficit via regulating oxidative stress and neuroinflammation in an ovariectomized rat model of sporadic dementia. *Neural Regen. Res.* **13**, 1827–1832 (2018).
67. Kim, J. K. et al. Protective effects of kaempferol (3,4',5,7-tetrahydroxyflavone) against amyloid beta peptide (Abeta)-induced neurotoxicity in ICR mice. *Biosci. Biotechnol. Biochem.* **74**, 397–401 (2010).
68. Zhang, Q. et al. Improved blood–brain barrier distribution: effect of borneol on the brain pharmacokinetics of kaempferol in rats by in vivo microdialysis sampling. *J. Ethnopharmacol.* **162**, 270–277 (2015).
69. Moradi-Afrapoli, F. et al. Validation of UHPLC-MS/MS methods for the determination of kaempferol and its metabolite 4-hydroxyphenyl acetic acid, and application to in vitro blood–brain barrier and intestinal drug permeability studies. *J. Pharm. Biomed. Anal.* **128**, 264–274 (2016).
70. Roupe, K. A., Yanez, J. A., Teng, X. W. & Davies, N. M. Pharmacokinetics of selected stilbenes: rhapontigenin, piceatannol and pinosylvin in rats. *J. Pharm. Pharmacol.* **58**, 1443–1450 (2006).
71. Stallings, N. R. et al. Pin1 mediates Abeta42-induced dendritic spine loss. *Sci. Signal* **11**, eaap8734 (2018).
72. Musuamba, F. T. et al. Advanced methods for dose and regimen finding during drug development: summary of the EMA/EFPIA workshop on dose finding (London 4–5 December 2014). *CPT Pharmacometrics Syst. Pharmacol.* **6**, 418–429 (2017).
73. Baell, J. B. & Holloway, G. A. New substructure filters for removal of pan assay interference compounds (PAINS) from screening libraries and for their exclusion in bioassays. *J. Med. Chem.* **53**, 2719–2740 (2010).
74. Dahlin, J. L. et al. PAINS in the assay: chemical mechanisms of assay interference and promiscuous enzymatic inhibition observed during a sulfhydryl-scavenging HTS. *J. Med. Chem.* **58**, 2091–2113 (2015).
75. Baell, J. B. & Nissink, J. W. M. Seven year itch: pan-assay interference compounds (PAINS) in 2017 – utility and limitations. *ACS Chem. Biol.* **13**, 36–44 (2018).
76. Baell, J. & Walters, M. A. Chemistry: chemical con artists foil drug discovery. *Nature* **513**, 481–483 (2014).
77. Hughes, J. P., Rees, S., Kalindjian, S. B. & Philpott, K. L. Principles of early drug discovery. *Br. J. Pharmacol.* **162**, 1239–1249 (2011).
78. Yoshino, M. et al. Nicotinamide mononucleotide increases muscle insulin sensitivity in prediabetic women. *Science* **372**, 1224–1229 (2021).
79. Cen, X. et al. Pharmacological targeting of MCL-1 promotes mitophagy and improves disease pathologies in an Alzheimer's disease mouse model. *Nat. Commun.* **11**, 5731 (2020).
80. Fang, E. F. Mitophagy and NAD(+) inhibit Alzheimer disease. *Autophagy* **15**, 1112–1114 (2019).
81. Landrum, G. RDKit: A software suite for cheminformatics, computational chemistry, and predictive modeling, Academic Press, https://doi.org/10.15252/embj.201899360 (2013).
82. Ehrlich, P. Über den jetzigen Stand der Chemotherapie. *Ber. Dtsch. Chem. Ges.* **42**, 17–47 (1909).
83. Landrum, G. A., Penzotti, J. E. & Putta, S. Feature-map vectors: a new class of informative descriptors for computational drug discovery. *J. Comput. Aided Mol. Des.* **20**, 751–762 (2006).
84. Brenner, S. The genetics of *Caenorhabditis elegans*. *Genetics* **77**, 71–94 (1974).
85. Fang, E. F. et al. NAD(+) augmentation restores mitophagy and limits accelerated aging in Werner syndrome. *Nat. Commun.* **10**, 5284 (2019).
86. Voglis, G. & Tavernarakis, N. A synaptic DEG/ENaC ion channel mediates learning in *C. elegans* by facilitating dopamine signalling. *EMBO J.* **27**, 3288–3299 (2008).
87. Bargmann, C. I. & Horvitz, H. R. Chemosensory neurons with overlapping functions direct chemotaxis to multiple chemicals in *C. elegans*. *Neuron* **7**, 729–742 (1991).
88. Fang, E. F. et al. NAD(+) replenishment improves lifespan and healthspan in ataxia telangiectasia models via mitophagy and DNA repair. *Cell Metab.* **24**, 566–581 (2016).
89. Sorrentino, V. et al. Enhancing mitochondrial proteostasis reduces amyloid-beta proteotoxicity. *Nature* **552**, 187–193 (2017).
90. Ianevski, A. et al. Chemical, physical and biological triggers of evolutionary conserved Bcl-xL-mediated apoptosis. *Cancers* **12**, 1694 (2020).
91. Matlack, K. E. et al. Clioquinol promotes the degradation of metal-dependent amyloid-beta (Abeta) oligomers to restore endocytosis and ameliorate Abeta toxicity. *Proc. Natl Acad. Sci. USA* **111**, 4013–4018 (2014).
92. Serrano-Saiz, E. et al. Modular control of glutamatergic neuronal identity in *C. elegans* by distinct homeodomain proteins. *Cell* **155**, 659–673 (2013).
93. Vorhees, C. V. & Williams, M. T. Morris water maze: procedures for assessing spatial and related forms of learning and memory. *Nat. Protoc.* **1**, 848–858 (2006).
94. Ghosal, K. et al. Alzheimer's disease-like pathological features in transgenic mice expressing the APP intracellular domain. *Proc. Natl Acad. Sci. USA* **106**, 18367–18372 (2009).
95. Leger, M. et al. Object recognition test in mice. *Nat. Protoc.* **8**, 2531–2537 (2013).
96. Iaccarino, H. F. et al. Gamma frequency entrainment attenuates amyloid load and modifies microglia. *Nature* **540**, 230–235 (2016).
97. Song, J. X. et al. A small molecule transcription factor EB activator ameliorates beta-amyloid precursor protein and Tau pathology in Alzheimer's disease models. *Aging Cell* **19**, e13069 (2020).

Acknowledgements

This project was supported by HELSE SØR-ØST (Nos. 2017056, 2020001 and 2021021), the Research Council of Norway (Nos. 262175 and 277813), the National Natural Science Foundation of China (No. 81971327), Akershus University Hospital (Nos. 269901 and 261973), the Civitan Norges Forskningsfond for Alzheimers sykdom (for a 3-year Ph.D. Fellowship, No. 281931) and the Czech Republic–Norway KAPPA programme (with Martin Vyhnálek, No. TO01000215) to E.F.F. The project was partially supported by the Science and Technology Development Fund, Macau SAR (Grants No. 0128/2019/A3 and 024/2017/AMJ), the University of Macau grants (Grant No. MYRG2019-00129-ICMS) awarded to J.H.L. H.N. was supported by grants from HELSE SØR-ØST

(No. 2019098) and the Research Council of Norway (No. 302483). G.Y. was supported by the British Heart Foundation (Project No. PG/16/78/32402), the Hangzhou Economic and Technological Development Area Strategical Grant (Imperial Institute of Advanced Technology), the European Research Council Innovative Medicines Initiative on Development of Therapeutics and Diagnostics Combatting Coronavirus Infections Award 'DRAGON: rapiD and secuRe AI imaging-based diaGnosis, stratification, fOllow-up and preparedness for coronavirus paNdemics' (H2020-JTI-IMI2 101005122), the AI for Health Imaging Award 'CHAIMELEON: Accelerating the Lab to Market Transition of AI Tools for Cancer Management' (H2020-SC1-FA-DTS-2019-1 952172) and the UK Research and Innovation Future Leaders Fellowship (MR/V023799/1). C.X. was supported by the National Science Foundation of China (No. 81600977), Wenzhou City Committee of Science and Technology (Y20180137) and the Natural Science Foundation of Zhejiang Province (Y19H090059). R.A. and H.W. were funded by the China Scholarship Council (http://www.csc.edu.cn/); the funders had no role in study design, data collection and analysis, decision to publish or preparation of the manuscript. Support for some of the transgenic nematode models used came from a Collaborative Innovation Award from the Howard Hughes Medical Institute to G.A.C. We thank B. Olaisen (KCL) and D. J. Patrick-Brown (UiO) for reading and comments on the manuscript. Cartoon images in Fig. 2a and Supplementary Fig. 4a were generated using BioRender via subscription through the Fang laboratory.

Author contributions

E.F.F. designed and coordinated the project. C.X., R.A., S.L., R.H., T.S.G., M.J.L.-D., D.C., W.-W.W., T.S.-M., J.Z., H.W., G.L., K.P. and H.N. did the worm experiments. K.A.C. and G.A.C. generated the worm strains and helped in data analysis on neurodegeneration. X.-X.Z., C.-Z.C., L.-M.X., W.Z. and J.-H.L. did the mouse experiments. S.C. did the Tau seeding experiments. Z.N., S.Z., Y.J., G.Y. and X.X. did the AI experiments. C.X. and E.F.F. wrote the manuscript, while X.-X.Z., Z.N., J.-H.L., K.A.C., G.A.C., H.N., K.P., H.M.S. and G.Y. edited the manuscript.

Competing interests

E.F.F. and H.N. have a cooperative research and development agreement with ChromaDex. E.F.F., G.Y. and H.N. are consultants to Aladdin Healthcare Technologies. E.F.F. is a consultant to the Vancouver Dementia Prevention Centre and Intellectual Labs. During the execution of this work, S.Z. was a paid part-time employee of MindRank AI Ltd. Z.N., Y.J. and X.X. are full-time employees of MindRank AI Ltd. E.F.F., J.-H.L, Z.N., C.X. and X.-X.Z. have filed a patent on the use of mitophagy inducers to treat Alzheimer's disease. The other authors declare no competing interests.

Additional information

Extended data is available for this paper at https://doi.org/10.1038/s41551-021-00819-5.

Supplementary information The online version contains supplementary material available at https://doi.org/10.1038/s41551-021-00819-5.

Correspondence and requests for materials should be addressed to Jia-Hong Lu or Evandro F. Fang.

Peer review information *Nature Biomedical Engineering* thanks Thomas Caulfield, Feixiong Cheng and Hongguang Xia for their contribution to the peer review of this work.

Reprints and permissions information is available at www.nature.com/reprints.

Publisher's note Springer Nature remains neutral with regard to jurisdictional claims in published maps and institutional affiliations.

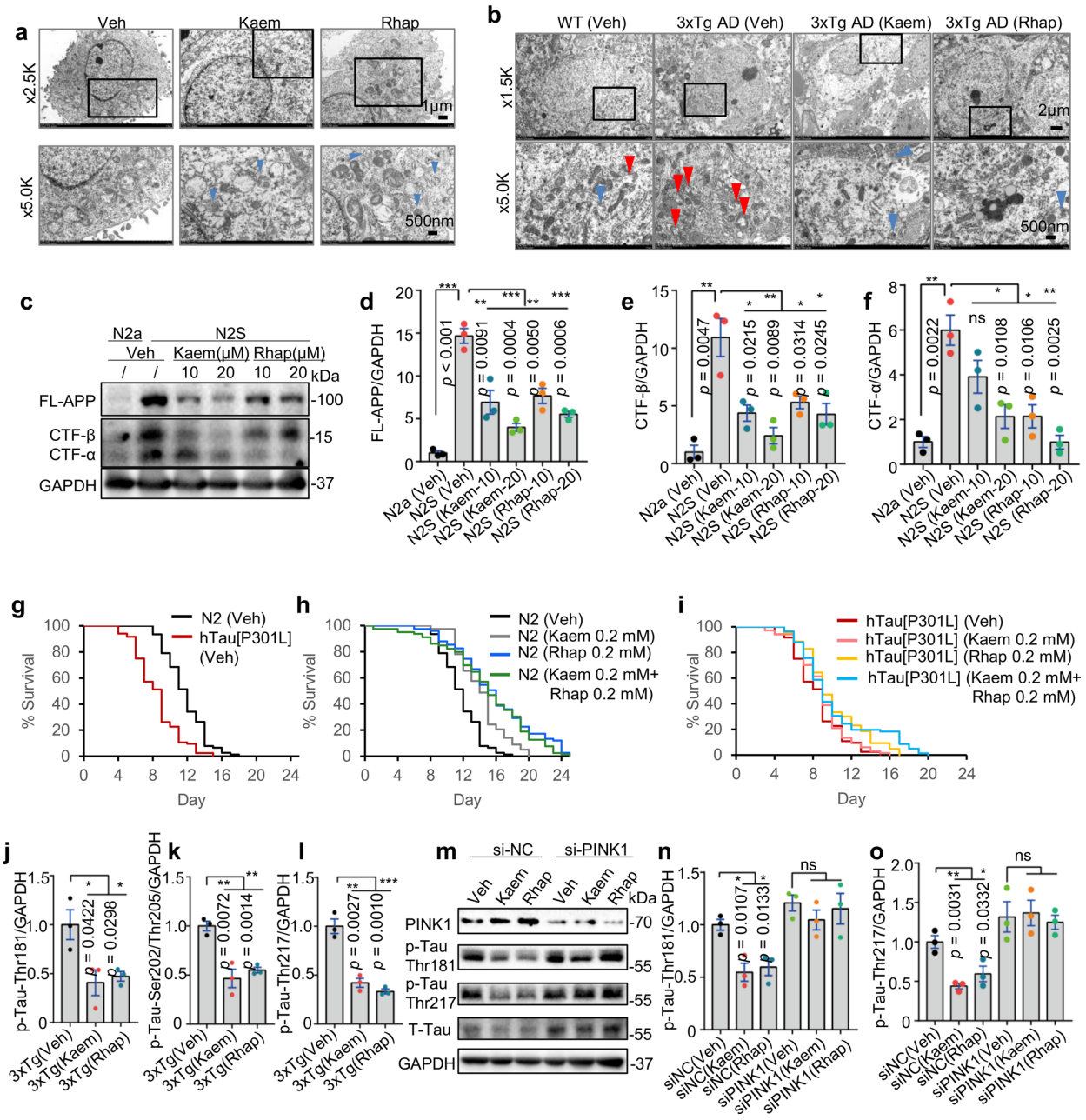

Extended Data Fig. 1 | See next page for caption.

Extended Data Fig. 1 | Kaem and Rhap induce mitophagy, abrogate disease pathologies, and improve healthspan and lifespan in cells, worm, or mouse models of AD. a, **b**, electron microscopic images showing effects of Kaem and Rhap on mitochondrial morphology and mitophagy-like events in mt-Keima HeLa cells (a, 20 μM for 24 h) and mouse hippocampal brain tissues (**b**, 100 mg/kg/d via oral gavage from 12 months for 7 consecutive days; n = 3 mice per group with 4 random hippocampal neuronal images per mouse), treated with Kaem and Rhap. Blue arrows indicate mitophagosome-like events, while red arrows point to damaged mitochondria. Quantitative data of a and b are shown in Fig. 3m and Fig. 3n, respectively. **c**–**f**, Effects of Kaem and Rhap on the expression of designated proteins involved in Aβ production. N2a and N2S (N2a stably transfected with human Swedish mutant APP695) cells were used. One set of western blot data is shown (**c**), with semi-quantifications from three biological replicates (**d**–**f**). All quantitative data were shown in mean ± S.E.M. One-way ANOVA followed by Šidák's multiple comparisons test (**d**–**f**) were used for data analysis. NS, no significance, $^{*}p < 0.05$, $^{**}p < 0.01$, $^{***}p < 0.001$. Original western blot gels for (**c**) are included in Source Data Fig. 2. **g**–**i**, Effects of Kaem and Rhap on lifespan of the N2 and hTau[P301L] (CK12) worms. Data shown are from one set of experiments from a total of two biological replicates (quantitative values in Supplementary Table 4). 90–120 worms were used for each group/biological repeat. All quantitative data were shown in mean ± S.E.M. Log-rank test was used for the statistics of lifespan data (**g**–**i**). NS, no significance, $^{*}p < 0.05$, $^{**}p < 0.01$, $^{***}p < 0.001$. **j**–**l**, Quantification of phosphorylated Tau sites (Thr181, Ser202/Thr205, Thr217) in hippocampal tissues from the 3xTg AD mice (n = 3 biological replicates). The western blotting gel data are shown in Fig. 6o. **m**–**o**, Effects of *PINK1* knockdown on p-Tau inhibition by Kaem and Rhap in HEK 293 3G-EGFP-Tau P301L/mCherry cells. While one biological set of blot data are shown (**m**), quantifications (**n**, **o**) were from 3 biological replicates. All quantitative data were shown in mean ± S.E.M. Two-way ANOVA followed by Tukey's multiple comparisons test (**j, k**. **l**) and one-way ANOVA followed by Šidák's multiple comparisons test (**n**, **o**) were used for data analysis. NS, no significance, $^{*}p < 0.05$, $^{**}p < 0.01$, $^{***}p < 0.001$. Original western blot gels for (**m**) were included in Source Data Fig. 2.

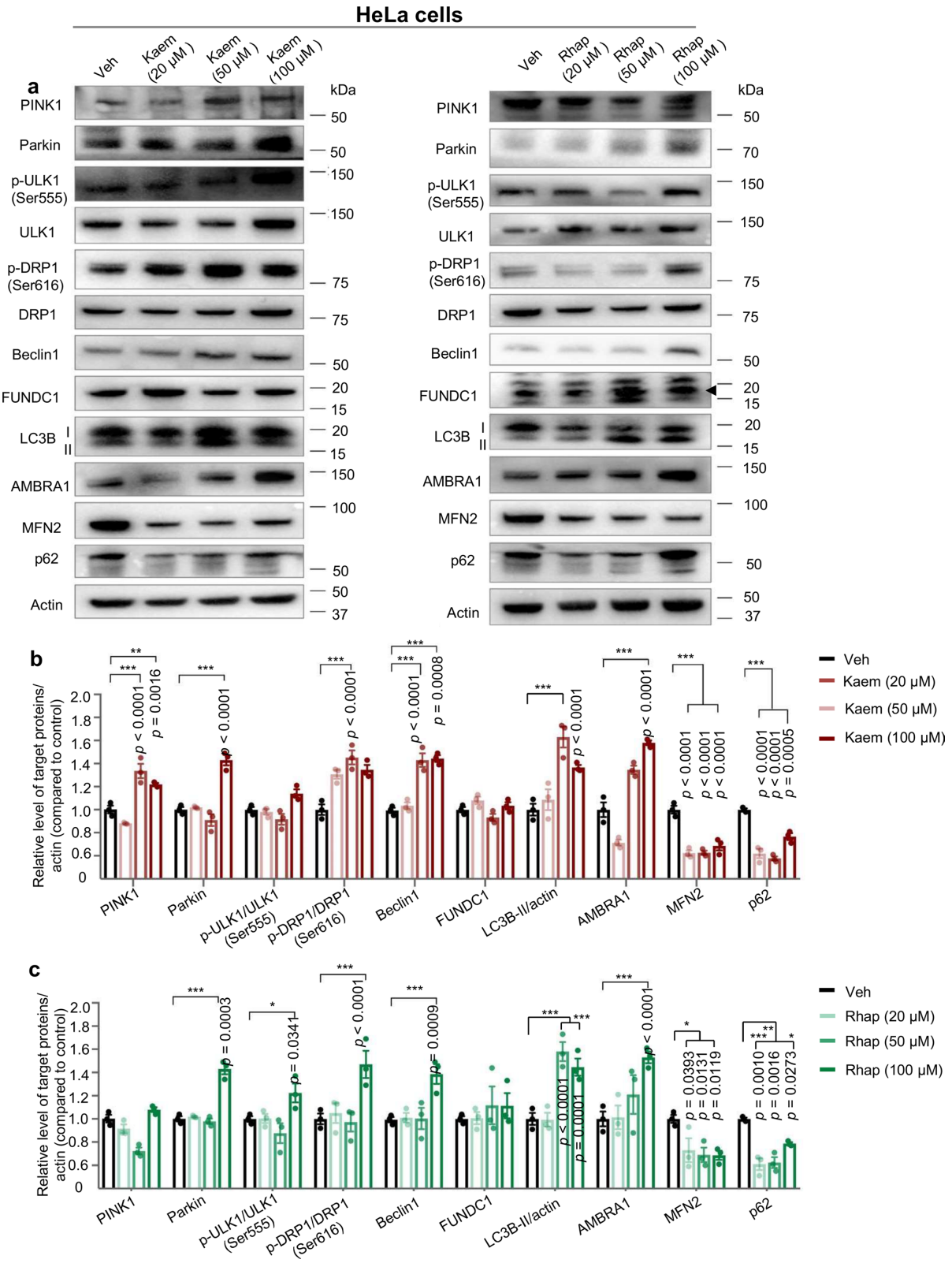

Extended Data Fig. 2 | See next page for caption.

Extended Data Fig. 2 | Kaem and Rhap induce expression of a broad spectrum of autophagy/mitophagy proteins. a, A representative set of western blot images for designated proteins upon Veh., Kaem (20, 50, 100 μM) or Rhap (20, 50, 100 μM) administration for 24 h. Arrow head in the right panel pointed to 'FUNDC1', with bands upper and lower were likely unknown or non-specific bands. **b**, **c**, Semi-quantification of **a** from three biological replicates with data shown in mean ± S.E.M. One-way ANOVA followed by Šidák's multiple comparisons test was used for data analysis, with $^{*}p < 0.05$, $^{**}p < 0.01$, $^{***}p < 0.001$. Original western blot gels for (**a**) were included in Source Data Fig. 1.

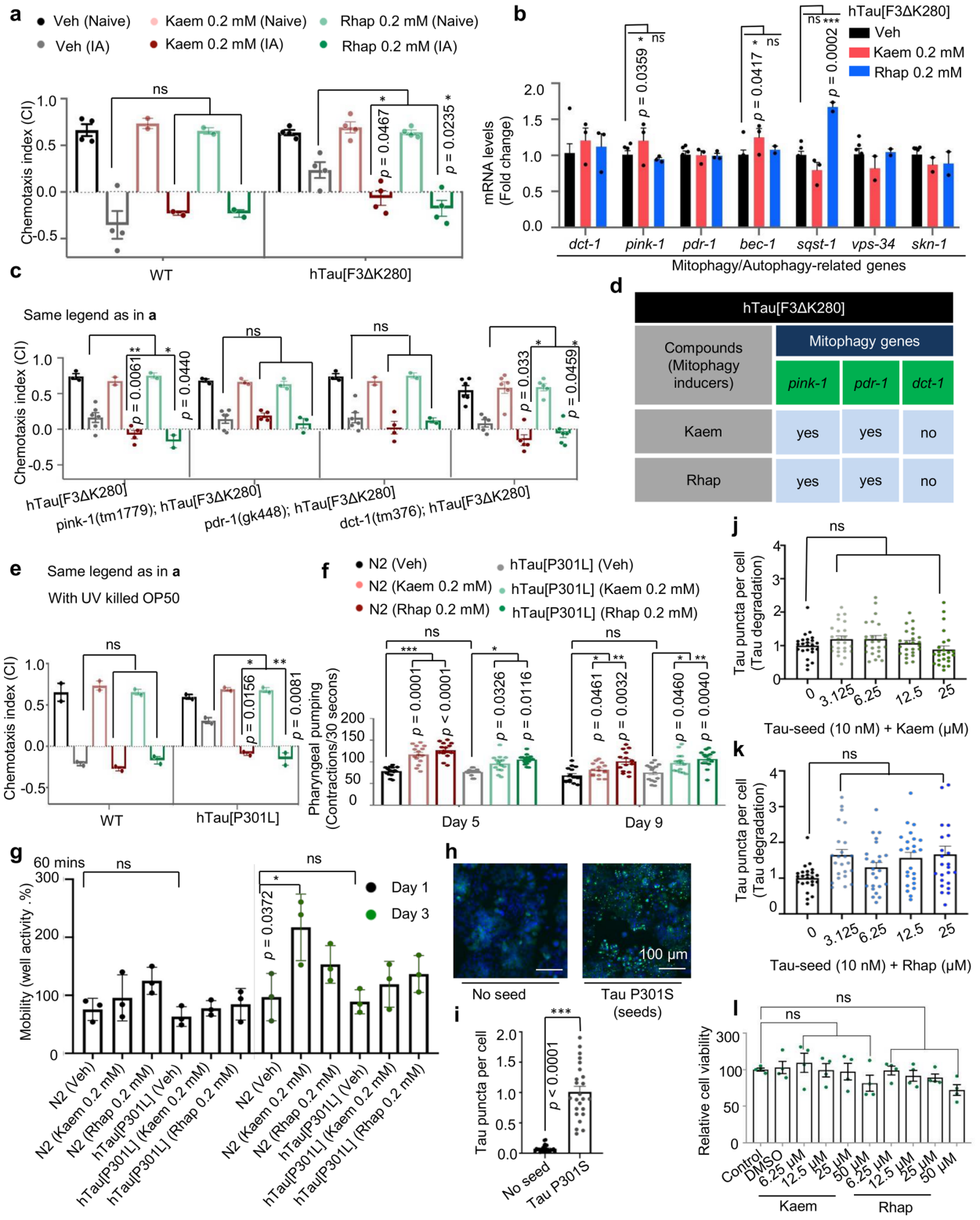

Extended Data Fig. 3 | See next page for caption.

Extended Data Fig. 3 | Mitophagy stimulation restores memory deficit and improves healthspan in the AD-like hTau[F3ΔK280] *C. elegans* model. **a**, Effects of Kaem and Rhap on associative memory in transgenic animals expressing hTau[F3ΔK280]. **b**, mRNA levels of genes affected by Kaem and Rhap in the hTau[F3ΔK280] worms. **c**, Effects of *pink-1*, *pdr-1*, *dct-1, sqst-1, and bec-1* on Kaem- and Rhap-induced associative memory in the hTau[F3ΔK280] worms. **d**, A summary of mitophagy genes involved in Kaem and Rhap-induced memory improvement in the hTau[F3ΔK280] worms. **e**, Memory assay of worms maintained on UV-killed OP50 treated with 0.2 mM Kaem, 0.2 mM Rhap or Veh. **f**, Pharyngeal pumping rates at days 1, 5 and 9 of adulthood in worms treated with 0.2 mM Kaem, 0.2 mM Rhap or Veh (n = 15). **g**, Mobility of hTau[P301L] worms treated with Kaem (n = 50–100 worms) or Rhap (n = 50–100 worms). Adult Day-1 worms were used. One set of data are shown from a total of two biological replicates. **h**–**k**, Effects of Kaem and Rhap on reduction of aggregated Tau in the HEK293 P301S Tau-Venus cells. Exogenous recombinant heparin-assembled P301S Tau (Tau seeds) induces conversion of endogenous Tau Venus from a dispersed distribution to bright foci (h, i). Tests to determine the mechanism of the effect of drugs affecting the degradation of aggregated Tau were performed (**j**, **k**). One image/well was taken, with a total of 8 technical repeats per biological replicate. Data were analysed using ImageJ with images from 3 biological replicates. **l**, Toxicity evaluation of Kaem or Rhap on PC12 cells using MTT. All quantitative data are shown in mean ± S.E.M. Two-way ANOVA followed by Tukey's multiple comparisons test (**a**–**c**, **e**–**g**), one-way ANOVA followed by Šidák's multiple comparisons test (**j**–**l**), and student *t*-test (**i**) were used for data analysis. NS, no significance, $^{*}p < 0.05$, $^{**}p < 0.01$, $^{***}p < 0.001$.

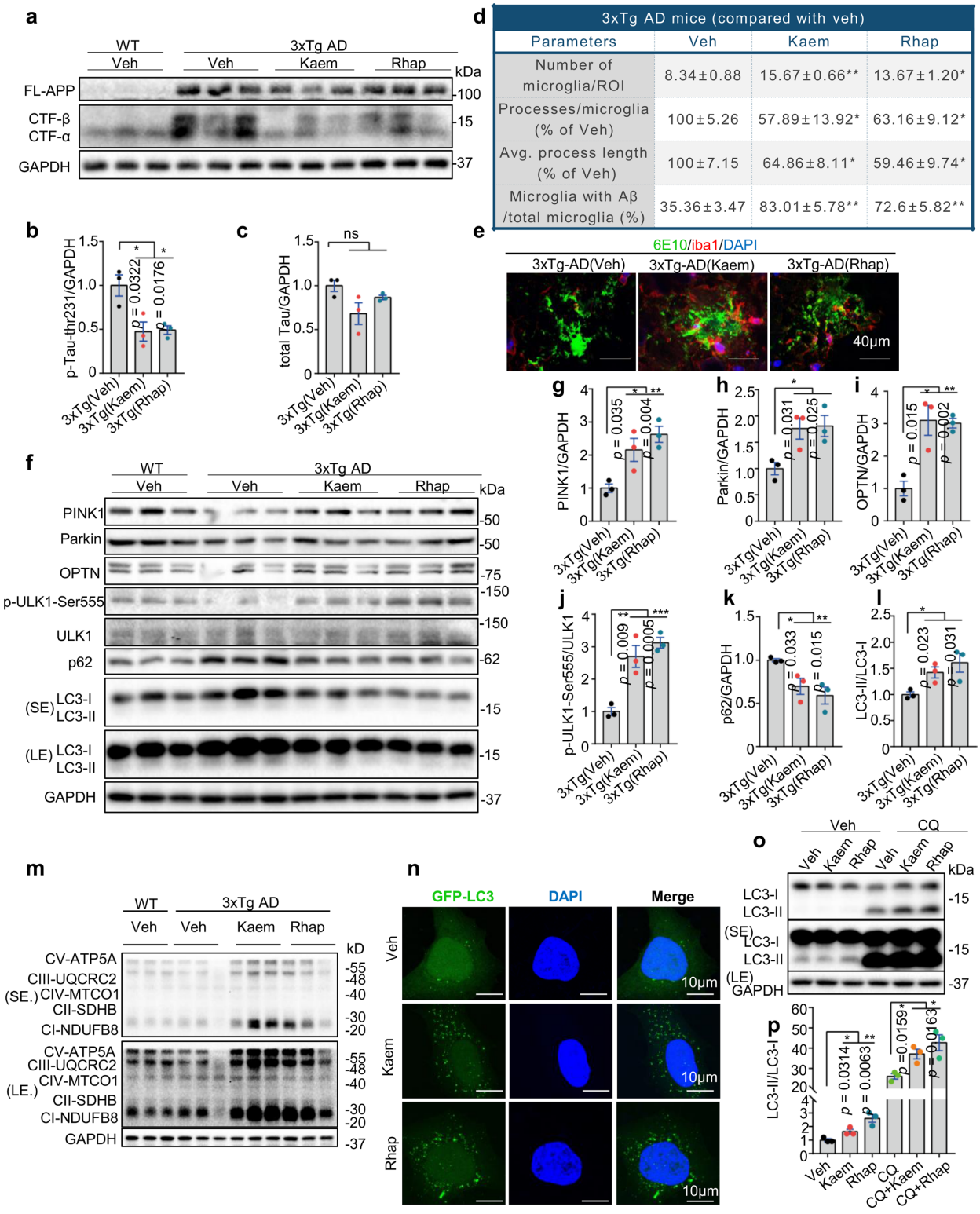

Extended Data Fig. 4 | See next page for caption.

Extended Data Fig. 4 | Kaem and Rhap inhibit Aβ production, increase microglial phagocytosis, and induce mitophagy and autophagy. a, Effects of Kaem and Rhap on protein levels of full-length APP (FL-APP), CTF-α and CTF-β in hippocampal tissues from 3xTg AD mice (n = 3 per group). **b**, **c**, Quantification of phosphorylated Tau sites (Thr231) and total Tau/GAPDH in hippocampal tissues from 3xTg AD mice (n = 3 biologically independent samples). **d**, **e**, Effects of Kaem and Rhap on microglial phagocytosis of Aβ plaques in hippocampal tissues from 3xTg AD mice. Data were quantified from 3 random images/mouse from a total of 3 mice (**d**). Aβ plaques are shown in green (6E10 antibody) and microglia (anti-Iba1 antibody) are in red (**e**). **f**, Western blot results showing the effects of Kaem and Rhap on the levels of proteins involved in mitophagy (PINK1, Parkin, OPTN, p-ULK1-Ser555 and ULK1) and substrates of autophagy (p62 and LC3-II/I) in the hippocampal tissues of the mice (n = 3 mice per group). **g**–**l**, Quantification of Western blot data in (**f**), n = 3 biologically independent samples. se: short-exposure; le: long-exposure. **m**, Western blot results showing the effects of Kaem and Rhap on the levels of proteins involved in OXPHOS in the hippocampal tissues of the mice (n = 3 mice per group). **n**, Effects of Kaem and Rhap on autophagy induction using a HeLa cell line stably expressing GFP-LC3 following Kaem (10 μM) or Rhap (10 μM) treatment for 12 h before imaging. **o**, **p**, Western blot data (o) with semi-quantification (p) showing the effects of Kaem and Rhap on levels of LC3-II/I in the HEK293 cells (n = 3 biologically independent samples). All quantitative data shown in mean ± S.E.M. One-way ANOVA followed by Šidák's multiple comparisons test (**b**–**d**, **g**–**l**, **p**) was used for data analysis. NS, no significance, $^{*}p < 0.05$, $^{**}p < 0.01$, $^{***}p < 0.001$. Original unprocessed western blots for **a**, **f**, **m**, **o** are available in Source Data Figs. 2–4.

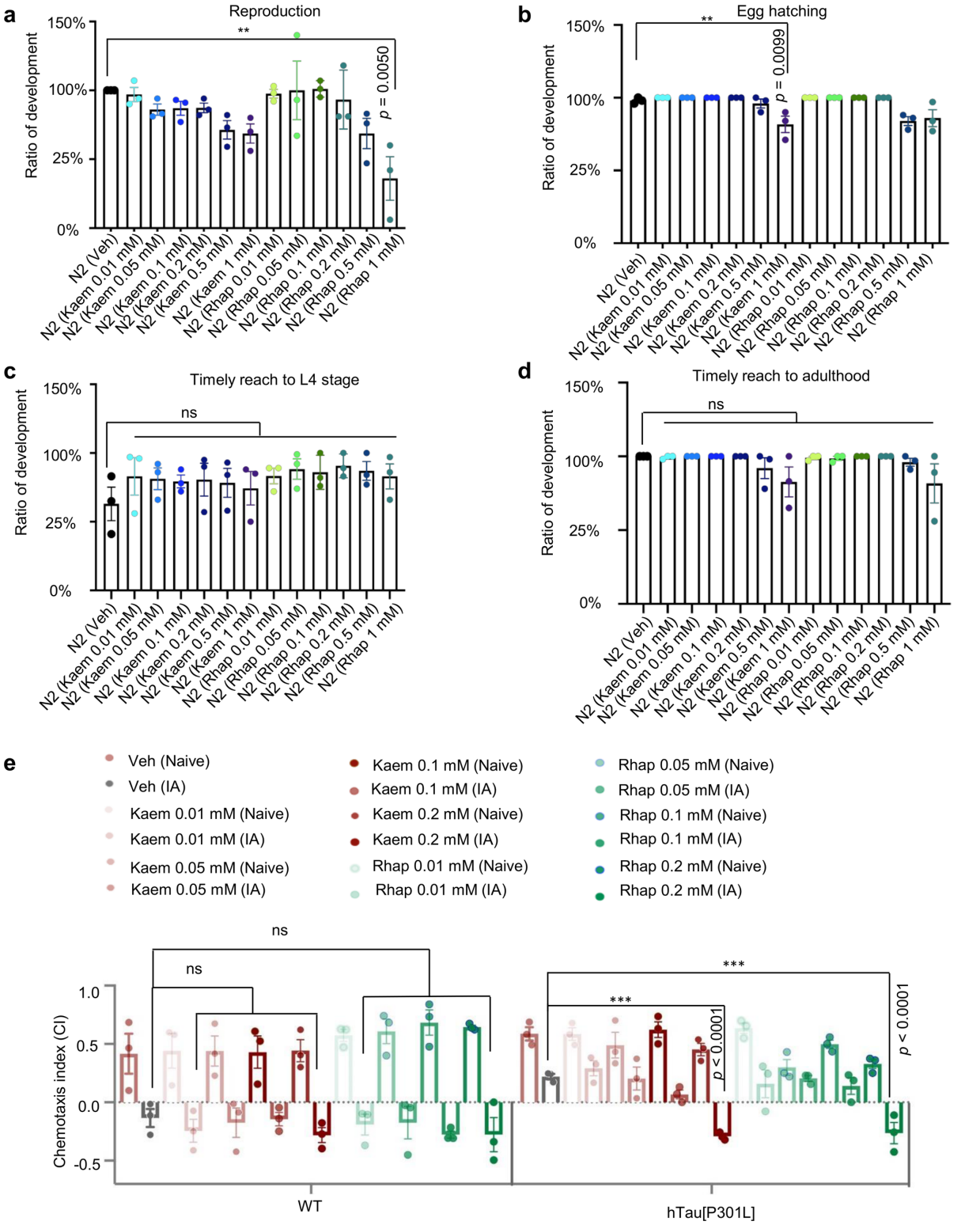

Extended Data Fig. 5 | See next page for caption.

Extended Data Fig. 5 | Kaem and Rhap are toxicologically safe to nematodes up to 1 mM and they do not show memory retention activity until reaching to 0.2 mM. Toxicological effects of Kaem or Rhap (0.01, 0.05, 0.1, 0.2 mM from egg hatching onwards) on fecundity (3-h egg-lay) (**a**), egg hatching (**b**), development to L4 (**c**), and time to reach adulthood (**d**). **e**, Effects of different doses of Kaem and Rhap (0.01, 0.05, 0.1, 0.2 mM from egg hatching onwards) on associative memory in transgenic animals expressing hTau[301 L]. All quantitative data are shown in mean ± S.E.M. from three biological repeats. Two-way ANOVA followed by Tukey's multiple comparisons test was used for data analysis. NS, no significance, ***$p < 0.001$.

nature portfolio

Corresponding author(s): Evandro F. Fang and Jia-Hong Lu

Last updated by author(s): Sep 15, 2021

Reporting Summary

Nature Portfolio wishes to improve the reproducibility of the work that we publish. This form provides structure for consistency and transparency in reporting. For further information on Nature Portfolio policies, see our Editorial Policies and the Editorial Policy Checklist.

Statistics

For all statistical analyses, confirm that the following items are present in the figure legend, table legend, main text, or Methods section.

n/a	Confirmed
☐	☒ The exact sample size (*n*) for each experimental group/condition, given as a discrete number and unit of measurement
☐	☒ A statement on whether measurements were taken from distinct samples or whether the same sample was measured repeatedly
☐	☒ The statistical test(s) used AND whether they are one- or two-sided *Only common tests should be described solely by name; describe more complex techniques in the Methods section.*
☒	☐ A description of all covariates tested
☒	☐ A description of any assumptions or corrections, such as tests of normality and adjustment for multiple comparisons
☐	☒ A full description of the statistical parameters including central tendency (e.g. means) or other basic estimates (e.g. regression coefficient) AND variation (e.g. standard deviation) or associated estimates of uncertainty (e.g. confidence intervals)
☐	☒ For null hypothesis testing, the test statistic (e.g. *F*, *t*, *r*) with confidence intervals, effect sizes, degrees of freedom and *P* value noted *Give P values as exact values whenever suitable.*
☒	☐ For Bayesian analysis, information on the choice of priors and Markov chain Monte Carlo settings
☒	☐ For hierarchical and complex designs, identification of the appropriate level for tests and full reporting of outcomes
☐	☒ Estimates of effect sizes (e.g. Cohen's *d*, Pearson's *r*), indicating how they were calculated

Our web collection on statistics for biologists contains articles on many of the points above.

Software and code

Policy information about availability of computer code

Data collection	RDkit-2019 was used for molecule operation and similarity calculation. Scikit-learn 0.23 was used for data processing and clustering. Custom code was specific to our computing infrastructure and mainly used for data input/output and parallelization across computers and graphics processors. The code, currently under a patent-examination process, is available from the corresponding author on reasonable request. Confocal Labmaze was used for behavioural tracking in the mouse studies. Nikon, ZEN (blue edition) and Leica TCS SP8 confocal Laser Scanning Microscope System software were used for taking images.
Data analysis	Microsoft Excel (2016) and Graphpad Prism 8 were used for data analysis. ImageJ with the plug in ObjectJ was used for the quantification of mitophagy levels.

For manuscripts utilizing custom algorithms or software that are central to the research but not yet described in published literature, software must be made available to editors and reviewers. We strongly encourage code deposition in a community repository (e.g. GitHub). See the Nature Portfolio guidelines for submitting code & software for further information.

Data

Policy information about availability of data

All manuscripts must include a data availability statement. This statement should provide the following information, where applicable:

- Accession codes, unique identifiers, or web links for publicly available datasets
- A description of any restrictions on data availability
- For clinical datasets or third party data, please ensure that the statement adheres to our policy

The main data supporting the findings of this study are available within the Article and its Supplementary Information. The raw wet-lab data generated in this study

are available from the corresponding author on reasonable request. Restrictions apply to the AI-related data: all requests for raw and processed data will be reviewed by Mindrank AI to verify whether the request is subject to any intellectual property or confidentiality constraints.

Field-specific reporting

Please select the one below that is the best fit for your research. If you are not sure, read the appropriate sections before making your selection.

☒ Life sciences ☐ Behavioural & social sciences ☐ Ecological, evolutionary & environmental sciences

For a reference copy of the document with all sections, see nature.com/documents/nr-reporting-summary-flat.pdf

Life sciences study design

All studies must disclose on these points even when the disclosure is negative.

Sample size	Sample sizes for the behavioral tests were determined by the current standard used for mice in behavioral experiments, as well as based on the minimal amount of mice required to detect statistical significance with an alpha rate set at 0.05 in a standardly powered experiment. Thus, a total 6 mice/group were used for behavioral tests. The sample sizes used for immuno-histochemistry, Western blotting and other analyses were 3–6, as specified in the figure captions. Sample sizes for the C. elegans studies were 200–400 worms/group for the memory assay and around 100 worms/group for the lifespan studies. The sample sizes used in other experiments are detailed in the respective figure captions.
Data exclusions	No data were excluded from analysis.
Replication	All the cell-culture and C. elegans experiments were performed with 3 biological repeats (with 3 technical repeats within each biological repeat), unless otherwise specified. All experiments were replicated successfully, with consistent data. The mouse data were from one biological experiment, as is common in the field.
Randomization	Animals and samples were assigned randomly to the various experimental groups. Mice were randomly selected for the behavioural experiments.
Blinding	In data collection and analysis (mouse behavioural studies, mouse imaging-data analysis, and the imaging and data analysis of electron microscopy), the investigators were blinded to the experimental design.

Reporting for specific materials, systems and methods

We require information from authors about some types of materials, experimental systems and methods used in many studies. Here, indicate whether each material, system or method listed is relevant to your study. If you are not sure if a list item applies to your research, read the appropriate section before selecting a response.

Materials & experimental systems

n/a	Involved in the study
☐	☒ Antibodies
☐	☒ Eukaryotic cell lines
☒	☐ Palaeontology and archaeology
☐	☒ Animals and other organisms
☒	☐ Human research participants
☒	☐ Clinical data
☒	☐ Dual use research of concern

Methods

n/a	Involved in the study
☒	☐ ChIP-seq
☒	☐ Flow cytometry
☒	☐ MRI-based neuroimaging

Antibodies

Antibodies used	Antibodies used in western blot as follows (all from Cell Signaling Technology unless otherwise stated): PINK1 antibody (catalog no. ab75487, Abcam; no. A7131, ABclonal); Parkin antibody (no.NB100-91921; Novus); FUNDC1 antibody (no. ab74834; Abcam); LC3B antibody (no.NB100-2220; Novus); Beclin1 antibody (no.3495s); phospho-DRP1 antibody (no.S616); DRP1 antibody (no.8570s); p62 antibody (no.8025s); MFN2 antibody (no.94823s); phospho-ULK1 antibody (no.5869s); ULK1 antibody (no.6439s); AMBRA1 antibody (no.24907s); OPTN antibody (no. A1845, ABclona); Tau antibody (no. 46687s); p-Tau-thr181 (no. 12285s); p-Tau-thr231 (no. ab151559, Abcam); p-Tau-ser202/thr205 (no. MN1020, ThermoFisher Scientific); p-Tau-thr217 (no. 44-744, ThermoFisher Scientific); beta Amyloid polyclonal antibody (no. 51-2700, ThermoFisher Scientific); β-actin antibody (no. A5441; Sigma). Secondary antibodies including anti-mouse immunoglobulin G (IgG; catalog no. 7076s) and anti-rabbit IgG (no. 7074s). Specific primary antibodies used in immunohistochemistry include: mouse anti-β-Amyloid, 1-16 antibody (clone 6E10, catalog no. 803002; BioLegend); and rabbit anti-iba1 antibody (019-19741; Wako); mouse anti-AT8 antibody (cat no. MN1020; ThermoFisher Scientific). For first antibodies, the dilution ratio was 1:1000 or otherwise as specified else where; for secondary antibodies, the dilution ration was 1:5000 or otherwise as specified else where.
Validation	All the antibodies were validated for use in cell, mouse/human tissues based on previous publications (Fang EF et al., Cell 2014; Fang

Validation	EF et al., Cell Metab 2016; Fang EF et al., Nat Neuroscu 2019; Fang EF et al., Nat Commun 2019). Detailed antibody validation profiles are available on the antibody-provider websites.

Eukaryotic cell lines

Policy information about cell lines

Cell line source(s)	Mt-Keima HeLa cells were used for mitophagy evaluation; HEK293 cells stably expressing the 0N4R isoform of human Tau, bearing the P301S mutation with a C-terminal venus were used for Tau aggregation and degradation. N2a and GFP-LC3 HeLa cells were cultured for mechanistic studies.
Authentication	None of the cell lines used were authenticated.
Mycoplasma contamination	All cell lines tested negative for mycoplasma contamination.
Commonly misidentified lines (See ICLAC register)	No commonly misidentified cell lines were used.

Animals and other organisms

Policy information about studies involving animals; ARRIVE guidelines recommended for reporting animal research

Laboratory animals	3xTg-AD mice were provided on a B6;129 genetic background (Stock No. 004807 B6;129-Tg(APPSwe,tauP301L)1Lfa Psen1tm1Mpm/Mmjax; https://www.jax.org/strain/004807) by the Jackson's laboratory. C57BL/6J mice were used as WT control. All animals were housed in individually ventilated cages on standardized rodent bedding. All animals were housed under constant-light cycle (12 h light/dark) with food and water provided. 12.5-month-old 3xTg-AD female mice were used for two-month drug treatments by oral gavage, followed by behavioural and biochemical studies.
Wild animals	The study did not involve wild animals.
Field-collected samples	The study did not involve samples collected from the field.
Ethics oversight	All animal care and experimental procedures were approved by the Committee on the Ethics of Animal Experiments of the University of Macau (UMARE-013-2019).

Note that full information on the approval of the study protocol must also be provided in the manuscript.